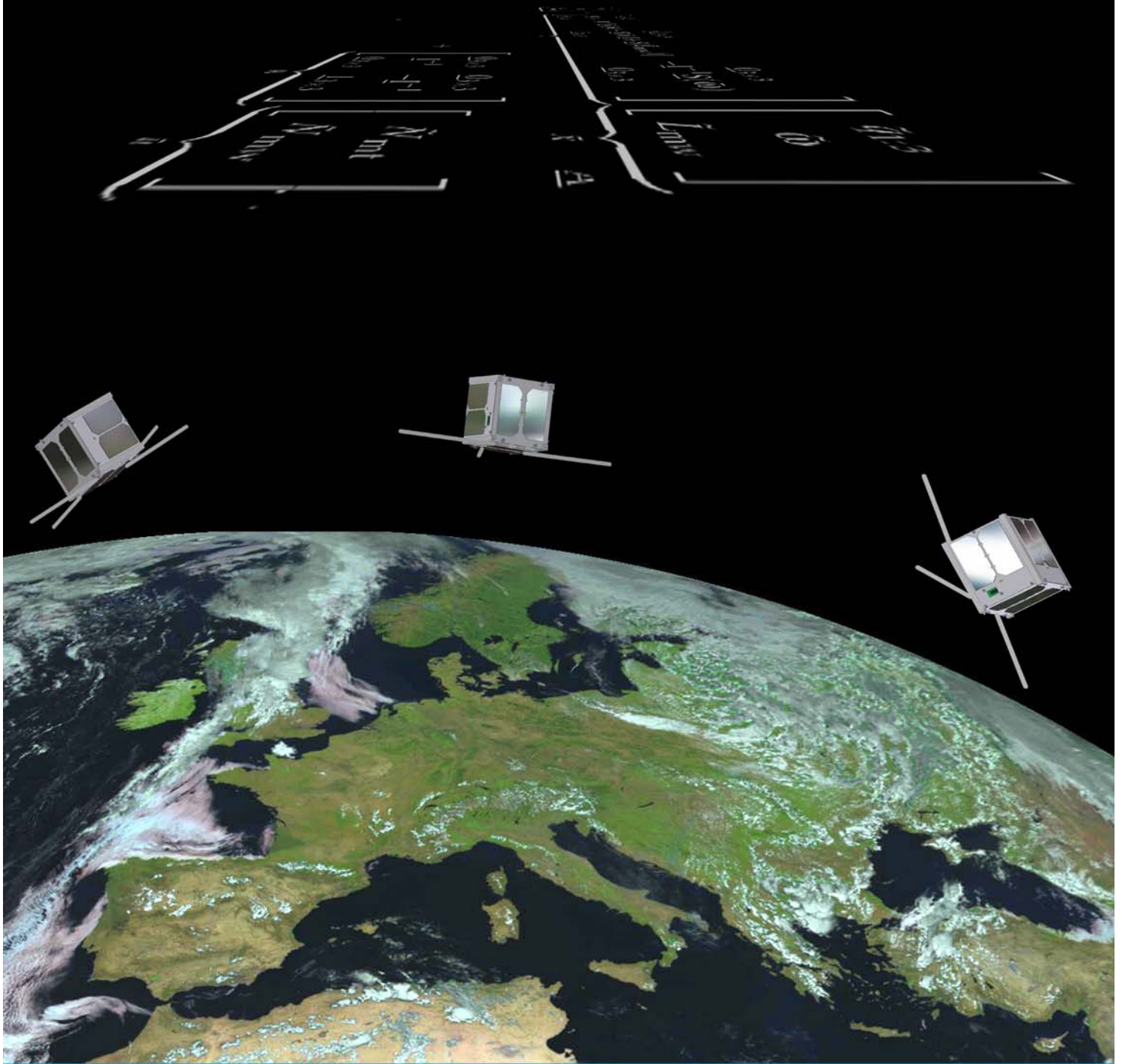
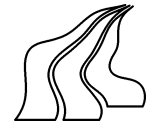


ATTITUDE CONTROL SYSTEM FOR AAUSAT-II





Title: Attitude Control System for AAUSAT-II

Theme: Modelling and Control

Project period: February 2nd 2005 - May 30th 2005

Project group:
IAS8-05GR834

Group members:
Bo Ørsted Andresen
Claus Grøn
Rasmus Hviid Knudsen
Claus Nielsen
Kresten Kjær Sørensen
Dan Taagaard

Supervisor:
Dan Bhanderi

Publications: 9
Pages: 113
Finished: May 30th 2005

Abstract

This report documents the work of group 05GR834, concerning the development of an attitude control system for the AAUSAT-II satellite.

A model of the satellite kinematics and dynamics has been implemented in a simulation environment containing relevant disturbances.

The attitude control system features both magnetorquers and momentum wheels to facilitate three axes control of the satellite and by the means of magnetic and mechanical actuation, the satellite is able to detumble and do slew manoeuvres.

To detumble the satellite, using only magnetic actuation, a controller based on the B-dot algorithm has been designed. For pointing purposes the attitude control system features a control supervisor to manage the attitude controllers. The attitude controllers consist of an optimal controller for controlling the momentum wheels and a desaturation controller to keep the momentum wheels from reaching their saturation limits.

The controllers have been tested in the simulation environment with successful results. The B-dot controller performs robustly and meets the demands, hence it is ready for implementation on the satellite. Simulations of the attitude controllers show that they meet the demands as well and enables the satellite to perform slew manoeuvres and maintain a given attitude.

Preface

This report documents the project of developing the attitude control system for AAUSAT-II. The project is made on 8th semester in the specialization of Intelligent Autonomous Systems at the Department of Control Engineering, Aalborg University.

The project was initiated February 2nd 2005 and finished May 30th 2005.

Throughout the report figures, tables and equations are numbered consecutively according to the chapters. Citation numbers are referring to the bibliography at page 79, e.g. [Wertz, page 571] is referring to page 571 in *Spacecraft Attitude Determination and Control* by James R. Wertz. Equations are referred to in parentheses e.g. (1.4) refers to Equation 1.4 on page 14.

The project is closely connected to the AAUSAT-II attitude determination system, hence Chapters 1, 2 and parts of the appendices have been written in collaboration with group 05GR833, who are developing the attitude determination system for AAUSAT-II. The project is a continuation of an earlier project concerning the attitude control system for AAUSAT-II made by group 04GR830a.

Simulation files, data sheets and other relevant documentation is available from the enclosed CD-ROM.

Aalborg University, May 30th 2005

Bo Ørsted Andresen

Claus Grøn

Rasmus Hviid Knudsen

Claus Nielsen

Kresten Kjær Sørensen

Dan Taagaard

Table of Contents

1	The AAUSAT-II Satellite	8
1.1	Background	8
1.2	Mission Objectives for AAUSAT-II	8
1.3	AAUSAT-II Subsystems	9
1.4	Satellite Modes	11
1.5	Requirements for the Attitude Determination and Control System	12
2	Modelling	18
2.1	Coordinate Systems	18
2.2	Ephemeris	25
2.3	Disturbance Modelling	28
2.4	Earth Albedo	32
2.5	Orbit Propagator	34
2.6	Magnetic Field Model	34
2.7	Satellite Dynamics and Kinematics	35
2.8	Transducers	42
2.9	Actuator Modelling	42
3	Controllers	51
3.1	Control Strategy	51
3.2	Control Supervisor	52
3.3	Controllability	55
3.4	Detumbling Controller	56
3.5	Optimal Controller for Attitude Control	61
3.6	Desaturation Controller	74
4	Conclusion	78
4.1	Future Work	79
	Bibliography	81
A	Quaternions	82
A.1	Quaternion Definitions	82
A.2	Quaternion Algebra	83
B	Rotations	85
B.1	Direction Cosine	85
B.2	Euler Angles	86
B.3	Euler's Eigenaxis Rotation Theorem	87
B.4	Attitude Matrix and Kinematics	88
C	Two Line Elements	91
D	Linearization	93
D.1	Linearization of the Satellite Kinematic Equation	93

D.2 Linearization of Satellite Dynamic Equation 96

D.3 Linear Equation for the Satellite Attitude 97

E Implementation of Simulation 98

E.1 Simulation Environment 98

F Orbit Propagator Accuracy 108

G Magnetic Field Model Accuracy 111

Nomenclature

Acronyms

ACS Attitude Control System

ADCS Attitude Determination and Control System

ADS Attitude Determination System

CDH Command and Data Handling

COM Communication system

DCM Direct Cosine Matrix

EPS Electrical Power Supply

GND Ground Station

ICD Interface Control Document

IGRF International Geomagnetic Reference Field

JD Julian Date. The number of days since January 1st, 4713 B.C., at 12.00AM UTC.

LEO Low Earth Orbit

MCC Mission Control Center

MECH Mechanical structure

OBC On-Board Computer

P/L Payload

SGP4 Simplified General Perturbations 4

TLE Two Line Element

Reference Frames

ECI Earth Centered Inertial reference frame. Abbreviated I in equations.

ECEF Earth Centered Earth Fixed reference frame. Abbreviated E in equations.

ORF Orbit Reference Frame. Abbreviated O in equations.

SBRF Satellite Body Reference Frame. Abbreviated S in equations.

CRF Controller Reference Frame. Abbreviated C in equations.

Notation

Vectors, Matrices and Rotations

- Vectors are typed as

v

- Unit vectors are typed as

\hat{u}

- Matrices are typed as

$\underline{\mathbf{M}}$

- Identity matrices are typed as

$\underline{\mathbf{1}}_{n \times n}$

(1)

e.g. a 3×3 identity matrix is written as

$$\underline{\mathbf{1}}_{3 \times 3} = \begin{bmatrix} 1 & 0 & 0 \\ 0 & 1 & 0 \\ 0 & 0 & 1 \end{bmatrix}$$

- Rotations (quaternions and matrices) are typed with source frame designation (preceding subscript) and destination frame designation (preceding superscript). E.g.,

${}^{\mathbf{I}}\underline{\mathbf{C}}_{\mathbf{E}}$, ${}^{\mathbf{I}}q_{\mathbf{E}}$

${}^{\mathbf{I}}q_{\mathbf{E}}$ is a quaternion describing a rotating from ECEF to ECI and ${}^{\mathbf{I}}\underline{\mathbf{C}}_{\mathbf{E}}$ is a matrix describing a rotating from ECI to CRF.

- Vector and quaternion components are typed as

${}^{\mathbf{E}}v_x$, ${}^{\mathbf{I}}q_{1:3}$

which denotes the component x of the vector v in ECEF, and the components 1 through 3 of the quaternion q in the ECI frame.

Signals

- Small signals are typed as

\tilde{q}

which denotes the small signal quaternion.

- Operating points are typed as

\bar{q}

which denotes the quaternion in the operating point.

The AAUSAT-II Satellite

This chapter describes the mission the AAUSAT-II satellite shall accomplish during the designated time of operation. This includes a description of the purpose and functionality of each subsystem on-board the satellite.

1.1 Background

The AAUSAT-II satellite is a pico satellite which is constructed by students primarily at Aalborg University. The project was initiated in September 2003 and the satellite is expected to be launched in December 2005. Another satellite, AAU CubeSat, has been developed at Aalborg University and was launched in April 2003, and was a great success.

The AAUSAT-II follows the CubeSat concept developed by California Polytechnic State University, San Luis Obispo and Space Systems Development Laboratory at Stanford University [CPSU]. This concept allows the satellite to have a mass of maximum 1 [kg] and the dimensions of 10 [cm] × 10 [cm] × 10 [cm], hence the name CubeSat. The size constrains the amount of power and space available which entails that low power consumption, small volume and low mass are important factors in the design process.

1.2 Mission Objectives for AAUSAT-II

A number of mission objectives have been formulated for the AAUSAT-II project. The mission objectives are defined in an order, such that the first objective has to be accomplished before trying to accomplish the second objective.

1. Education of the students and staff involved with the AAUSAT-II project.

The primary mission for the satellite project is to educate the students and the staff working on it. The satellite shall be built by students mostly. Staff related to the project are only meant to act as advisors and final arbitrators. The purpose of this is to enable the students to make important decisions based on their own experience which is an important part of engineering studies, since a satellite is a complicated system which requires a lot of coordination between all groups working with the project.

2. Communication.

In order to ensure the communication with the satellite is functioning, one-way communication is established when a basic beacon with the correct syntax is received at the ground station. When two-way communication is established, by sending a command to the satellite and a correct answer corresponding to the command, is received from the satellite, the communication objective is fulfilled.

3. Payload.

The AAUSAT-II carries a gamma ray burst detector as a payload. The gamma ray burst detector is developed at the Danish National Space Center (DNSC), and is used for measuring the radiation from gamma bursts in space. This objective is fulfilled when correct and usable data has been received from the satellite.

4. The attitude determination and control system.

It is a scientific purpose that the attitude of the satellite is to be controlled by an active on-board Attitude Determination and Control System (ADCS). The primary goal for the ADCS is to detumble the satellite to ensure a more reliable radio link to Earth. A secondary goal is controlling the attitude of the satellite using magnetorquers and momentum wheels. Controlling the attitude of the satellite makes it possible to do experiments and prove the accuracy of the ADCS. The ADCS can then be used on future missions which may demand a high pointing accuracy such as an optical downlink for high speed data transfer to the ground station.

5. Upload new software.

As a science mission the satellite shall also include the possibility of uploading new software, such as new determination algorithms or a new controller for the ADCS. This is done to verify how writing to flash memory acts in space. Furthermore, this establishes the possibility for future students to upload and test their determination and control algorithms.

6. Deployment of solar arrays.

Since CubeSats have a limited size, the energy from the solar panels is limited, reflecting on the power budget. Therefore the possibility of adding solar cells is tested by deploying solar arrays. The solar array does not have solar cells on them, but is deployed to verify the functionality of the mechanical system.

7. Co-operation with the AMSAT¹ community.

When all previous mission objectives are fulfilled, upload of new software will be performed. This software will give radio amateurs access to the satellite using commands that are published on the homepage of AAUSAT-II, <http://www.aausatii.aau.dk>.

Furthermore, to make it easier to construct a new satellite for other types of missions, the subsystems are designed using a generic architecture platform meaning that integration and implementation of new subsystems would have no effect on the other subsystems. This way the integration and testing of the single subsystems will be less complex. As a part of the project all data accumulated on the satellite as housekeeping data will be downloaded and saved in a database. Using the data it will be possible to analyze how different parts of the satellite perform in space. The results will then be used for improving the performance in future satellite projects.

1.3 AAUSAT-II Subsystems

The AAUSAT-II consists of different subsystems, each with a specific task. This section provides an overview of these subsystems and explains their tasks on-board the satellite.

1.3.1 Subsystem Overview

A block diagram of the AAUSAT-II subsystems is depicted in Figure 1.1. The satellite itself consists of seven subsystems, five of these are electrical and communicates through a CAN bus. MECH is the mechanical structure of the satellite, and command and data handling (CDH) is software running on the on-board computer (OBC). Besides that, the AAUSAT-II project comprises a ground station (GND) and a mission control center (MCC). The communication link between the satellite and the ground station transfers data at either 1200, 2400 or 4800 [bps], half duplex [COM, page 49].

¹ The Radio Amateur Satellite Corporation, <http://www.amsat.org>.

1.3. AAUSAT-II SUBSYSTEMS

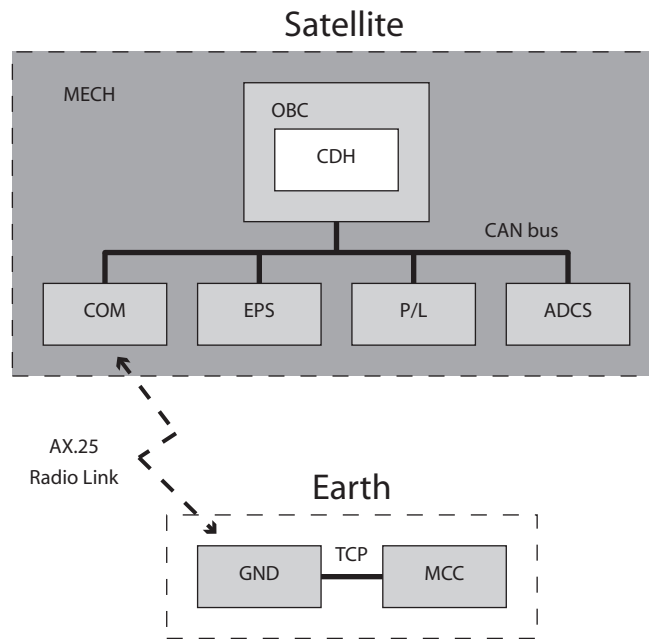


Figure 1.1: Block diagram depicting the subsystems in the AAUSAT-II and a conceptual visualization of their respective interfaces to other subsystems.

1.3.2 Subsystem Descriptions

MCC (Mission Control Center) is responsible for handling and storing all transmission data from the satellite and sending flight plans etc. to the satellite. The MCC provides a user interface and a database to store housekeeping data from the satellite. The mission control center is furthermore able to control multiple ground stations, both the ground station located in Aalborg and a ground station placed at Svalbard in Norway which is currently in the final stages of development.

GND (Ground Station) is responsible for the communication between the MCC and the satellite. The task of the ground station is to track the satellite throughout each pass and adjust the radio frequency, so data between the satellite and the MCC can be sent and received correctly. Furthermore, the ground station is designed to be autonomously controlled by the MCC, both for communicating with the AAUSAT-II satellite and the ESA SSETI Express satellite².

COM (Communication System) is designed to function as a pipeline for the communication between the ground station and the CDH. COM modulates and sends data from CDH to the ground station. Data received from the ground station is demodulated and sent via the CAN bus to the CDH subsystem.

EPS (Electrical Power Supply) is responsible for generating power from the solar cells and storing it in the batteries in order to be able to deliver continuous power during eclipse and peak demands. The EPS subsystem also conditions and distributes the power to other satellite subsystems.

ADCS (Attitude Determination and Control System) is responsible for determining and controlling the attitude of the satellite. This primarily implies detumbling and stabilization of the satellite.

P/L (Payload) consists of a gamma ray burst detector. The gamma ray burst detector is a newly developed detector crystal supplied by Danish National Space Center.

OBC (On-Board Computer) is the main computer on the satellite. The CDH subsystem software is executed on the OBC. The OBC subsystem also provides processing facilities for other satellite subsystems.

²<http://sseti.gte.tuwien.ac.at/WSW4/express1.htm>

CDH (Command and Data Handling) is implemented as software running on the OBC. The CDH subsystem is responsible for maintaining the flight plan, accumulating housekeeping data, managing the subsystems and controlling the communication with the ground station.

MECH (Mechanical Structure) provides the physical satellite frame structure and casing in which the other satellite subsystems are mounted. Besides the satellite frame, also an additional solar cell array is designed to be mounted on the satellite frame.

The satellite is an intelligent autonomous system which interacts on tele commands sent from the MCC using the ground station. The communication path is illustrated in Figure 1.2. A tele command is transmitted through the ground station and received by the COM system. The communication system then passes the tele command on to the CDH system which decodes and executes the command. It is not possible to send a command directly through the communication system to a specific subsystem. All tele commands is directed through the CDH system.

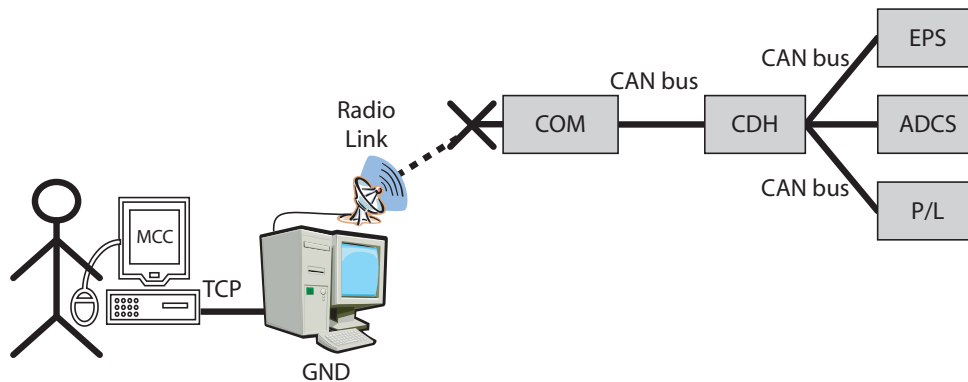


Figure 1.2: The communication path for the AAUSAT-II.

1.3.3 Description of the Attitude Determination and Control System

During development of the AAUSAT-II the ADCS is divided into three parts, each developed by three separate groups; Attitude Determination System (ADS), Attitude Control System (ACS) and ADCS Hardware (ADCS HW). The ADS consists mainly of development of algorithms allowing determination of the attitude of the satellite, whereas development of the control strategy and algorithms are done by the ACS. The ADCS HW consists of sensors and actuators needed by the ADS and ACS and provides an interface platform connected to the on-board CAN bus allowing the ADS and ACS to run on the OBC. The ADCS HW sensor and actuator system consists of three momentum wheels, three magnetorquers, one three-axis magnetometer, six one-axes gyros, six photodiodes, and six temperature sensors.

1.4 Satellite Modes

Four different modes of operation have been defined for the satellite. Each subsystem has different tasks to perform within each mode. The four different modes each defines which subsystems are to be powered up and individual actions for the subsystems. The modes are as follows:

Initialization mode

Systems powered up: EPS.

1.5. REQUIREMENTS FOR THE ATTITUDE DETERMINATION AND CONTROL SYSTEM

Actions: EPS checks if the antennas have been deployed and deploys them if they have not. Afterwards the satellite changes to safe mode.

Safe mode

Systems powered up: EPS.

Actions: EPS charges the batteries in case of low battery voltage or conditions the batteries in case of extreme temperatures etc.

Recovery mode

Systems powered up: EPS and COM.

Actions: COM sends a basic beacon including the current battery voltage to Earth and EPS checks if the battery voltage is sufficient to advance to nominal mode.

Nominal mode

Systems powered up: EPS, COM, OBC/CDH, ADCS and P/L.

Actions: CDH is responsible for transmitting a nominal beacon through COM to Earth. Besides that CDH controls the flight plan and instructs EPS to turn on or off ADCS and P/L.

1.5 Requirements for the Attitude Determination and Control System

This section will describe the requirements to the ADCS according to each of the mission objectives presented in Section 1.2. All requirements for the ADCS are within a confidence interval of 2σ equal to 95.44 [%] according to [Anderson et al., page 232]. Since the exact orbit height the satellite is released into after deployment is unknown, the requirements for ADCS on AAUSAT-II are made for worst case scenarios for orbit heights between 500 [km] and 700 [km].

1.5.1 Education of the Students and Staff Involved with the AAUSAT-II Project

The students shall follow the courses and theme for the semester. This includes modelling and controlling an autonomous system, as the satellite is.

1.5.2 Communication

In order to reduce the pointing loss³, the ADCS shall point the antenna on the satellite towards the ground station during an overflight. In order to do this, the satellite shall be detumbled to reduce the rotation of the satellite.

³Pointing loss is a loss of signal, caused if the direction of optimal gain of the satellite antenna does not point towards the ground station.

Detumbling

The initial maximum angular velocity is assumed to be 0.1 [rad/s] on all three axes. In order to consider the satellite as detumbled, the satellite shall follow the magnetic field around the Earth as this rotation is known. This minimizes the risk of constantly having a low antenna gain in the direction of the Earth. The worst case scenario will be if a "blind spot", meaning an antenna gain so low that no signal reaches the ground station, points towards the ground station during an entire overflight of the ground station. This problem has the same properties as the requirements for rotation, which are described under rotation.

As shown in Figure 1.3 the magnetic field causes the vector field to rotate two times during an orbit.

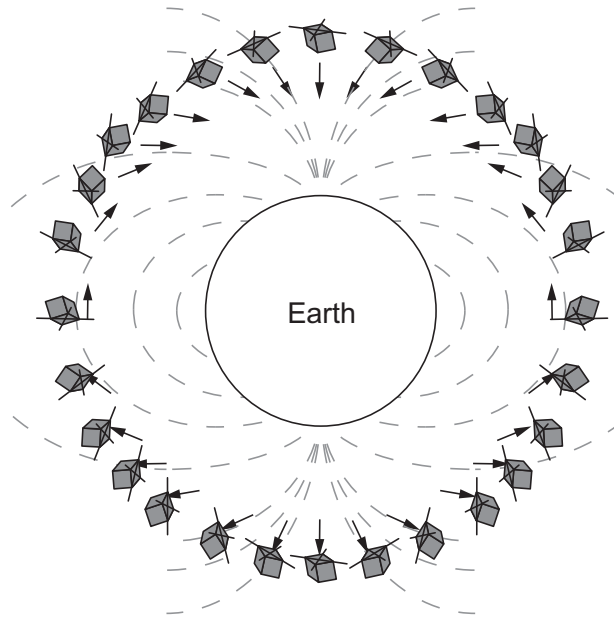


Figure 1.3: Rotation of a satellite in a circular orbit due to the magnetic field of the Earth.

According to [Wertz & Larson, Earth Satellite Parameters table col:52] the orbit time for a satellite in an orbit height of 700 [km] is $98.77 \text{ [min]} \sim 5926.2 \text{ [s]}$. This yields a maximum angular velocity of the satellite ω , given by

$$\omega_{\text{Detumble}} = 2 \cdot \frac{2\pi}{5926.2 \text{ [s]}} = 0.0021 \text{ [rad/s]} \approx 12 \text{ [°/s]}. \quad (1.1)$$

The satellite is considered detumbled when the angular velocity on each axis is 0.0021 [rad/s] or lower.

Rotation

To ensure higher efficiency during transmission at high data rates, the antenna on the satellite shall point directly towards the ground station. Therefore the satellite shall rotate $\pi \text{ [rad]}$ during an overflight which is worst case when an ideal overflight at an orbit height of 500 [km] occurs.

According to Figure 1.4 the maximum arch section, α , of the orbit visible from a groundstation can be calcu-

1.5. REQUIREMENTS FOR THE ATTITUDE DETERMINATION AND CONTROL SYSTEM

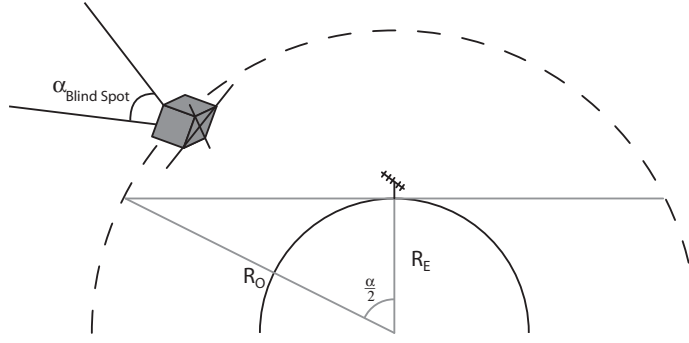


Figure 1.4: Satellite during overflight of a ground station.

lated as

$$\begin{aligned}\alpha &= 2 \cdot \arccos\left(\frac{R_E}{R_O}\right) \\ &= 2 \cdot \arccos\left(\frac{6378166 \text{ [m]}}{6378166 \text{ [m]} + 500000 \text{ [m]}}\right) \approx 0.7673 \text{ [rad]} \approx 44 \text{ [}^\circ\text{]}.\end{aligned}\quad (1.2)$$

This gives, using an orbit time of $T_O = 5677.2 \text{ [s]}$ at an orbit height of 500 [km] [Wertz & Larson, Earth Satellite Parameters table col: 52], a maximum time in view, T_v ,

$$\begin{aligned}T_v &= \frac{\alpha}{2\pi} \cdot T_O \\ &= \frac{0.7673 \text{ [rad]}}{2\pi \text{ [rad]}} \cdot 5677.2 \text{ [s]} = 693 \text{ [s]}.\end{aligned}\quad (1.3)$$

This yields a minimum angular velocity of the satellite of

$$\omega_{\min} = \frac{\pi}{693 \text{ [s]}} = 0.0045 \text{ [rad/s]} \approx 0.26 \text{ [}^\circ\text{/s]}.\quad (1.4)$$

The satellite shall be able to maintain an angular velocity of minimum 0.0045 [rad/s] during an overflight to ensure a stable communication link.

According to the problem having a "blind spot" pointing towards the ground station described in Subsection 1.5.2, will not be a problem, as the maximum angular velocity requirements for detumbling in (1.1), is lower than the angular velocity requirements for rotation in (1.4). This of course yields that the "blind spot" is smaller than

$$\begin{aligned}\alpha_{\text{Blind spot}} &< T_v \cdot \omega_{\text{Detumble}} \\ &< 693 \text{ [s]} \cdot 0.0021 \text{ [rad/s]} = 1.4553 \text{ [rad]} \approx 84 \text{ [}^\circ\text{]}.\end{aligned}\quad (1.5)$$

If the measurements for the antenna gain shows that the satellite has a "blind spots" larger than 1.4553 [rad] , the demands for ADCS for detumbling have to be reconsidered.

1.5.3 Payload

This mission objective does not provide any requirements for the ADCS.

1.5. REQUIREMENTS FOR THE ATTITUDE DETERMINATION AND CONTROL SYSTEM

1.5.4 The Attitude Determination and Control System

The purpose of having an ADCS on-board the satellite is to make it possible to control the attitude of the satellite. Besides detumbling the satellite, the ADCS is also brought as a payload to test the accuracy of an ADCS on a CubeSat using momentum wheels as actuators, i.e., the goal of this objective is to accumulate data to verify simulations of the ADCS on ground.

Depending on how accurate the ADCS on the satellite is, it will be possible to implement optical downlink. This requires the satellite to point within a certain area of the Earth surface, e.g., $10\text{ [m]} \times 10\text{ [m]}$, which will require an accuracy of

$$\arctan\left(\frac{10\text{ [m]}}{700000\text{ [m]}}\right) = 0.000014\text{ [rad]} \approx 0.00008\text{ [}^\circ\text{]}. \quad (1.6)$$

However this will most likely not be possible, as former studies shows that an accuracy below 0.087 [rad] is not possible with the sensors available [04GR830b, page 111].

1.5.5 Upload New Software

The design of the software for both ADS and ACS shall be designed such that it can be uploaded and implemented by using the communication system of the satellite. This is only possible through the modules implemented on the OBC and not on the hardware controllers. The purpose of this is to have the possibility to upload new determination and/or controller algorithms.

1.5.6 Deployment of Solar Arrays

A mission for the AAUSAT-II is to deploy arrays of solar cells. The purpose of deploying solar arrays is to produce more power on-board a CubeSat. However, this mission objective is of low priority, since the power budget is satisfactory with solar cells on the side panels only. This, however, requires the ADCS to point three side panels towards the Sun, when not running a specific flight plan or using the ADCS for other tasks. After the solar arrays have been deployed, the solar arrays shall point towards the Sun, requiring new software uploaded for ADCS as deployment of the solar arrays will change the dynamics of the satellite.

The power from the solar cells is proportional with the area projected to the plane normal to the sunlight, assuming rays of sunlight are parallel. Figure 1.5 shows an illustration of the sunlight projected to the plane orthogonal to the sunlight.

When a corner of the satellite points towards the Sun, the area of the projected plane is maximum as depicted in Figure 1.5. Figure 1.6 shows the area normal to the sunlight as a function of the angle from the direction where the satellite points a corner towards the Sun.

Based on the ADCS hardware Interface Control Document (ICD) [ADCS HW ICD] which states that attitude manoeuvres consumes 97 [mW] , the satellite shall point a corner towards the Sun within $0.3\text{ [rad]} \approx 17\text{ [}^\circ\text{]}$, see Figure 1.6. This shall be done when no other tasks are present for the ADCS.

1.5.7 Co-operation with the AMSAT Community

In order to make it possible for radio amateurs from the community of AMSAT to communicate with the satellite, commands must be defined in such a way that radio amateurs can control the ADCS by using the

1.5. REQUIREMENTS FOR THE ATTITUDE DETERMINATION AND CONTROL SYSTEM

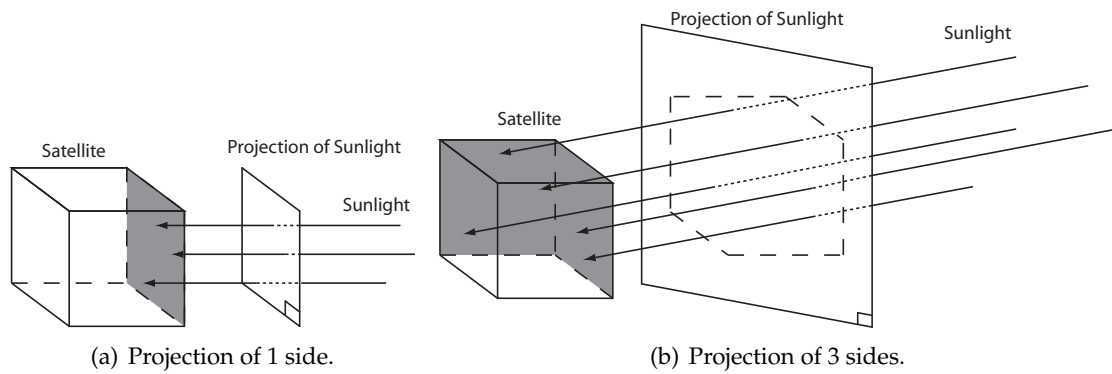


Figure 1.5: Illustration of the area of the satellite which is covered by the sunlight projected to the plane orthogonal to the sunlight.

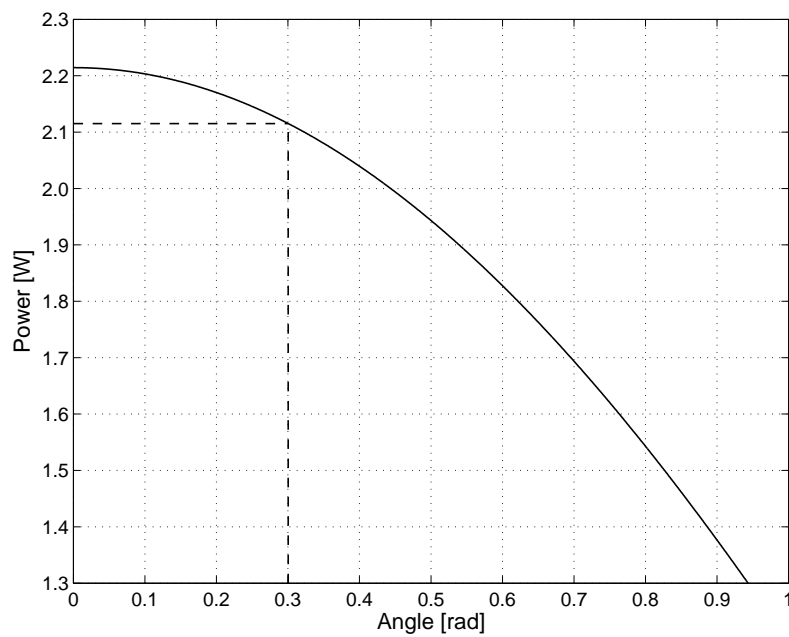


Figure 1.6: Area of the sunlight absorbed by the satellite, described by the angle between the diagonal of the Satellite Body Reference Frame and the sunlight, assuming rays of sunlight are parallel.

1.5. REQUIREMENTS FOR THE ATTITUDE DETERMINATION AND CONTROL SYSTEM

AX.25 protocol after the previous mission objectives have been fulfilled.

1.5.8 System Demands for ADCS

All the requirements shall be met with a confidence interval of 2σ equal to 95.44 [%].

1. The ADCS shall be able to detumble the satellite from 0.1 [rad/s] to 0.0021 [rad/s] or below around each axis within 3 orbits.
2. The ADCS shall be able to rotate the satellite at an angular velocity of at least 0.0045 [rad/s].
3. The ADCS shall be designed so it is possible to upload new determination and control algorithms.
4. The ADCS shall be able to maintain a given attitude for the satellite within 0.087 [rad] ≈ 5 [°].

Modelling

To be able to test the ADCS a simulation environment must be available. The models needed for this are described in the following chapter.

To define vectors in space a reference frame is required, and to ease calculations a number of different coordinate systems are defined. After defining the coordinate systems, the environment will be modelled. This includes an ephemeris model, modelling of the disturbances affecting the satellite in LEO, an Earth albedo model and an orbit propagator model, which is needed in the modelling of the disturbances and the modelling of the magnetic field model.

Furthermore, to determine how the environment is affecting the satellite, the dynamics and kinematics of the satellite are modelled.

In order to simulate the ACS the actuators on the satellite, which includes magnetorquers and momentum wheels, will be modelled.

The simulation environment is implemented in SIMULINK, and is presented in the end of this chapter.

2.1 Coordinate Systems

In this section the coordinate systems used for describing the attitude and the orbit of the satellite are introduced.

2.1.1 Orbital Elements

Before describing the coordinate systems used, the basic theory and the terms used in orbital mechanics are presented. As source for this section [Wertz, Chapter 2 and 3] are used.

Kepler's First Law: If two objects in space interact gravitationally, each will describe an orbit that is a conic section with the center of mass at one focus. If the bodies are permanently associated, their orbits will be ellipses; if they are not permanently associated, their orbits will be hyperbolas.

Kepler's Second Law: If two objects in space interact gravitationally (whether or not they move in closed elliptical orbits), a line joining them sweeps out equal areas in equal intervals of time.

Kepler's Third Law: If two objects in space revolve around each other due to their mutual gravitational attraction, the sum of their masses multiplied by the square of their period of mutual revolution is proportional to the cube of the mean distance between them. Hence

$$(m + M)P^2 = \frac{4\pi^2}{G}a^3, \quad (2.1)$$

where P is their mutual period of revolution, a is the mean distance between them, m and M are the two masses, and G is Newton's gravitational constant.

Of the two revolving objects the one with the greatest mass is called the primary, and the less massive object is called the secondary. If the mass of the satellite is denoted m , and the mass of the Earth is denoted M the mass of the satellite is considered negligible,

$$m + M \approx M. \quad (2.2)$$

Thus in the case of a satellite orbiting the Earth it follows from Kepler's laws, that the trajectory of the satellite is an ellipse with the center of the Earth at the one focus.

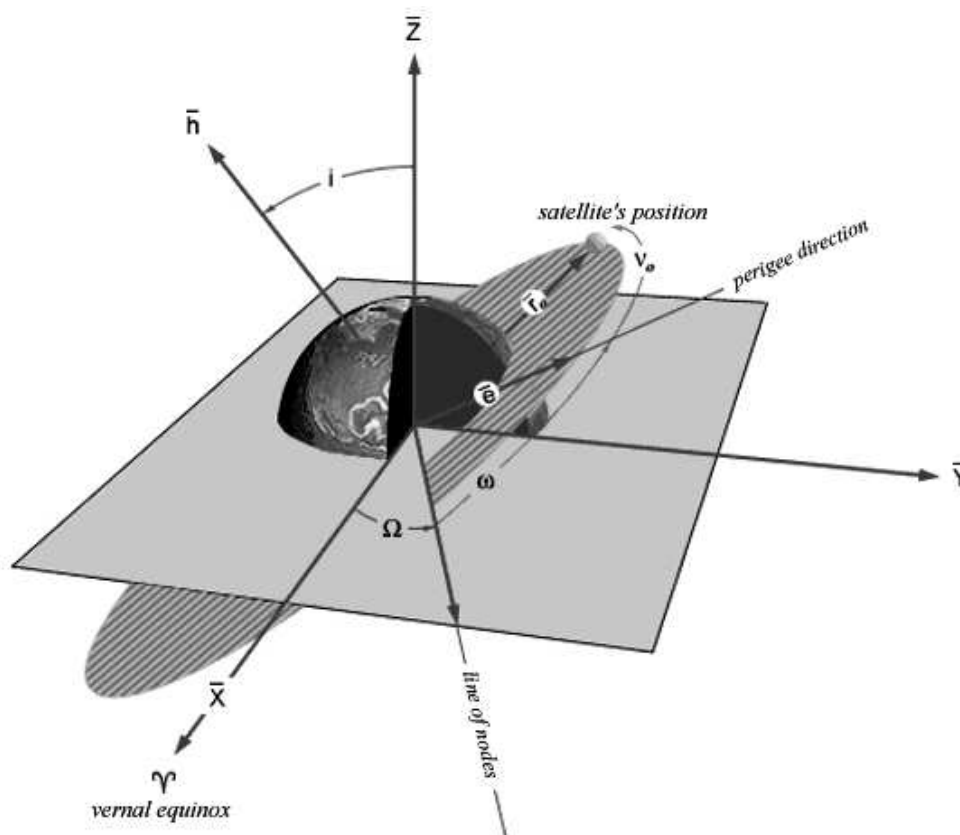


Figure 2.1: Satellite orbit.

An example of a satellite orbit is depicted in Figure 2.1 and an orthogonal view of the orbit is shown in Figure 2.2. In order to mathematically describe orbits the following terms are used.

Vernal equinox (γ) is the line connecting the center of the Earth and the center of the Sun where the ecliptic, which is the plane of the Earth's orbit around the Sun, crosses the equator, i.e., spring equinox. Due to the precession and nutation of the Earth the direction of vernal equinox must be associated with a specific year to give an unambiguous definition of the direction in space.

Line of nodes is the line through the two points of intersection between the satellite orbit and the reference plane, typically the equatorial plane of the Earth. The point in the orbit where the satellite crosses from south to north is called the ascending node.

2.1. COORDINATE SYSTEMS

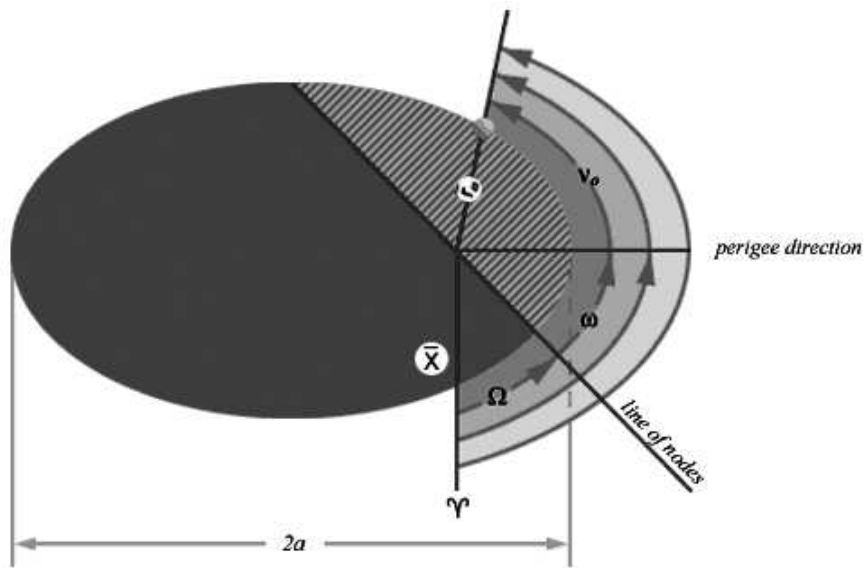


Figure 2.2: Orthogonal view of an orbit.

Longitude of ascending node (Ω) is the angle from vernal equinox to the ascending node. Note that this angle lies in the equatorial plane.

Perigee direction is the point in the orbit closest to the center of mass of the primary (the center of the Earth) this is often referred to as the barycenter.

Argument of perigee (ω) is the angle from the ascending node to the perigee direction.

Inclination (i) is the angle from the equatorial plane to the orbit plane.

The geometry of an ellipse is shown in Figure 2.3.

An ellipse is one of the four conic sections. Given two arbitrary points called foci an ellipse is described geometrically as the set of points for which the sum of the distances to the two foci is a given constant, $2a$. The quantity $2a$ is also called the major axis of the ellipse, i.e., the width of the ellipse measured on a line through the two foci.

The eccentricity, e , describes the shape of an ellipse and is defined as the ratio

$$e = \frac{c}{a} = \frac{\sqrt{a^2 - b^2}}{a}, \quad (2.3)$$

where c is half the distance between the two foci. For a circular orbit this ratio is, $e = 0$, meaning that the two foci coincides, and for an elliptic orbit $0 < e < 1$. The terms a , b and c are shown in Figure 2.3. For further information about ellipses see [Weisstein Ellipse].

2.1.2 Reference Frames

When dealing with ADCS for a satellite certain features as its orbit, the environment and attitude need to be described. To describe the orientation of an object in space, a reference frame must be defined. As the satellite can be observed from different points of view, a number of reference frames suitable for attitude determination and control purposes need to be defined. The reference frames used in this project is defined as a right-handed 3-dimensional cartesian coordinate system described by three mutually perpendicular unit

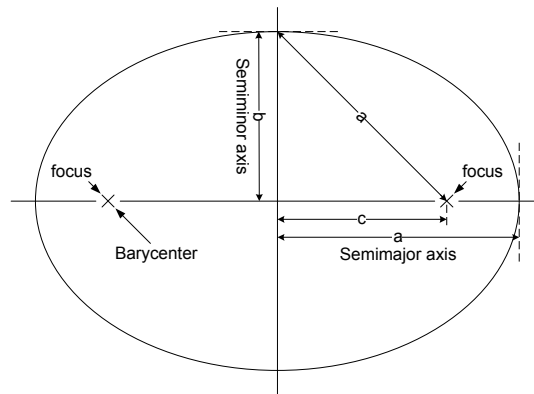


Figure 2.3: The geometry of an ellipse.

vectors. When the reference frames are defined, it is possible to model the satellite and the environment of the satellite. Below is the list of the reference frames used in the AAUSAT-II project.

- Earth Centered Inertial reference frame - ECI
- Earth Centered Earth Fixed reference frame - ECEF
- Orbit Reference Frame - ORF
- Satellite Body Reference Frame - SBRF
- Controller Reference Frame - CRF

Earth Centered Inertial Reference Frame

An inertial reference frame is needed to have a non-accelerating point of view in which Newton's laws of motion applies. As the AAUSAT-II will be launched into a Low Earth Orbit (LEO) the Earth will be the primary object, and therefore an Earth Centered Inertial reference frame (ECI) system could be used as the inertial reference frame.

Unfortunately the ECI reference frame is not an ideal inertial reference frame as it is accelerating, due to the fact that the Earth is orbiting the Sun. Thus a more precise inertial reference frame eliminating this acceleration would be a Sun centered inertial reference frame. However, the Sun orbits the center of the Milky Way galaxy and so forth. So unless the inertial reference frame is defined with its origo in the center of the Universe (hard to determine) it will never be ideal. However, choosing a non Earth centered reference frame complicates the required calculations, and because the acceleration caused by the Earth orbiting the Sun is considered negligible, the ECI reference frame is used in this project.

The ECI reference frame is illustrated in Figure 2.4. It is defined as a right handed cartesian coordinate system, having its origo in the center of the Earth. The x-axis is in the direction of vernal equinox Υ , the z-axis is perpendicular to the equatorial plane with the positive direction going through the geographic North Pole of the Earth, and the y-axis is the cross product between the z-axis and the x-axis.

Earth Centered Earth Fixed Reference Frame

Some calculations can be simplified by using a reference frame that rotates with the Earth. This means that points on the Earth surface such as ground stations are fixed in this frame. Also some environmental modeling depends on the spacecraft position relative to a specific point on the Earth surface. For this purpose the Earth Centered Earth Fixed (ECEF) reference frame is introduced.

2.1. COORDINATE SYSTEMS

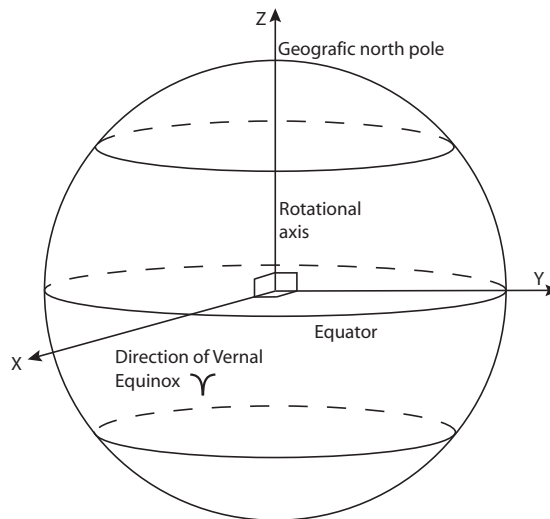


Figure 2.4: The Earth Centered Inertial reference frame.

The ECEF is illustrated in Figure 2.5. It is defined with origo in the center of the Earth. The z-axis is the Earth rotation axis and the positive direction is through the North Pole. The x-axis is in the direction of the intersection between the equatorial plane (0° latitude) and the Greenwich meridian (0° longitude). The y-axis is the cross product between the z- and x-axis, thus forming a right handed cartesian coordinate system.

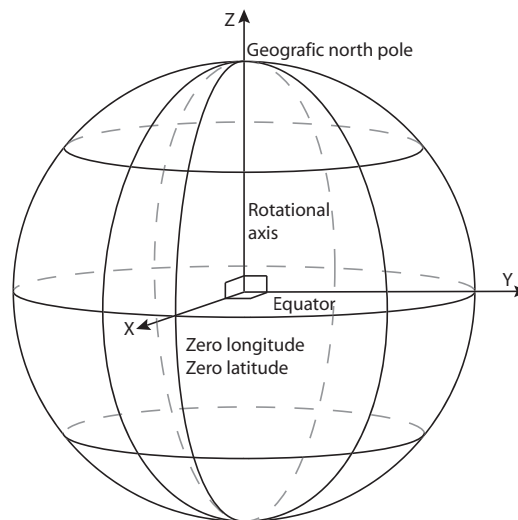


Figure 2.5: The Earth Centered Earth Fixed reference frame.

Orbit Reference Frame

The Orbit Reference Frame (ORF) is an accelerating, thus non-inertial reference frame, with origo in the center of mass of the satellite. For the AAUSAT-II satellite this point is in orbit around the Earth. The x-axis of the right perpendicular coordinate system is in the nadir direction (towards the center of the Earth). The z-axis is perpendicular to the orbit plane with the positive direction in the direction of the angular velocity vector of the orbit. The y-axis is the cross product between the z-axis and the x-axis. Notice that for a circular orbit the y-axis is parallel to the translatory velocity of the spacecraft orbit as depicted in Figure 2.6.

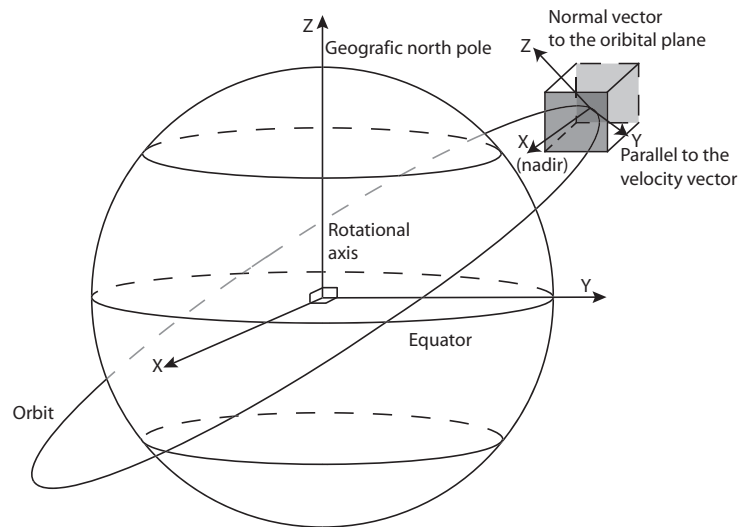


Figure 2.6: The Orbit Reference Frame for a circular orbit.

Satellite Body Reference Frame

The Satellite Body Reference Frame (SBRF) is fixed with respect to the body of the satellite. It is used to determine the orientation of the on-board instrumentation. If some of the on-board instruments are dependent on the orientation of the satellite e.g. a camera, it is convenient to define the SBRF with one of the axes parallel to the field of view of this instrument.

As the payload of the AAUSAT-II has no requirements to the pointing direction, the SBRF is defined such that it is convenient for use with the attitude determination and control system. The SBRF has its center in the corner of the satellite opposite of the vertical momentum wheel according to [MECH-WWW]. The axes forms a right-handed coordinate system with the axes perpendicular to the satellite sides. Thereby the on-board sensors and actuators direction is defined by the SBRF. The SBRF is depicted in Figure 2.7. In the figure only the momentum wheels are shown.

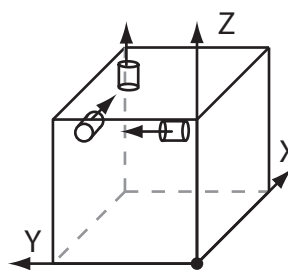


Figure 2.7: The AAUSAT-II Satellite Body Reference Frame.

Controller Reference Frame

Figure 2.8 shows the Controller Reference Frame (CRF) which is convenient for calculations involving the satellite dynamics as all products of inertia are eliminated.

The origo of the CRF is in the center of mass of the satellite and the axes are defined with respect to the

2.1. COORDINATE SYSTEMS

principal axes of the satellite. The x-axis is the major axis of inertia, the y-axis the minor axis of inertia and the z-axis is the cross product between the x-axis and the y-axis, thus forming a right handed cartesian coordinate system.

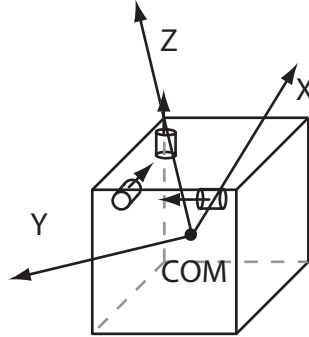


Figure 2.8: The AAUSAT-II Controller Reference Frame with respect to the principal axes, with origo placed in the center of mass (COM).

Because the satellite is non-spherical and have a non-uniform mass distribution, the center of mass will obviously not coincide precise with the geometric center of the satellite. The mass distribution of the satellite must be computed in order to determine the center of mass and the principal axes, which are required for defining the CRF. The mechanical team affiliated with the AAUSAT-II project, MECH [MECH-Mail] has calculated and measured the inertia matrix relative to the SBRF to be

$${}^S\mathbf{I} = \begin{bmatrix} I_{xx} & I_{xy} & I_{xz} \\ I_{yx} & I_{yy} & I_{yz} \\ I_{zx} & I_{zy} & I_{zz} \end{bmatrix} = \begin{bmatrix} 1377 & -40.427 & 3.199 \\ -40.427 & 1623 & -69.578 \\ 3.199 & -69.578 & 1569 \end{bmatrix} \cdot 10^{-6}, \quad (2.4)$$

where ${}^S\mathbf{I}$ is given in $[\text{kg} \cdot \text{m}^2]$, and the center of mass in the SBRF to be

$${}^S\mathbf{P} = \begin{bmatrix} P_{com,x} \\ P_{com,y} \\ P_{com,z} \end{bmatrix} = \begin{bmatrix} 56.11 \\ 49.829 \\ 50.788 \end{bmatrix} \cdot 10^{-3}, \quad (2.5)$$

where ${}^S\mathbf{P}$ is given in $[\text{m}]$. The principal axes can be found by calculating the eigenvalues of the inertia matrix. The major axis is the eigenvector corresponding to the largest eigenvalue. The intermediate axis is the eigenvector corresponding to the intermediate eigenvalue, and the minor axis is the eigenvector corresponding to the smallest eigenvalue [Wie, page 331-339]. The eigenvalues of ${}^S\mathbf{I}$ on matrix form corresponding to ${}^C\mathbf{I}$ are

$${}^S\mathbf{I}_\lambda = {}^C\mathbf{I} = \begin{bmatrix} 1.3702 & 0 & 0 \\ 0 & 1.5240 & 0 \\ 0 & 0 & 1.6748 \end{bmatrix} \cdot 10^{-3}. \quad (2.6)$$

The matrix comprised of the eigenvectors can be used for rotating the SBRF into the CRF.

2.1.3 Coordinate System Transformations

Rotations of coordinate systems can be described by quaternions. Quaternions provide a singularity-free representation of kinematics and provide a convenient product rule for successive rotations. In Appendix A quaternions are defined and the fundamental algebraic properties of quaternions are described.

2.2 Ephemeris

In the following section a model of the rotation of the Earth, i.e. a rotation of ECI to ECEF, will be derived.

As input to the gravitational disturbance model, the position of the Earth, the Sun, and the Moon is needed. The description of the orbit of the Sun around the Earth is further used to determine the vector from the satellite to the Sun.

2.2.1 Earth Rotation

In the following the rotation of the Earth will be modelled as the ECI frame rotation with respect to the ECEF frame about the common z-axis. The rotation is measured with respect to the fixed stars and is called a Sidereal day, which in the year 2003 was 23 [h] 56 [min] 04.09053 [s] [Hmnao, page B6]. This yields an angular velocity of $\omega = 7.29211 \cdot 10^{-5}$ [rad/s].

The rotation will be described as the angle ψ between the frame axes ${}^I\hat{e}_x$ and ${}^E\hat{e}_x$, i.e. the angle between the Vernal equinox and Greenwich. To be able to determine ψ , the time of alignment of the two frames must be known, i.e. the time when $\psi = 0$. According to [Princeton] this took place on December 31st 1996, 17 [h] 18 [min] 21.8256 [s]. In Julian Date this is $J = 2450449.221076389$ [JD]. It is now possible to express ψ as

$$\begin{aligned} T_r &= \frac{2\pi}{\omega} \\ N_r &= ((t - J) \cdot 86400) \bmod (T_r) \\ \psi &= \omega(t - N_r \cdot T_r), \end{aligned} \quad (2.7)$$

where T_r is the time of one revolution, N_r is the number of revolutions since alignment, i.e., since J , and t is the current time in JD. The factor 86400 is the conversion from JD to seconds.

Since the rotation is only about the z-axis the quaternion notation is equal to

$${}^I_{E}q = \begin{bmatrix} 0 \\ 0 \\ \sin\left(\frac{\psi}{2}\right) \\ \cos\left(\frac{\psi}{2}\right) \end{bmatrix}. \quad (2.8)$$

The direction of the spin axis, i.e. the z-axis of the ECI frame, with respect to the fixed stars is not constant. In fact the spin axis of the Earth is performing a circular motion sweeping out a cone with a wavy edge. The cone motion, called precession, is primarily caused by the gravitational force of the Sun and has a period of 25800 years and an amplitude of 23.5° . Another contribution, nutation, making the wavy edge, is caused

2.2. EPHEMERIS

by the Moon. The period is 18,6[years] and has an amplitude of $0^{\circ}0'9''21$ [Sidi, page 22]. Nutation and precession are not covered further since the effects of these are considered negligible.

2.2.2 Sun Position

The position of the Sun is described using keplerian orbit elements, as introduced in Section 2.1.1 and further in this section. The model places the Earth in the center with the Sun orbiting. Actually the Earth is orbiting the Sun, but it makes no difference to the result. This section is based on [Wertz, page 140-145].

Since the eccentricity of the orbit of the Sun is small [Wertz, equation (5-46)] the following approach can be used. A starting point in time is needed where the exact position and velocity of the Sun is known. The mean anomaly M_{SE} , of the Sun and the mean motion n_s , of the Sun both on the 1st of January, 2000 at noon UTC, can be found in Table 2.1.

Parameter	Value	Unit
e	0.016751	[.]
M_{SE}	357.528	[°]
n_s	0.9856003	[°/day]
c	23.4387	[°]

Table 2.1: Sun orbit elements obtained from [Princeton].

The mean anomaly M_s for a given time T_s , can be calculated as:

$$M_s = M_{SE} + n_s \cdot T_s, \quad (2.9)$$

where T_s is the time measured in days since the 1st of January, 2000 at noon UTC. [Braeunig, Equation (1.29)]

The mean longitude of the Sun in the ecliptic plane can be described by L_{OS} [Wertz, Equation (5-46) & (5-47)]

$$L_{OS} = 279.696678^{\circ} + 0.9856473354 \cdot M_s + 1.918 \sin(M_s) + 0.02 \sin(2M_s). \quad (2.10)$$

Including the inclination of the ecliptic plane denoted c , leads to the following unit vector description of the Sun orbiting the Earth in the ECI reference coordinate system

$${}^I\hat{R}_S = \begin{bmatrix} \cos(L_{OS}) \\ \cos(c) \sin(L_{OS}) \\ \sin(c) \sin(L_{OS}) \end{bmatrix} \quad (2.11)$$

The distance between the Sun and the Earth is described by [Wertz, Equation (5-48)]

$$D_s = \frac{1.495 \cdot 10^8 (1 - e^2)}{1 + e \cos(M_s)}. \quad (2.12)$$

2.2.3 Sunlight Eclipse

Since the satellite is orbiting the Earth the line of sight from the satellite to the Sun will eventually be blocked by the Earth, i.e. the satellite is in eclipse, and as a consequence the sun sensor input will not be usable. Not only the Earth but also the Moon will cause the satellite to be in eclipse. However, eclipses caused by the moon are relatively rare and have a short duration and are therefore not considered in the model.

Eclipse caused by the Earth happens when the distance from the center of the Earth perpendicular to the line of sight from the satellite to the Sun, ${}^I R_E$, is smaller than the radius of the Earth, r_{Earth} . The problem is depicted in Figure 2.9. The incident light on the satellite due to light from the Sun being deflected in the atmosphere of the Earth in the short period after entering eclipse will be ignored.

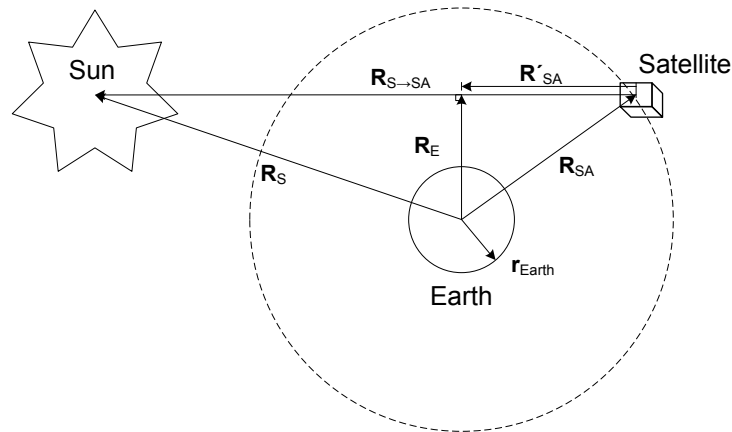


Figure 2.9: Sunlight eclipse model. All the vectors are given in ECI.

The vector ${}^I R_E$ can be expressed as

$${}^I R_E = {}^I R_{SA} + {}^I R'_{SA}. \quad (2.13)$$

Furthermore ${}^I R'_{SA}$ can be described as

$${}^I R'_{SA} = \frac{-{}^I R_{SA} \cdot {}^I R_{SA \rightarrow S}}{\|{}^I R_{SA \rightarrow S}\|^2} {}^I R_{SA \rightarrow S} \quad (2.14)$$

where ${}^I R_{SA \rightarrow S} = {}^I R_S - {}^I R_{SA}$ is the vector from the satellite to the Sun.

Inserting (2.14) into (2.13) result in a term for $\|{}^I R_E\|$, which for $\|{}^I R_E\| < r_{Earth}$ entails that the satellite is in eclipse, yields

$$\|{}^I R_E\| = \left\| {}^I R_{SA} - \frac{{}^I R_{SA} \cdot {}^I R_{SA \rightarrow S}}{\|{}^I R_{SA \rightarrow S}\|^2} {}^I R_{SA \rightarrow S} \right\|. \quad (2.15)$$

2.2.4 Moon Position

The orbit of the Moon is rather complex and will not be described, since ephemeris modelling is not the main topic in this project.

2.3. DISTURBANCE MODELLING

In the SIMULINK implementation position of the Moon will be handled by a toolbox from Princeton Satellite System. A few corrections has been made by the previous groups (see [04GR830b] and [04GR830a]) to allow continuous position updates.

2.3 Disturbance Modelling

This section describes the main disturbances affecting the attitude of the satellite. Four disturbances are considered for the model, these are

- Aerodynamic drag
- Gravity gradient
- Magnetic residual
- Solar radiation

This implies that the total disturbance torque on the satellite can be calculated in the SBRF as

$${}^S N_{\text{ext}} = {}^S N_{\text{drag}} + {}^S N_{\text{GG}} + {}^S N_{\text{mag}} + {}^S N_{\text{R}}. \quad (2.16)$$

Where ${}^S N_{\text{drag}}$ is the torque caused by the aerodynamic drag, ${}^S N_{\text{GG}}$ is the torque caused by the gravity gradient, ${}^S N_{\text{mag}}$ is the torque caused by the interaction between the Earth's magnetic field and the satellites magnetic residual dipole and ${}^S N_{\text{R}}$ is the torque caused by the solar radiation.

2.3.1 Aerodynamic Drag Disturbance

For a satellite in LEO the main disturbance torque is exerted by aerodynamic drag [Wertz, page 573]. The drag arises from the friction between the satellite and the atmosphere and is in the opposite direction of the satellites velocity vector. The force df_{drag} acting on an infinitesimal surface element dA with the normal vector \hat{N} , is given by

$$df_{\text{drag}} = -\frac{1}{2}\rho C_D \|V\|^2 (\hat{N} \cdot \hat{V}) \hat{V} dA, \quad (2.17)$$

where \hat{V} is a unit vector in the direction of the satellites translational velocity, ρ is the atmospheric density and C_D is the drag coefficient. Since there is no measured value available for C_D , it can be set to 2, according to [Wertz, page 573-574]. By integrating (2.17) over the exposed area, the total aerodynamic drag can be calculated. For objects with a simple and symmetric structure this can be simplified to

$$f_{\text{drag}} = -\frac{1}{2}\rho C_D A \|V\|^2 \hat{V}, \quad (2.18)$$

where A is the total exposed area of the satellite, measured in a plane perpendicular to the motion [Serway & Beichner, page 165-166]. This means that the aerodynamic torque ${}^S N_{\text{drag}}$ acting on the satellite due to f_{drag} can be written as

$${}^S N_{\text{drag}} = {}^S C_P \times f_{\text{drag}}, \quad (2.19)$$

where ${}^S C_P$ is a vector from the center of mass to the center of pressure on the satellite. The center of pressure is the geometrical center of the exposed cross sectional area¹.

2.3.2 Gravitational Disturbances

The gravitational disturbance model must contain the following forces

- Gravitational forces from the Sun and the Moon
- The Earth's zonal harmonics
- The gravity gradient

The gravitational forces from the Sun and the Moon, will influence the orbit of the satellite and should therefore be included in the disturbance model.

The Earth's zonal harmonics arise from the fact that the Earth is not a perfect sphere, i.e., the radius is larger at the equator than at the poles, which entail that the Earth's gravity field varies. This will affect the orbit of the satellite and should therefore be included in the disturbance model.

As the satellite is non-spherical and has a non-uniform mass distribution, it will experience a gravitational torque around the center of mass, due to Earth's gravitational force.

Sun and Moon Gravity Disturbance

For calculating the gravitational disturbance from the Sun and the Moon, Newton's law of universal gravitation [Serway & Beichner, page 424-425] is used. A vector from the satellite to the Sun is calculated as ${}^I R_{SA \rightarrow S} = {}^I R_S - {}^I R_{SA}$, as seen in Figure 2.9. The vector ${}^I R_S$ is from the center of the Earth to the Sun in the ECI and ${}^I R_{SA}$ is a vector from the center of the Earth to the satellite in the ECI. ${}^I R_{SA \rightarrow S}$ is used to calculate the force the Sun exerts on the satellite

$${}^I F_{GS} = G \frac{m_S m_{SA}}{\|{}^I R_{SA \rightarrow S}\|^2} \cdot \frac{{}^I R_{SA \rightarrow S}}{\|{}^I R_{SA \rightarrow S}\|} = G \frac{m_S m_{SA}}{\|{}^I R_{SA \rightarrow S}\|^3} {}^I R_{SA \rightarrow S}, \quad (2.20)$$

where G is the gravitational constant, m_S is the mass of the Sun and m_{SA} is the mass of the satellite. The equation for the force between the satellite and the Moon are of the same structure.

$${}^I F_{GM} = G \frac{m_M m_{SA}}{\|{}^I R_{SA \rightarrow M}\|^3} {}^I R_{SA \rightarrow M}, \quad (2.21)$$

where m_M is the mass of the Moon and ${}^I R_{SA \rightarrow M}$ is a vector from the satellite to the Moon.

Earth Zonal Harmonics

Because the Earth have a non-uniform mass distribution the gravitational field vary, depending on the position of the satellite. This is known as the Earth's zonal harmonics. This section is based on [Serway &

¹In the same way that the weight of all the satellite components act through a single point, the center of mass, the aerodynamic forces act through a single point called the center of pressure.

2.3. DISTURBANCE MODELLING

Beichner, page 435-437] and [Wertz, page 123-126]. If a particle is placed in the Earth's gravitational field, it will experience a force

$$F = -G \frac{M_E m}{\|r\|^2} \cdot \hat{r}, \quad (2.22)$$

where M_E is the mass of the Earth, G is the gravitational constant, r is a vector from the center of the Earth to the particle. The minus indicates that the field points toward the center of the Earth. Now the Earth gravitational potential, U can be defined as

$$U = -\frac{GM_E}{\|r\|}. \quad (2.23)$$

From (2.23), (2.22) can be expressed as the gradient of a scalar potential

$$F = -\frac{GM_E m}{\|r\|^2} \hat{r} = -m \nabla U, \quad (2.24)$$

where U can be expressed as

$$U \cong \frac{GM_E}{\|r\|} [U_0 + U_{J_2} + U_{J_3} + U_{J_4}], \quad (2.25)$$

where

$$U_0 = -1, \quad (2.26)$$

$$U_{J_2} = \left(\frac{r_{Earth}}{\|R_{SA}\|} \right)^2 J_2 \frac{1}{2} (3 \cos^2 \theta - 1), \quad (2.27)$$

$$U_{J_3} = \left(\frac{r_{Earth}}{\|R_{SA}\|} \right)^3 J_3 \frac{5}{2} \left(\cos^3 \theta - \frac{3}{5} \cos \theta \right), \quad (2.28)$$

$$U_{J_4} = \left(\frac{r_{Earth}}{\|R_{SA}\|} \right)^4 J_4 \frac{35}{8} \left(\cos^4 \theta - \frac{6}{7} \cos^2 \theta + \frac{3}{35} \right). \quad (2.29)$$

The radius of the Earth is denoted r_{Earth} and J_2 , J_3 and J_4 are the zonal harmonic coefficients. Now the gradient of U can be found as

$$\nabla U = \begin{bmatrix} \frac{\partial U}{\partial \|R_{SA}\|} \\ \frac{1}{\|R_{SA}\|} \frac{\partial U}{\partial \phi} \\ \frac{1}{\|R_{SA}\| \sin \phi} \frac{\partial U}{\partial \theta} \end{bmatrix}, \quad (2.30)$$

which yields

$$\nabla U = \begin{bmatrix} -GM_E \left(-\frac{1}{\|R_{SA}\|^2} + \frac{3}{2} \frac{r_E J_2 (3 \cos^2 \theta - 1)}{\|R_{SA}\|^4} + 10 \frac{r_E^3 J_3 (\cos^3 \theta - \frac{3}{5} \cos \theta)}{\|R_{SA}\|^5} + \frac{175}{8} \frac{r_E^4 J_4 (\cos^4 \theta - \frac{6}{7} \cos^2 \theta + \frac{3}{35})}{\|R_{SA}\|^6} \right) \\ 0 \\ \frac{GM_E}{\|R_{SA}\|^2 \sin \phi} \left(-3 \frac{r_E^2 J_2 \cos \theta \sin \theta}{\|R_{SA}\|^2} + \frac{5}{2} \frac{r_E^3 J_3 (-3 \cos^2 \theta \sin \theta + \frac{3}{5} \sin \theta)}{\|R_{SA}\|^3} + \frac{35}{8} \frac{r_E^4 J_4 (-4 \cos^3 \theta \sin \theta + \frac{12}{7} \cos \theta \sin \theta)}{\|R_{SA}\|^4} \right) \end{bmatrix}, \quad (2.31)$$

where $c \equiv \cos$ and $s \equiv \sin$ and r_E is the radius of the Earth. Now, the force exerted by the zonal harmonics can be found according to (2.24).

Gravity Gradient

The gravity between a satellite of mass, m_{SA} , and the Earth with mass, M_E , at a distance, $\|R_{SA}\|$, from the Earth's center, has a magnitude of

$$\|F\| = G \frac{M_E m_{SA}}{\|R_{SA}\|^2}, \quad (2.32)$$

where G is the gravitational constant. If m_1 and m_2 , in Figure 2.10, are two equal mass elements of the satellite, they will not experience the same gravity. This is due to the fact, that the gravity depends on the inverse square of the distance between the mass elements and the Earth's center. In the scenario depicted in Figure 2.10 F_1 will be greater than F_2 and the satellite will experience a counter-clockwise torque around the center of mass.

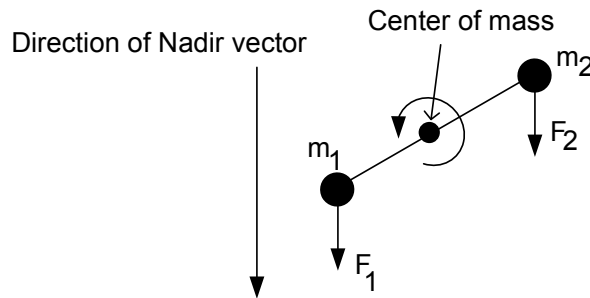


Figure 2.10: Illustration of the gravity gradient torque.

The equation for the torque can be expressed as [Wertz, page 567]

$${}^S N_{GG} = \frac{3\mu}{\|{}^S R_{SA}\|^3} \left[{}^S \hat{R}_{SA} \times ({}^S \underline{I} \cdot {}^S \hat{R}_{SA}) \right], \quad (2.33)$$

where μ is the gravitational constant multiplied with the mass of the Earth, ${}^S R_{SA}$ is a vector from the center of the Earth to the satellite and ${}^S \underline{I}$ is the moment of inertia tensor².

2.3.3 Magnetic Residual Disturbance

The magnetic field of the Earth interacts with the residual magnetic dipole of the satellite, which causes a torque around the center of mass of the satellite. The residual magnetic dipole of the satellite is caused by the current running through the wires and PCBs on the satellite. The magnetic disturbance can, according to [Wertz, page 575], be expressed as

$${}^S N_{mag} = S_m \times S_B, \quad (2.34)$$

² \underline{I} is called a tensor because it has specific transformation properties under a real orthogonal transformation.

2.3. DISTURBANCE MODELLING

where ${}^S m$ is the residual magnetic dipole of the satellite and ${}^S B$ is the magnetic field of the Earth. The residual magnetic dipole of the satellite should be modelled, since it cannot be assumed to be constant, because it depends on the amount of current running through the wiring on the satellite. However, at the time of this writing the PCBs of the satellite are subjected to changes, whereby the residual magnetic dipole of the satellite will not be modelled.

2.3.4 Radiation Disturbance

Radiation hitting the surface of the satellite will cause a torque around the center of mass. There are several radiation sources for this torque, but the major ones are direct solar radiation, solar radiation reflected by the Earth and its atmosphere, i.e. the Earth's albedo and radiation emitted from the Earth. The radiation emitted from the Earth will not be considered since it is small compared to the others [Wertz, page 571]. The magnitude of the solar radiation force, F_R , is given by

$$\|F_R\| = KAP, \quad (2.35)$$

where P is the momentum flux from the Sun, given by $P = 4.4 \cdot 10^{-6}$ [kg/ms²], K is a dimensionless constant in the range $0 \leq K \leq 2$, depending on the amount of the sunlight the satellite surface reflects and A is the cross-sectional area perpendicular to the vector from the satellite to the Sun exposed to the Sun [Wertz, page 64-65].

The force will act in the opposite direction of the vector from the satellite to the Sun, ${}^I R_{SA \rightarrow S} = {}^I R_S - {}^I R_{SA}$ shown in Figure 2.9. Therefore a negative unit vector in the direction of ${}^I R_{SA \rightarrow S}$ is multiplied with the force.

$${}^I F_R = -KAP {}^I \hat{R}_{SA \rightarrow S}. \quad (2.36)$$

A rotation of ${}^I F_R$ to SBRF can be made, and the disturbance torque in SBRF can be expressed as

$${}^S N_R = {}^S F_R \times {}^S R_{com}, \quad (2.37)$$

where ${}^S R_{com}$ is a vector from the center of mass of the satellite, to the geometrical center. This equation considers only the radiation coming directly from the Sun and not from the albedo of the Earth.

2.3.5 Total Disturbance Torque

The disturbances have been analyzed and modelled and an equation expressing the total disturbance torque can now be derived as

$${}^S N_{ext} = {}^S N_{drag} + {}^S N_{GG} + {}^S N_R \Leftrightarrow \quad (2.38)$$

$${}^S N_{ext} = {}^S C_P \times {}^S f_{drag} + \frac{3\mu}{\|{}^S R_{SA}\|^3} \left({}^S \hat{R}_{SA} \times ({}^S \mathbf{I} \cdot {}^S \hat{R}_{SA}) \right) + {}^S F_R \times {}^S R_{com}. \quad (2.39)$$

The torque generated by magnetic residuals has been omitted since no model of the residual magnetic dipole of the satellite is available.

2.4 Earth Albedo

The reflectivity of the surface of the Earth causes a percentage of the incident sunlight to be reflected back into space where the satellite is orbiting. This phenomenon is called the Earth albedo effect. The Earth's reflectivity is on average 30 [%] [Wertz & Larson, page 428], but varies depending on the position on the surface of the Earth. E.g., at the poles the reflectivity can be as high as 95 [%] and at the equator as low as 10 [%].

NASA is in co-operation with Goddard Space Flight Center mapping the reflectivity in the Total Ozone Mapping Spectrometer (TOMS) experiment [NASA/GSFC], and measurements from the TOMS experiment are shown in Figure 2.11.

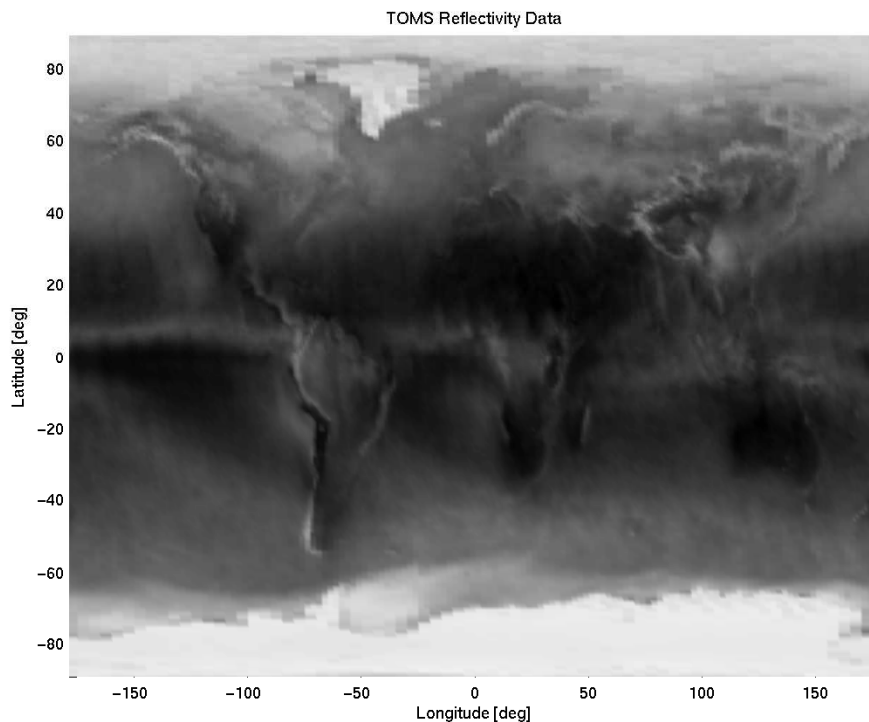


Figure 2.11: Reflectivity of the Earth. Bright is high reflectivity and dark is low reflectivity (generated using SIMULINK albedo toolbox).

Using data from the TOMS experiment [Bhanderi] has developed an albedo toolbox including the albedo SIMULINK library model shown in Figure 2.12. This library block will be used in the simulations as a black box model with sun and satellite vectors in the ECEF as input and a matrix describing the albedo in $[\text{W}/\text{m}^2]$ within the entire field of view of the satellite is provided as the output. In the albedo toolbox there is also a MATLAB function taking the zenith vector, a normal vector to a sun sensor plane and the albedo matrix from the albedo library block as input and providing the total albedo contribution to the sun sensor in the given plane as output. However, this function has been modified to accommodate two normal vector input as this is enough to describe all normal vectors to the sun sensor planes for the cubic AAUSAT-II. The modified function then returns the albedo received on each sun sensor as a vector.

2.5. ORBIT PROPAGATOR

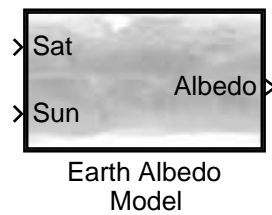


Figure 2.12: SIMULINK library block providing a black box model of the Earth albedo.

2.5 Orbit Propagator

As previously described, some of the models are dependent on the velocity and position of the satellite. To describe the orbit of the satellite a model could be used. Alternatively a specific orbit using position measurement data of a existing satellite could be used. However, the satellite used for position measurement must have physical properties similar to the AAUSAT-II, and an orbit comparable to the expected orbit of AAUSAT-II.

Two examples of orbital models are the Kepler orbit model and the Simplified General Perturbations 4 (SGP4) orbit model. The SGP4 model is based on Keplerian orbit calculation, but also addresses some perturbations such as the oblateness of the Earth and the atmospheric drag asserted on the satellite. The precision of the two orbit models are examined in Appendix F on page 108 by comparing the position output of the models to position data obtained from the Ørsted satellite.

The conclusion is that the SGP4 orbit model over time has a smaller error compared to the Kepler model and based on this, the SGP4 model will be used.

2.5.1 SGP4 Orbit Model

The SGP4 model is one of five mathematical models commonly used for prediction of satellite position and velocity. Three are used for near-earth satellites, namely the SGP, the SGP4 and the SGP8 orbit models and two can be used for deep space orbits namely the Simplified Deep-space Perturbations 4 (SDP4) and the Simplified Deep-space Perturbations 8 (SDP8) models. A near-earth orbit is defined as an orbit with a period less than 225 minutes and a deep-space orbit is defined as an orbit with a period greater than or equal to 225 minutes. This implies that only the first three of the five mathematical models are relevant for the orbit of AAUSAT-II. The SGP4 model is chosen since an implementation is currently available.

The SGP4 model is complex and will therefore not be described here. For a complete description of the model including an implementation example, see [Hoots & Roehrich]. As a consequence of the complexity the SGP4 orbit model will be considered as a black box as depicted in Figure 2.13. The position and velocity is calculated at a given time (Julian Date) based on the data from a Two Line Element (TLE) which is described in Appendix C on page 91. The implementation of the orbit propagator is described in Appendix E on page 98.



Figure 2.13: The SGP4 orbit model is considered a black box.

2.6 Magnetic Field Model

To be able to emulate the output of the magnetometer of the satellite a model describing the magnetic field of the Earth is needed. In the following, a short introduction to the magnetic field of the Earth is given and the chosen model is described.

The magnetic field observable on the surface of the Earth can be categorized in internal sources and external sources. The primary internal contribution to the magnetic field is generated in the fluid outer core by a self-exciting dynamo process. Electrical currents flowing in the slowly moving molten iron generate the magnetic field. The other internal source is the magnetic field generated by magnetic materials in the crust of the Earth. The external sources are due to magnetic fields induced by currents in the Ionosphere and Magnetosphere. The external sources can be omitted since the magnitude of the magnetic field due to external sources are low compared to the magnetic field of the Earth and furthermore the orbit of the AAUSAT-II is expected to be in a higher altitude than the upper bounds of the Ionosphere [BGS].

2.6.1 International Geomagnetic Reference Field model

The International Geomagnetic Reference Field (IGRF) model is used to describe the magnetic field of the Earth. It is an empirical representation of the main field without any external sources. The IGRF model uses a set of coefficients which has been modelled using data from geomagnetic measurements from observatories, ships, aircrafts and satellites, e.g., the Danish Ørsted satellite. Omitting external sources, the main magnetic field B , is the negative gradient of a scalar potential V , $B(r, \theta, \phi, t) = -\nabla V(r, \theta, \phi, t)$, which according to [IAGA V-MOD] can be represented by a truncated series expansion as

$$V(r_{Earth}, \theta, \phi, t) = R \sum_{n=1}^n \left(\frac{R}{r_{Earth}} \right)^{n+1} \sum_{m=0}^n (g_n^m(t) \cos(m\phi) + h_n^m(t) \sin(m\phi)) P_n^m(\theta) \quad (2.40)$$

where,

r_{Earth} Distance from the center of the Earth

θ Colatitude, i.e. 90 [°]- latitude

ϕ Longitude

R Reference radius (6371.2 [km])

$g_n^m(t), h_n^m(t)$ coefficients at time t

$P_n^m(\theta)$ Schmidt semi-normalized associated Legendre functions of degree n and order m .

The main-field coefficients change with time as the core-generated field changes. This variation is assumed to be constant over intervals of five years.

2.7 Satellite Dynamics and Kinematics

This section contains the derivation of the dynamic and kinematic equations of the satellite. The dynamic differential equation of the satellite describes how torques acting on the satellite influence the rotational acceleration of the satellite. The kinematic differential equation of the satellite describes the time dependent relationship between different reference frames. The following section is based on [Wertz, page 516-523]. For the section concerning kinematics [Wie, page 307-328] is used. Whenever an equation is copied from a source a citation will be given. Appendix A provides a description of the fundamental algebraic properties of quaternions which are extensively used for these equations.

2.7.1 Dynamic Equation of the Satellite

This subsection contains the dynamic differential equation of the satellite, which is based on Newton's laws of motion and Euler's laws of angular momentum.

When modelling a system it is basically a good idea to choose a simple model structure that gives an adequate description of the system. In order to derive the dynamic equation for the satellite a rigid body model structure is chosen.

Euler's second equation given in inertial coordinates can be expressed as

$$\frac{d^1L}{dt} = {}^1N_{ext}, \quad (2.41)$$

where L is the angular momentum and N_{ext} are the external torques acting on the satellite. These external torques are disturbance torques which include aerodynamic drag, solar radiation, gravity gradient and magnetic residual cf. Section 2.3. The internal torques are cancelled due to Newton's third law.

The angular momentum of the satellite is defined as

$$L_{SA} = \underline{I}\omega, \quad (2.42)$$

where \underline{I} is the moment of inertia tensor.

In order to express 1L in the CRF the following equation is used

$${}^C L = {}^C \underline{C} {}^1 L, \quad (2.43)$$

where ${}^C \underline{C}$ is an attitude matrix from ECI to CRF. Taking the derivative yields

$$\begin{aligned} {}^C \dot{L} &= {}^C \dot{\underline{C}} {}^1 L + {}^C \underline{C} \dot{{}^1 L} \\ {}^C \dot{L} &= {}^C \dot{\underline{C}} {}^1 L + {}^C \dot{L}. \end{aligned} \quad (2.44)$$

Comparing (2.44) with the translation theorem given in (2.45)

$$\frac{d^C L}{dt} = \frac{d^1 L}{dt} - \omega \times {}^1 L, \quad (2.45)$$

yields the following expression for the change in angular momentum given in the CRF

$${}^C\dot{L} = {}^C N_{\text{ext}} - \boldsymbol{\omega} \times {}^C L, \quad (2.46)$$

Besides the disturbance torques the satellite is also influenced by control torques from the magnetorquers and momentum wheels. The control torques from the momentum wheels will be modelled in the dynamic differential equation of the satellite. Control torques from the magnetorquers will be modelled separately, however the contribution from the magnetorquers will be included in the dynamic differential equation.

Due to the fact that the satellite contains momentum wheels, it cannot be considered a rigid body. However, it is still possible to derive the dynamic equation of the satellite using the equations for a rigid body model. With the angular momentum from the momentum wheels included the total angular momentum of the satellite becomes

$$L = L_{SA} + L_{mw}, \quad (2.47)$$

where L_{mw} is the angular momentum of the momentum wheels. Inserting (3.39) in (2.47) yields

$$\begin{aligned} L &= \mathbf{I}\boldsymbol{\omega} + L_{mw} \\ \mathbf{I}\boldsymbol{\omega} &= L - L_{mw} \\ \boldsymbol{\omega} &= \mathbf{I}^{-1}(L - L_{mw}). \end{aligned} \quad (2.48)$$

Substituting (2.48) into (2.46) yields the following equation for the total angular momentum of the satellite

$${}^C\dot{L} = {}^C N_{\text{ext}} - (\mathbf{I}^{-1}({}^C L - {}^C L_{mw})) \times {}^C L. \quad (2.49)$$

It is important that the dynamic equation of the satellite is calculated in the CRF, otherwise the moment of inertia will be a time varying tensor. By choosing the CRF as consisting of the principle axes the product of inertia becomes 0, thereby yielding the moment of inertia tensor matrix [Wertz, page 519]

$${}^C\mathbf{I} = \begin{bmatrix} I_1 & 0 & 0 \\ 0 & I_2 & 0 \\ 0 & 0 & I_3 \end{bmatrix}. \quad (2.50)$$

Since the CRF will be used in the expression of the dynamic equation the superscript denoting the reference frame, will not be used in the further derivation of the dynamic equation.

Inserting (2.50) in (2.49) and calculating the cross product yields

$$\begin{bmatrix} \dot{L}_1 \\ \dot{L}_2 \\ \dot{L}_3 \end{bmatrix} = \begin{bmatrix} N_{\text{ext},1} - (L_2 - L_{mw,2})L_3I_2^{-1} + (L_3 - L_{mw,3})L_2I_3^{-1} \\ N_{\text{ext},2} - (L_3 - L_{mw,3})L_1I_3^{-1} + (L_1 - L_{mw,1})L_3I_1^{-1} \\ N_{\text{ext},3} - (L_1 - L_{mw,1})L_2I_1^{-1} + (L_2 - L_{mw,2})L_1I_2^{-1} \end{bmatrix}. \quad (2.51)$$

Instead of expressing the dynamic differential equations in terms of the time derivative of the total angular momentum as in (2.51) it is simpler to express it in terms of the time derivative of the angular velocity. This is done by expressing (2.49) as

2.7. SATELLITE DYNAMICS AND KINEMATICS

$$\begin{aligned}\underline{\mathbf{I}}\dot{\boldsymbol{\omega}} + \dot{L}_{\text{mw}} &= N_{\text{ext}} - (\underline{\mathbf{I}}^{-1}(L - L_{\text{mw}})) \times L \\ \underline{\mathbf{I}}\dot{\boldsymbol{\omega}} &= N_{\text{ext}} - \dot{L}_{\text{mw}} - \boldsymbol{\omega} \times (\underline{\mathbf{I}}\boldsymbol{\omega} + L_{\text{mw}}).\end{aligned}\quad (2.52)$$

Then by introducing the skew symmetric matrix shown in (2.53) it is possible to substitute the cross product in (2.52) with a multiplication [Hughes, page 524-525]

$$\begin{aligned}\underline{\mathbf{S}}(\boldsymbol{\omega}) &= \boldsymbol{\omega}^T \times \boldsymbol{\omega} = -\boldsymbol{\omega} \times \boldsymbol{\omega}^T = - \begin{bmatrix} \hat{\boldsymbol{\omega}}_1 \\ \hat{\boldsymbol{\omega}}_2 \\ \hat{\boldsymbol{\omega}}_3 \end{bmatrix} \times \begin{bmatrix} \hat{\boldsymbol{\omega}}_1 & \hat{\boldsymbol{\omega}}_2 & \hat{\boldsymbol{\omega}}_3 \end{bmatrix} \\ &= - \begin{bmatrix} \hat{\boldsymbol{\omega}}_1 \times \hat{\boldsymbol{\omega}}_1 & \hat{\boldsymbol{\omega}}_1 \times \hat{\boldsymbol{\omega}}_2 & \hat{\boldsymbol{\omega}}_1 \times \hat{\boldsymbol{\omega}}_3 \\ \hat{\boldsymbol{\omega}}_2 \times \hat{\boldsymbol{\omega}}_1 & \hat{\boldsymbol{\omega}}_2 \times \hat{\boldsymbol{\omega}}_2 & \hat{\boldsymbol{\omega}}_2 \times \hat{\boldsymbol{\omega}}_3 \\ \hat{\boldsymbol{\omega}}_3 \times \hat{\boldsymbol{\omega}}_1 & \hat{\boldsymbol{\omega}}_3 \times \hat{\boldsymbol{\omega}}_2 & \hat{\boldsymbol{\omega}}_3 \times \hat{\boldsymbol{\omega}}_3 \end{bmatrix} \\ &= \begin{bmatrix} 0 & -\hat{\boldsymbol{\omega}}_3 & \hat{\boldsymbol{\omega}}_2 \\ \hat{\boldsymbol{\omega}}_3 & 0 & -\hat{\boldsymbol{\omega}}_1 \\ -\hat{\boldsymbol{\omega}}_2 & \hat{\boldsymbol{\omega}}_1 & 0 \end{bmatrix},\end{aligned}\quad (2.53)$$

(2.52) can now be expressed as

$$\dot{\boldsymbol{\omega}} = \underline{\mathbf{I}}^{-1} [N_{\text{ext}} + N_{\text{ctrl}} - \underline{\mathbf{S}}(\boldsymbol{\omega})(\underline{\mathbf{I}}\boldsymbol{\omega} + L_{\text{mw}})], \quad (2.54)$$

where the control torque, N_{ctrl} is defined as

$$N_{\text{ctrl}} = N_{\text{mt}} - N_{\text{mw}}. \quad (2.55)$$

N_{mt} is the torque contributed by the magnetorquers and the N_{mw} is the torque applied to the momentum wheels which is defined as

$$N_{\text{mw}} = \dot{L}_{\text{mw}}. \quad (2.56)$$

The equation derived in (2.54) will be used in the system equations for the satellite.

2.7.2 Kinematic Equation for the Satellite

There are different methods to represent the kinematic differential equation of the satellite. These are the direct cosine matrix (DCM) denoted the attitude matrix, Euler angles and quaternions. However, the attitude matrix representation suffers from redundancy and the Euler angles suffer from singularities, which is why this section contains the kinematic differential equation represented in terms of quaternions which only has one redundant parameter.

In order to derive the kinematic differential equation in terms of quaternions the attitude matrix given by Euler's eigenaxis rotation theorem is used. This attitude matrix is derived in Appendix B and is expressed as

$$\underline{C} = \begin{bmatrix} c\theta + e_1^2(1 - c\theta) & e_1e_2(1 - c\theta) + e_3s\theta & e_1e_3(1 - c\theta) - e_2s\theta \\ e_2e_1(1 - c\theta) - e_3s\theta & c\theta + e_2^2(1 - c\theta) & e_2e_3(1 - c\theta) + e_1s\theta \\ e_3e_1(1 - c\theta) + e_2s\theta & e_3e_2(1 - c\theta) - e_1s\theta & c\theta + e_3^2(1 - c\theta) \end{bmatrix}, \quad (2.57)$$

where $c\theta \equiv \cos(\theta)$, $s\theta \equiv \sin(\theta)$ and e_i are the direction cosines of the Euler axis, which is bounded by $e_1^2 + e_2^2 + e_3^2 = 1$

Based on Appendix A the following definitions for the quaternions are used in deriving the kinematic differential equation.

$$q_{1:3} = e_{1:3} \sin(\theta/2). \quad (2.58)$$

$$q_4 = \cos(\theta/2) \quad (2.59)$$

$$q = (q_{1:3}, q_4) \quad (2.60)$$

$$q_1^2 + q_2^2 + q_3^2 + q_4^2 = 1. \quad (2.61)$$

It is now possible to express the attitude matrix given in (2.57) in terms of quaternions [Wie, page 318] yielding

$$\underline{C}(q_{1:3}, q_4) = \begin{bmatrix} 1 - 2(q_2^2 + q_3^2) & 2(q_1q_2 + q_3q_4) & 2(q_1q_3 - q_2q_4) \\ 2(q_2q_1 - q_3q_4) & 1 - 2(q_1^2 + q_3^2) & 2(q_2q_3 - q_1q_4) \\ 2(q_3q_1 + q_2q_4) & 2(q_3q_2 - q_1q_4) & 1 - 2(q_1^2 + q_2^2) \end{bmatrix}. \quad (2.62)$$

The kinematic differential equation for the attitude matrix method which is derived in Appendix B yields

$$\dot{\underline{C}} + \underline{S}(\omega)\underline{C} = 0, \quad (2.63)$$

where \underline{C} is the attitude matrix from one reference frame to another, $\dot{\underline{C}}$ is the time derivative of the same attitude matrix and $\underline{S}(\omega)$ is a 3×3 skew symmetric matrix containing the angular velocity.

From (2.63) the following vector composition for the angular velocity is given.

$$\omega_1 = \dot{C}_{21}C_{31} + \dot{C}_{22}C_{32} + \dot{C}_{23}C_{33} \quad (2.64)$$

$$\omega_2 = \dot{C}_{31}C_{11} + \dot{C}_{32}C_{12} + \dot{C}_{33}C_{13} \quad (2.65)$$

$$\omega_3 = \dot{C}_{11}C_{21} + \dot{C}_{12}C_{22} + \dot{C}_{13}C_{23}. \quad (2.66)$$

2.7. SATELLITE DYNAMICS AND KINEMATICS

In order to express (2.64), (2.65) and (2.66) in terms of quaternions (2.62) is used. This yields the following equations

$$\omega_1 = 2(\dot{q}_1 q_4 + \dot{q}_2 q_3 - \dot{q}_3 q_2 - \dot{q}_4 q_1) \quad (2.67)$$

$$\omega_2 = 2(\dot{q}_2 q_4 + \dot{q}_3 q_1 - \dot{q}_1 q_3 - \dot{q}_4 q_2) \quad (2.68)$$

$$\omega_3 = 2(\dot{q}_3 q_4 + \dot{q}_1 q_2 - \dot{q}_2 q_1 - \dot{q}_4 q_3). \quad (2.69)$$

One more equation is needed in order to obtain 4 equations with 4 unknowns. By differentiating (2.61) the last equation is obtained

$$0 = 2(\dot{q}_1 q_1 + \dot{q}_2 q_2 + \dot{q}_3 q_3 + \dot{q}_4 q_4). \quad (2.70)$$

The four equations (2.67), (2.68), (2.69) and (2.70) can be combined into matrix form which yields

$$\begin{bmatrix} \omega_1 \\ \omega_2 \\ \omega_3 \\ 0 \end{bmatrix} = 2 \begin{bmatrix} q_4 & q_3 & -q_2 & -q_1 \\ -q_3 & q_4 & q_1 & -q_2 \\ q_2 & -q_1 & q_4 & -q_3 \\ q_1 & q_2 & q_3 & q_4 \end{bmatrix} \begin{bmatrix} \dot{q}_1 \\ \dot{q}_2 \\ \dot{q}_3 \\ \dot{q}_4 \end{bmatrix}. \quad (2.71)$$

Since the 4×4 matrix in (2.71) is orthonormal the kinematic differential equation for the satellite in terms of quaternions is given in the matrix form [Wie, page 327]

$$\begin{bmatrix} \dot{q}_1 \\ \dot{q}_2 \\ \dot{q}_3 \\ \dot{q}_4 \end{bmatrix} = \frac{1}{2} \begin{bmatrix} 0 & \omega_3 & -\omega_2 & \omega_1 \\ -\omega_3 & 0 & \omega_1 & \omega_2 \\ \omega_2 & -\omega_1 & 0 & \omega_3 \\ -\omega_1 & -\omega_2 & -\omega_3 & 0 \end{bmatrix} \begin{bmatrix} q_1 \\ q_2 \\ q_3 \\ q_4 \end{bmatrix}. \quad (2.72)$$

By defining a vector $\omega = [\omega_1 \ \omega_2 \ \omega_3]^T$ it is possible to express (2.72) in the compact form shown in (2.73)

$$\dot{q} = \frac{1}{2} \begin{bmatrix} q_4 \omega - \omega \times q_{1:3} \\ -\omega^T q_{1:3} \end{bmatrix} = \frac{1}{2} \begin{bmatrix} -\underline{S}(\omega) & \omega \\ -\omega^T & 0 \end{bmatrix} q = \frac{1}{2} \underline{\Omega} q, \quad (2.73)$$

where $\underline{\Omega}$ is defined as

$$\underline{\Omega} = \begin{bmatrix} 0 & \omega_3 & -\omega_2 & \omega_1 \\ -\omega_3 & 0 & \omega_1 & \omega_2 \\ \omega_2 & -\omega_1 & 0 & \omega_3 \\ -\omega_1 & -\omega_2 & -\omega_3 & 0 \end{bmatrix}$$

There are certain advantages in using quaternions as a representation of rigid body rotation. As already mentioned the quaternions eliminate the redundancy and singularities that appear when expressing rigid body rotation with the attitude matrix or Euler angles. Furthermore, the quaternion representation only

consists of products and sums and it does not contain any trigonometric functions like the attitude matrix and Euler angles. This makes the rigid body rotation expressed in quaternions more suited for software implementation as it is less computational demanding.

2.7.3 System Equations

Based on the derived dynamic and kinematic differential equations for the satellite, it is possible to express the system equations as

$$\underbrace{\begin{bmatrix} \dot{\omega} \\ \dot{q} \end{bmatrix}}_{\dot{x}} = \underbrace{\begin{bmatrix} \mathbf{I}^{-1}(N_{\text{ext}} + N_{\text{ctrl}} - \mathbf{S}(\omega)(\mathbf{I}\omega + L_{\text{mw}})) \\ \frac{1}{2}\mathbf{\Omega}q \end{bmatrix}}_{f(x,u,w)} \quad (2.74)$$

$$\underbrace{\begin{bmatrix} \omega \\ q \end{bmatrix}}_y = \underbrace{\begin{bmatrix} \mathbf{1}_{3 \times 3} & \mathbf{0}_{3 \times 4} \\ \mathbf{0}_{4 \times 3} & \mathbf{1}_{4 \times 4} \end{bmatrix}}_{\mathbf{C}} \underbrace{\begin{bmatrix} \omega \\ q \end{bmatrix}}_x \quad (2.75)$$

The system equations are constructed, based on the desire of an output containing the angular velocity, ω , and the attitude in terms of a quaternion, q . In order to keep the output matrix \mathbf{C} simple, the angular velocity and the attitude quaternion are suitable choices for the state vector, x . In (2.74) the states are given by a function, containing the state variables, the control signals and the disturbances denoted $f(x, u, w)$. In (2.75) the notation $\mathbf{1}_{3 \times 3}$ means a 3×3 identity matrix, i.e. the output matrix \mathbf{C} becomes a 7×7 identity matrix.

Because the function $f(x, u, w)$ is nonlinear it needs to be linearized, before it is possible to obtain the system equations in state space form. The linearization of (2.74) can be found in Appendix D and it yields the following linearized expression

$$\underbrace{\begin{bmatrix} \dot{\tilde{q}}_{1:3} \\ \dot{\tilde{\omega}} \\ \dot{\tilde{L}}_{\text{mw}} \end{bmatrix}}_{\dot{\tilde{x}}} = \underbrace{\begin{bmatrix} -\mathbf{S}(\tilde{\omega}) & \frac{1}{2}\mathbf{1}_{3 \times 3} & \mathbf{0}_{3 \times 3} \\ \mathbf{0}_{3 \times 3} & \mathbf{I}^{-1}[\mathbf{S}(\mathbf{I}\tilde{\omega}) - \mathbf{S}(\tilde{\omega})\mathbf{I} + \mathbf{S}(\tilde{L}_{\text{mw}})] & -\mathbf{I}^{-1}\mathbf{S}(\tilde{\omega}) \\ \mathbf{0}_{3 \times 3} & \mathbf{0}_{3 \times 3} & \mathbf{0}_{3 \times 3} \end{bmatrix}}_{\mathbf{A}} \underbrace{\begin{bmatrix} \tilde{q}_{1:3} \\ \tilde{\omega} \\ \tilde{L}_{\text{mw}} \end{bmatrix}}_{\tilde{x}} + \underbrace{\begin{bmatrix} \mathbf{0}_{3 \times 3} & \mathbf{0}_{3 \times 3} \\ \mathbf{I}^{-1} & -\mathbf{I}^{-1} \\ \mathbf{0}_{3 \times 3} & \mathbf{1}_{3 \times 3} \end{bmatrix}}_{\mathbf{B}} \underbrace{\begin{bmatrix} \tilde{N}_{\text{mt}} \\ \tilde{N}_{\text{mw}} \end{bmatrix}}_{\tilde{u}} \quad (2.76)$$

Furthermore, the output equation is rewritten to include the same state vector as in (2.76). This yields the following expression

$$y = \tilde{y} + \bar{y}, \quad (2.77)$$

where

2.8. TRANSDUCERS

$$\tilde{y} = \underbrace{\begin{bmatrix} \underline{1}_{3 \times 3} & \underline{0}_{3 \times 3} & \underline{0}_{3 \times 3} \\ \underline{0}_{3 \times 3} & \underline{1}_{3 \times 3} & \underline{0}_{3 \times 3} \\ \underline{0}_{3 \times 3} & \underline{0}_{3 \times 3} & \underline{1}_{3 \times 3} \end{bmatrix}}_{\underline{C}} \underbrace{\begin{bmatrix} \tilde{q}_{1:3} \\ \tilde{\omega} \\ \tilde{L}_{mw} \end{bmatrix}}_{\tilde{x}} \quad \text{and} \quad \bar{y} = \underbrace{\begin{bmatrix} \underline{1}_{3 \times 3} & \underline{0}_{3 \times 3} & \underline{0}_{3 \times 3} \\ \underline{0}_{3 \times 3} & \underline{1}_{3 \times 3} & \underline{0}_{3 \times 3} \\ \underline{0}_{3 \times 3} & \underline{0}_{3 \times 3} & \underline{1}_{3 \times 3} \end{bmatrix}}_{\underline{C}} \underbrace{\begin{bmatrix} \bar{q}_{1:3} \\ \bar{\omega} \\ \bar{L}_{mw} \end{bmatrix}}_{\bar{x}}$$

The linear system equations in (2.76) and (2.77) can be used for both the control of the satellite in the form of a state space model and for the determination of the attitude.

2.8 Transducers

The design of ACDS includes a full model of the system to be able to simulate the behaviour of the attitude of the satellite in space. Therefore the sensors and the actuators need to be included in the model too.

On the AAUSAT-II three different types of sensors will be used.

Gyro A gyro measures the angular velocity of the satellite or the angle of rotation from an initial reference point, without any use of external references.

Magnetometer A magnetometer measures the direction and size of the magnetic field of the Earth which is why it can only be used in the vicinity of Earth (LEO).

Photo diode A photo diode is used to measure the current induced from the exposure of the diode to sunlight. This current induced is dependent of the angle of attack of the sunlight.

The actuators used on the AAUSAT-II will be

Magnetorquers The magnetorquers consist of 3 coils, one placed perpendicular to each axis on the satellite relative to the SBRF. The magnetorquers are able to create a magnetic field which can create a torque on the satellite when the magnetic field is perpendicular to the magnetic field of the Earth. When using the magnetorquers, the magnetometers must be turned off to avoid contamination of the magnetometer readings.

Momentum Wheels The momentum wheels consist of 3 motors on which a load is mounted. The momentum wheels are placed one on each axis of the satellite. Spinning a momentum wheel up and down loads and unloads angular momentum from the satellite into the momentum wheels and makes the satellite change attitude.

The modelling of the sensors has been made and implemented in the SIMULINK model by the ADS group, 05gr833 [ADS05], and this will not be further described in this report. The following section describes the modelling of the actuators used on AAUSAT-II.

2.9 Actuator Modelling

In this section the models for the attitude control actuators on-board the spacecraft will be described. The momentum wheels are used for quick and small changes in attitude and the magnetorquers are used to desaturate the momentum wheels or for slow changes in attitude.

2.9.1 Magnetorquer Model

The magnetorquers used on AAUSAT-II are rectangular coils with the sides $S_{x1}, S_{x2}, S_{y1}, S_{y2}$, as shown in Figure 2.14. The arrows indicate the direction of the current in the coil.

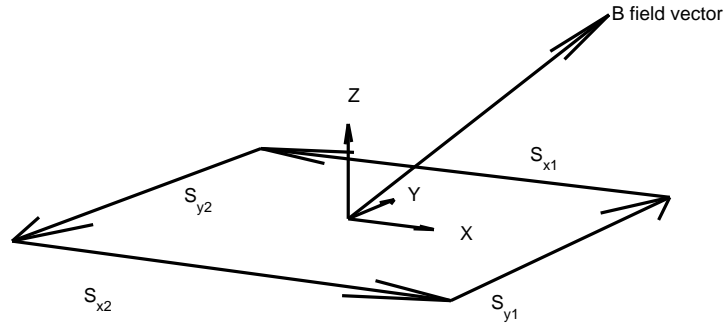


Figure 2.14: Diagram of a magnetorquer.

When placed in a magnetic field the force F acting on each side of the coil can be described by (2.78)

$$F = n \cdot I \cdot S \times B \quad (2.78)$$

where n is the number of windings of the coil, I is the current in the coil and B is the magnetic field vector. The resulting force F_{res} is then

$$F_{res} = \sum_{i=1}^2 n \cdot I \cdot S_{xi} \times B + \sum_{i=1}^2 n \cdot I \cdot S_{yi} \times B \quad (2.79)$$

Figure 2.15 shows the magnetorquer in a magnetic field and the forces acting on each side of the coil.

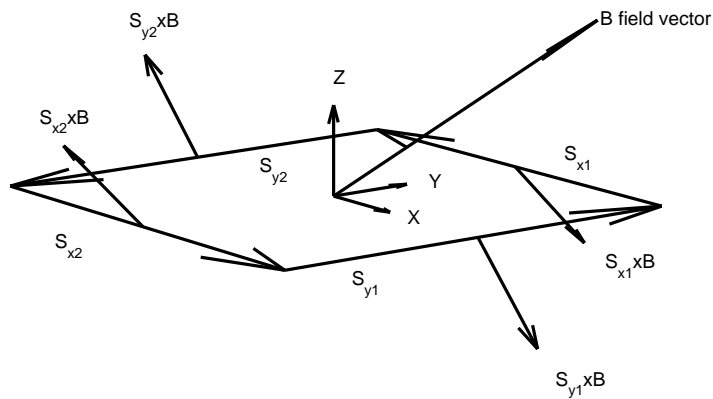


Figure 2.15: Diagram of a magnetorquer, the B-field and the resulting forces.

Because the current runs in a loop the resulting force F_{res} will be equal to zero. This means that the orbit of the satellite cannot be changed by the magnetorquer. It can, however, create a torque because the forces are acting on the sides of the coil, and this torque can be used to adjust the attitude of the satellite.

The magnitude of the torque can be found by projecting the force vectors found in (2.78) onto the plane with a normal vector that lies in the coil plane and is perpendicular to the coil element vector on which the force

2.9. ACTUATOR MODELLING

acts. One such normal vector is the coil vectors orthogonal to the coil vector on which the force acts. The projection matrix is calculated from a normal vector with unit length:

$$\hat{N}_{xu} = \frac{S_{x2}}{|S_{x2}|} \quad (2.80)$$

The projection matrix:

$$\underline{Q}_x = I - N_{xu} \cdot N_{xu}^T \quad (2.81)$$

Figure 2.16 shows the force vectors projected onto the planes defined by the normals of the coil vectors.

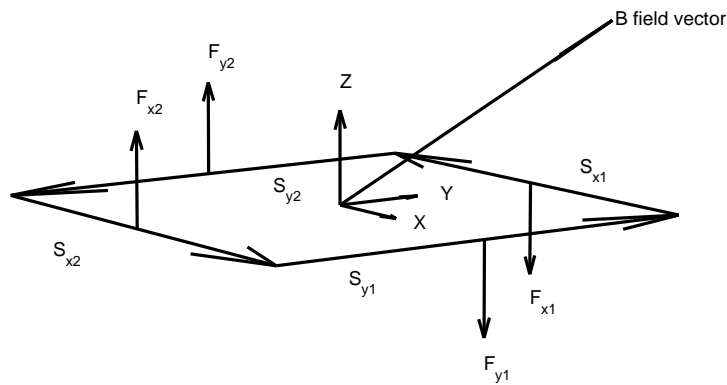


Figure 2.16: Diagram of a magnetorquer and the B-field with the resulting forces projected onto the planes defined by the normals of the coil vectors.

The resulting torque on the coil is the product of the distance from the center of the coil to the coil element and the length of the force vector. Thus the torque N_{y1} is given by

$$N_{y1} = \frac{S_{x2}}{2} \times F_{y1} \quad (2.82)$$

Since the force vectors F_{y1} and F_{y2} are equal in size the torques from each of them are also equal. Therefore the total torque around the x- and y-axis can be written as

$$N_y = S_{x2} \times F_{y1} \quad (2.83)$$

$$N_x = S_{y1} \times F_{x1} \quad (2.84)$$

Implementation of Magnetorquers in SIMULINK

The magnetic moment of the magnetorquers can be written as

$$m_{mt} = n \cdot I \cdot A \cdot \hat{n} \quad (2.85)$$

where n is the number of turns in the coil, I is the current running through the coils, A is the area enclosed by the coils and \hat{n} is a normal vector to the plane, where the individual coils are mounted. The torque produced by the magnetorquers depends on the magnetic field of the Earth. The torque is the cross product between the magnetorquers magnetic moment and the magnetic field of the Earth

$$N_{mt} = m_{mt} \times B = n \cdot I \cdot A \cdot \hat{n} \times B. \tag{2.86}$$

This means that the magnetorquers can be implemented in SIMULINK as depicted in Figure 2.17.

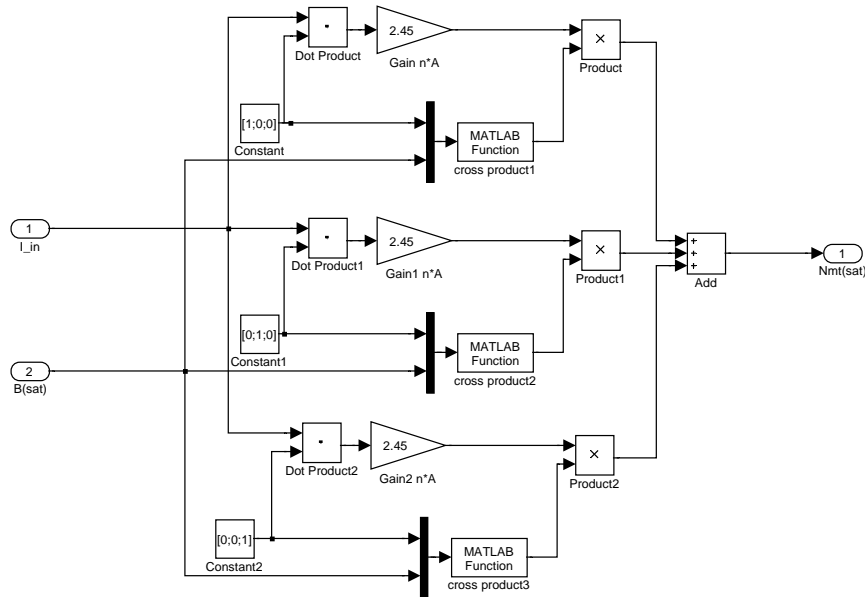


Figure 2.17: SIMULINK implementation of the magnetorquers.

2.9.2 Momentum Wheel Model

The momentum wheels utilized on AAUSAT-II consist of a flywheel mounted on a DC motor. When the flywheel is accelerated by the motor it picks up angular momentum which is transferred from the satellite. The change in angular momentum generates a torque, which makes the satellite rotate.

The satellite is equipped with three momentum wheels. To make it easy to control the attitude of the satellite the momentum wheels are aligned parallel to the axes of the satellite body reference model and hence perpendicular to each other.

The DC motor chosen for the momentum wheels, is a Maxon RE 10 (Order No. 256086) [Maxon RE10]. It runs at a nominal voltage of 3 [V] and is available in a space qualified version. The motor is fitted with a 4.4 [g] flywheel made out of steel.

Electrical Model

The torque of the DC motor is generated by moving a conductor in a magnetic field. Since the orientation of the conductors is approximately orthogonal to the magnetic field, the torque of the motor, N_m is proportional

2.9. ACTUATOR MODELLING

to the current, i_{mw} with the motor torque constant, K_t as the proportionality factor. Hence the torque of the motor is given by

$$N_m = K_t \cdot i_{mw}. \quad (2.87)$$

When a conductor is moved in a magnetic field an electromotive force, e_{mw} is generated. It is approximated by a linear combination of the angular velocity of the rotor, ω_{mw} and the motor speed constant, K_s of the motor. Thus the electromotive force can be approximated by

$$e_{mw} \approx K_s \cdot \omega_{mw}. \quad (2.88)$$

Figure 2.18 shows the electrical equivalent diagram of a brushless DC motor. From this diagram it is possible to derive the relation between the armature voltage, v_{mw} and the current, i_{mw} of the motor and the angular velocity, ω_{mw} . The armature voltage is given by

$$v_{mw} = R_{mw} \cdot i_{mw} + L_{mw} \frac{di_{mw}}{dt} + e_{mw} = R_{mw} \cdot i_{mw} + L_{mw} \frac{di_{mw}}{dt} + K_s \cdot \omega_{mw}. \quad (2.89)$$

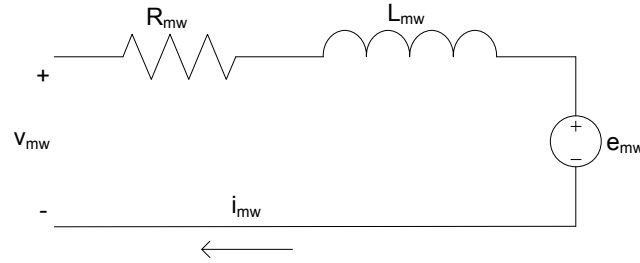


Figure 2.18: Electrical equivalent diagram of a brushless DC motor. v_{mw} is the armature voltage, i_{mw} is the current through the motor, R_{mw} is the resistance in the coils, L_{mw} is the inductance of the coils and e_{mw} is the electromotive force.

Mechanical Model

Figure 2.19 shows a free body diagram of the motor and load. I_{mw} is the moment of inertia of the momentum wheel, N_m is the torque generated by the motor and N_f is the torque generated due to friction. The moment of inertia of the momentum wheel is given by the sum of the moment of inertia of the rotor, I_r and the moment of inertia of the load, I_l . The load is the flywheel.

From the free body diagram and Newton's second law it is possible to derive the torque of the momentum wheel

$$N_{mw} = I_{mw} \frac{d\omega_{mw}}{dt} = (I_r + I_l) \frac{d\omega_{mw}}{dt} = N_m - N_f \quad (2.90)$$

In order to be able to use a linear model and avoid unnecessary wear of the motors, they will only be utilized around a bias point, never reaching zero or negative voltages in operation. Thus only viscous friction is included in the model.

The torque generated by friction, N_f is proportional to the angular velocity, ω_{mw} with the viscous friction coefficient, b_f as the proportionality factor:

$$N_f = b_f \cdot \omega_{mw} \quad (2.91)$$

From (2.87), (2.90) and (2.91) follows the torque of the momentum wheel

$$N_{mw} = I_{mw} \frac{d\omega_{mw}}{dt} = K_t \cdot i_{mw} - b_f \cdot \omega_{mw}. \quad (2.92)$$

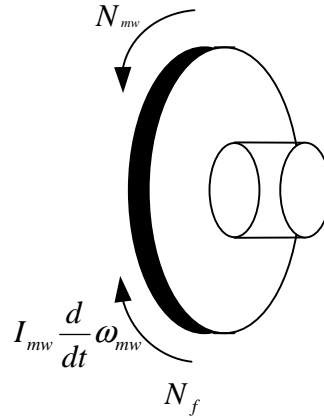


Figure 2.19: Free body diagram of the motor and load. I_{mw} is moment of inertia of the momentum wheel, N_m is the torque generated by the motor and N_f is the torque generated due to friction.

In Figure 2.20 the MATLAB implementation of the momentum wheel can be seen. The contribution from the coil inductance is very small compared to the other components and therefore it has been removed in order to speed up simulations.

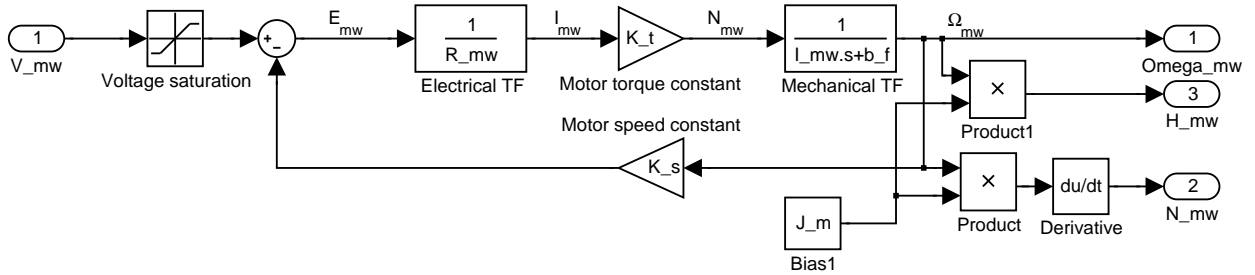


Figure 2.20: MATLAB implementation of a momentum wheel.

The motor for the momentum wheel is controlled by a hardware PID controller on the ADCS subsystem PCB. This controller must be included in the model of the momentum wheel in order to get a realistic simulation result. The Laplace transformed transfer function for the MATLAB implementation of the momentum wheel is given by

$$\frac{\Omega_{mw}(s)}{V_{mw}(s)} = \frac{\frac{K_t}{R_{mw}(I_{mw}s+b_f)}}{1 + K_s \cdot \frac{K_t}{R_{mw}(I_{mw}s+b_f)}} \quad (2.93)$$

$$= \frac{K_t}{R_{mw} \cdot I_{mw} \cdot s + R_{mw} \cdot b_f + K_s \cdot K_t}, \quad (2.94)$$

and it has a DC gain of

$$g_{mw} = \frac{K_t}{R_{mw} \cdot b_f + K_s \cdot K_t} = 370.9. \quad (2.95)$$

A discrete PID controller is inserted into the momentum wheel model and the full implementation can be seen in Figure 2.21.

A continuous transfer function for the PID controller is calculated using the constants from the data sheet for the hardware controller [LM628], and then discretized with the function `C2D` in MATLAB, whereafter it

2.9. ACTUATOR MODELLING

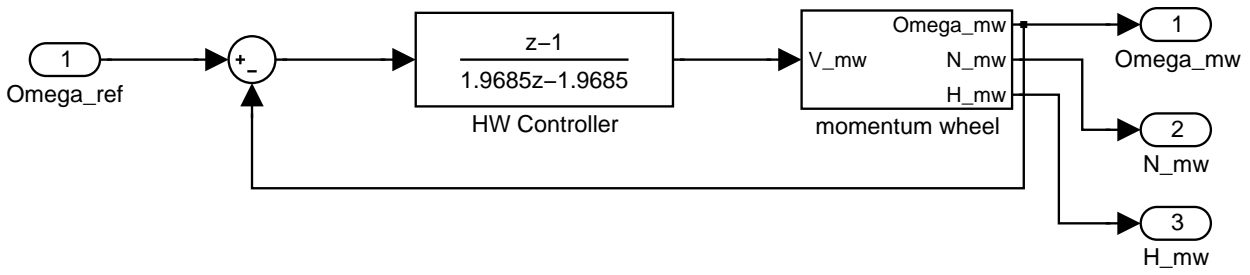


Figure 2.21: MATLAB implementation of a momentum wheel with a hardware PID controller.

is inserted into the SIMULINK model. The standard form for a PID controller transfer function is [Powell et al., Page 218]

$$\frac{K_d \cdot s^2 + K_p \cdot s + K_i}{s} \quad (2.96)$$

The PID controller is equipped with a 5 [MHz] clock and therefore the sample rate is [LM628, Page 9]

$$f_s = \frac{f_{clk}}{2048} = \frac{5 \cdot 10^6}{2048} = 2.441 \text{ [kHz]} \quad (2.97)$$

The sampling theorem requires that

$$\frac{f_s}{f_b} > 2 \quad (2.98)$$

where f_b is the closed loop system bandwidth [Franklin et al., Page 450] in order to get a stable system. Therefore the maximum bandwidth of the system is 1.221 [kHz].

Since the DC gain of the motor model is 370.9 the initial gain for the hardware controller is set to $\frac{1}{370.9}$ in order to get a unit gain. The frequency response of the closed loop system is plotted in Figure 2.22.

The gain at the bandwidth frequency is -45.5 [dB] and therefore the hardware controller gain can be increased by 45.5 [dB] and the system will still be stable. So the gain of the hardware controller shall be

$$10^{\frac{45.5}{20}} \cdot \frac{1}{370.9} = 0.508 \quad (2.99)$$

and the resulting bode plot is shown in Figure 2.23.

It can be seen that the system bandwidth now is 1221 [Hz], however a pure P controller with unit feedback has a small DC error and therefore an integrator is introduced. The integration constant is set to $\frac{1}{10}$ of the P gain.

The resulting system is tested with a ramp as reference because this generates a continuous torque and therefore it is easy to verify. The test result can be seen in Figure 2.24.

As it can be seen the reference and the angular velocity is very close to each other so the controller works as intended. The torque forms a square wave which is expected because the torque is the derivative of the angular velocity times the moment of inertia.

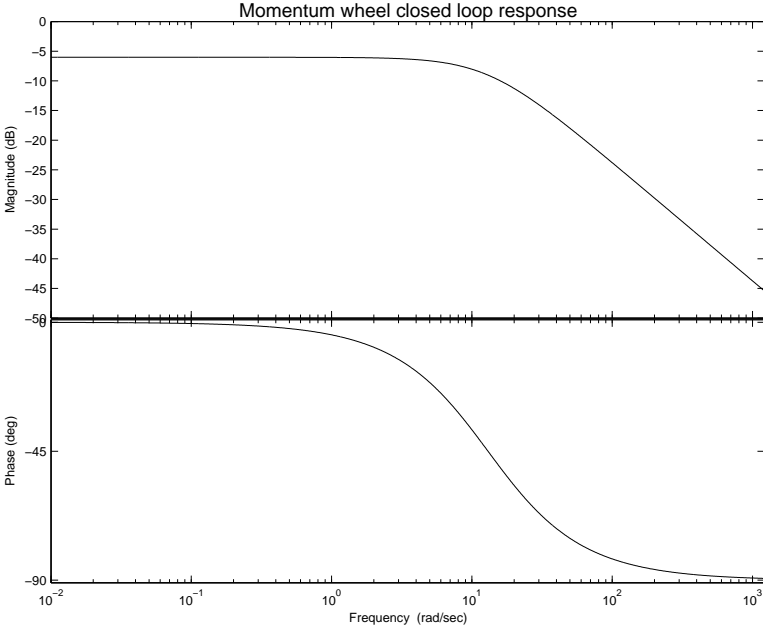


Figure 2.22: Frequency response of the momentum wheel with hardware PID controller with unit gain.

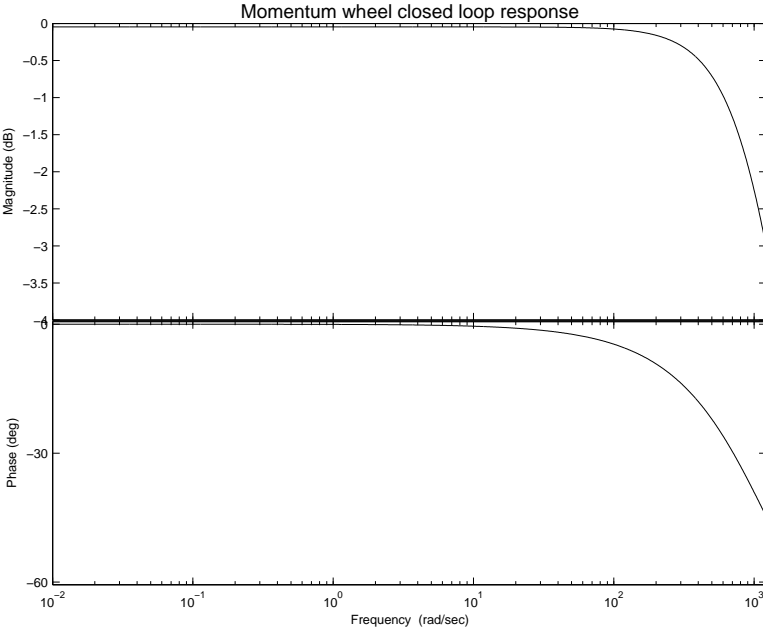


Figure 2.23: Frequency response of the momentum wheel with hardware PID controller with maximum gain.

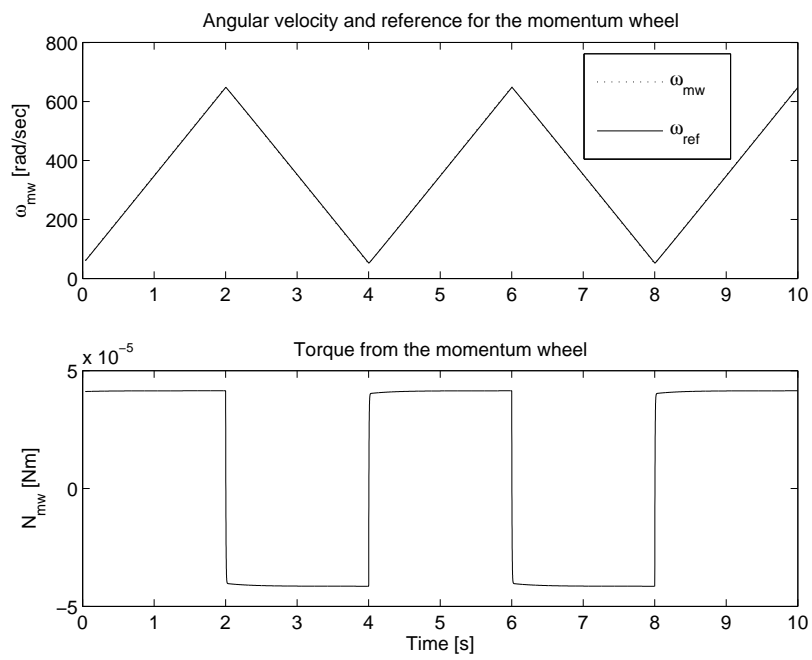


Figure 2.24: Torque generated by the momentum wheel with a ramp as input.

Controllers

This chapter describes different control strategies of the attitude control system. Detumbling and pointing control algorithms are designed, implemented and tested in the simulation environment.

3.1 Control Strategy

There are two sets of actuators on-board the AAUSAT-II satellite, magnetorquers and momentum wheels one of each on each axis of the SBRF.

The magnetorquers generate a magnetic field which can be used for moving angular momentum from the satellite to the magnetic field of the Earth, the B field. Each magnetorquer is only able to actuate when it is not perpendicular to the B field.

The momentum wheels actuate by loading or unloading angular momentum from the satellite to the momentum wheels by accelerating or decelerating them. This means the sum of the angular momentum of the satellite and the momentum wheels does not change. Since the motors used for the momentum wheels have a maximum speed, the momentum wheels are only able to load a certain amount of angular momentum from the satellite. Therefore the angular momentum of the momentum wheels has to be unloaded. This can be done using the magnetorquers, by unloading the angular momentum from the momentum wheels to the magnetic field of the Earth.

Three modes for ADCS are defined to describe the control strategy.

Idle is when no actuators are active, meaning that ADCS is disabled and the satellite is tumbling uncontrolled in its orbit.

Detumble is when the satellite has been released from the launch vehicle. The satellite is then tumbling around and needs to be detumbled in order to stabilize the satellite.

Pointing is when the satellite shall maintain a given attitude or a given rotation e.g. in order to point the antenna towards a ground station.

In order to make sure that the correct control strategy is used in each mode a supervisor is designed.

3.1.1 Idle

In idle mode, the ADCS is off, meaning the satellite is tumbling uncontrolled. This mode will be active right after deployment of the satellite or when power is so low that the ADCS is turned off to save power.

3.2. CONTROL SUPERVISOR

3.1.2 Detumbling

The detumbling mode is active after deployment, where the satellite needs to be detumbled in order to stabilize it for more reliable communication with the ground station. In addition detumbling also prevents the possibility of having the satellite spinning with a certain frequency such that a "blind spot" in the antenna gain would make communication impossible.

In detumbling mode the primary purpose is to minimize the rotation of the satellite, which should be below 0.0021 [rad/s] on all axes, according to statement 1 in the system demands for ADCS described in Subsection 1.5.8 on page 17. This average angular velocity is equivalent to following the magnetic field around the Earth, for which reason a B-dot controller is chosen. The B-dot controller actuates on the derivative of the B field of the Earth meaning the changes in the B field are minimized, causing the satellite to follow the magnetic field of the Earth.

3.1.3 Pointing

In pointing mode the satellite shall be stabilized at a given attitude or point towards a certain point by renewing the reference quaternion. This will e.g. enable the satellite to point the antennas towards the ground station during an overflight and thereby give a better communication link. This mode also enables the satellite to point a corner towards the Sun when no other tasks are performed by the ADCS, meaning that charging of the batteries is optimized. Because of the low amount of power available an optimal controller is chosen because it gives the opportunity to easily weigh performance against energy consumption.

The system demands for the ADCS in pointing mode, is to maintain a certain attitude of the satellite within 0.087 [rad] during 95 [%] of the orbit, as described in statement 4 in Subsection 1.5.8 on page 17. Actuating is done using the momentum wheels, because only two axis control is possible with the magnetorquers and they are not as fast as momentum wheels. The momentum wheels will, however saturate over time and therefore it is necessary to desaturate the momentum wheels from time to time. The magnetorquers are used for desaturation by unloading angular momentum from the satellite to the Earth's magnetic field. Therefore it is necessary to design a desaturation controller that can be activated when the speed of the momentum wheels deviate too much from their bias speed.

3.2 Control Supervisor

A supervisor is introduced in order to apply the correct control strategy in each mode. The strategy for each of the modes where the ADCS is activated is described in the following.

Detumbling

In detumbling mode the detumbling controller is activated in order to reduce the angular velocity of the satellite.

Pointing

In pointing mode the control supervisor supply the attitude controller with a reference quaternion from the flight plan. Before the reference quaternion is sent to the attitude controller it must be checked if the satellite is able to turn to the new attitude in one step because the momentum wheel attitude controller can only stabilize the satellite within a limited range as described in Section 3.3.1. If the satellite is unable to turn to the new attitude in one step the manoeuvre must be divided into smaller steps. The steps are then carried out one at a time and the momentum wheels are desaturated between each step. With this approach the satellite can be stabilized at any attitude.

Desaturation

It is only necessary to activate the desaturation controller when using the momentum wheels, that is when

the pointing controller is active. Therefore the desaturation mode is a sub mode to the pointing mode, hence it can only be activated when the pointing controller is active.

3.2.1 Mode Switching

The supervisor can switch between the modes and the rules for mode switching are listed in Table 3.1.

Mode	Initiation trigger	Termination trigger
Idle	Flight plan command	Flight plan command
Detumbling	Flight plan command Satellite tumbling	Flight plan command
Pointing	Flight plan command	Flight plan command Satellite tumbling

Table 3.1: Mode switching rules.

Transitions between the different modes can be triggered by a flight plan command $FP.event$ or a conditional event $C.event$ IF[*condition*] that is carried out when *condition* becomes true. Some $FP.event$ commands can only be carried out if a certain condition is true, an example is: $FP.event$ IF[*condition*]. One transition can be triggered by multiple flight plan commands and conditional events.

3.2.2 Main Supervisor

The states and transitions for the pointing controller supervisor are shown in Figure 3.1. The supervisor is started in Idle mode when the ADCS system is turned on. It is possible to switch between all modes with flight plan commands sent from the mission control center. The supervisor has a security function built in to terminate faulty controllers if the angular velocity of the satellite increases. If the supervisor detects that the satellite is tumbling in Pointing mode, it will stop the controller and go to Detumbling mode.

3.2.3 Desaturation Supervisor

The states and transitions for the desaturation controller supervisor are shown in Figure 3.2. The desaturation supervisor is started when the main supervisor sets the system to Pointing mode. It is in Off mode by default and can be activated by the $FP.Desat$ on command that sends it into Wait mode. In Wait mode it will automatically switch to Desaturate mode, if the momentum wheel bias error l_{err} is smaller than $l_{err\ off}$. In Desaturate mode it will automatically switch to Wait mode, if the momentum wheel bias error l_{err} is larger than $l_{err\ off}$. The two different levels create a Schmitt trigger coupling that prevents on/off oscillations of the desaturation controller. A conditional transition sends the desaturation supervisor into Off mode, when the main supervisor leaves the Pointing mode.

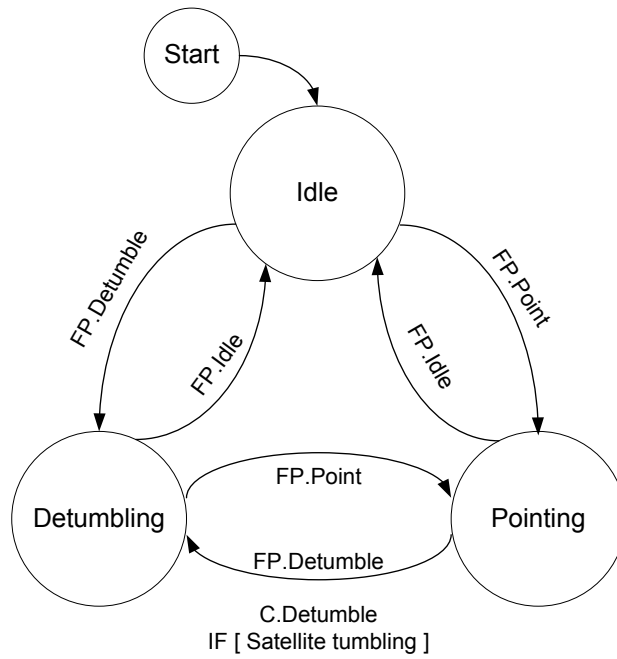


Figure 3.1: States and transitions for the main supervisor.

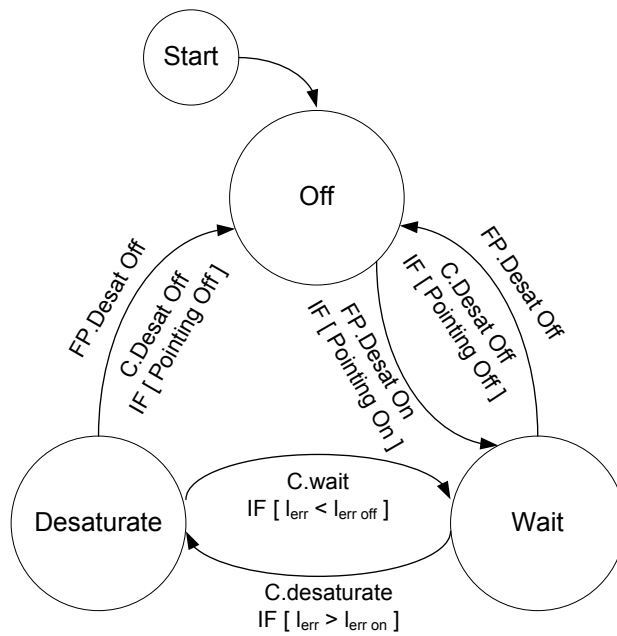


Figure 3.2: States and transitions of desaturation controller supervisor.

3.3 Controllability

In order to be able to control all states of the system, it must be controllable. The system is considered to be controllable if, for all initial times and all initial states, there exists an input function that changes the state vector to any desired final state within a finite time.

With the system defined as $\dot{x} = \underline{A}x + \underline{B}u$, the rank of the controllability matrix should equal the order, n , of the system matrix \underline{A} . The controllability matrix, \underline{C} , is calculated as [Powell et al., page 849]

$$\underline{C} = [\underline{B} \quad \underline{A}\underline{B} \quad \underline{A}^2\underline{B} \quad \dots \quad \underline{A}^{n-1}\underline{B}]. \quad (3.1)$$

The linearized system, Equation 2.76 on page 41, contains nine state variables, ($\tilde{q}_{1:3}$, $\tilde{\omega}$ and \tilde{L}_{mw}) and six input variables (\tilde{N}_{mt} and \tilde{N}_{mw}). By the definition, this system is fully controllable because it has full rank. But in order to be able to design a linear controller to control the attitude of the satellite, the contribution from the magnetic B field has to be included in the linearized system equations, as the magnetorquers depend on this for actuation. Since this is not the case, linear control using magnetorquers is not possible.

By omitting the magnetorquers from the input matrix, the rank of the controllability matrix is reduced to six. This means that only six of the nine states are controllable thus leaving the angular momentum of the momentum wheels uncontrollable.

3.3.1 Attitude Controllability

Because the magnetorquers will not be used for attitude changes, the momentum wheels will be used for both disturbance rejection and the attitude changes. If the satellite is to be stable at a given attitude, it is necessary to transfer all the angular momentum of the satellite to the momentum wheels, as described in the following equation

$$L_{total} = L_{mw}. \quad (3.2)$$

This means that the momentum wheels must be able to store the angular momentum coming from the disturbance torques and the attitude changes from the attitude controller. Disregarding the disturbance torques and the magnetorquers, there are no external torques affecting the satellite, this means that the law of conservation of angular momentum applies. The law states that "The total angular momentum of a system is constant in both magnitude and direction if the resultant external torque acting on the system is zero" [Serway & Beichner, page 340]. This means that if the satellite is to be stable at any given attitude, the momentum wheels must be able to store the total angular momentum independently of the attitude of the satellite. However since the configuration of the momentum wheels states that they should only rotate in one direction, they are only able to produce angular momentum in the first octant in the SBRF frame. This means that (3.2) cannot be fulfilled for any given attitude, as depicted in Figure 3.3.

In Figure 3.3(a) the total angular momentum is in the first octant of the SBRF frame and the momentum wheels will be able to stabilize the satellite at this attitude. In Figure 3.3(b) the total angular momentum is outside the first octant of the SBRF frame and the momentum wheels will not be able to produce an angular momentum in this direction, which entails that they cannot stabilize the satellite at this attitude.

When the satellite is stabilized at an attitude and the momentum wheels are at their bias point, the total angular momentum of the satellite will be equal to the bias angular momentum of the momentum wheels, meaning

3.4. DETUMBLING CONTROLLER

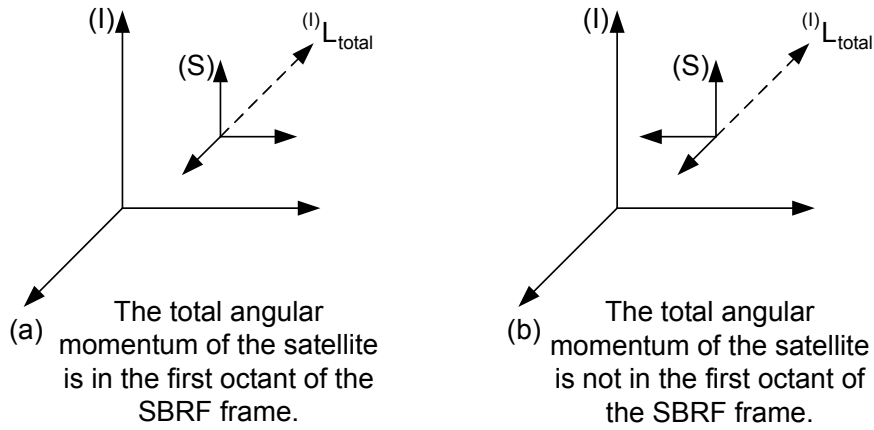


Figure 3.3: Total angular momentum of the satellite for two different attitudes of the satellite.

$$L_{total} = L_{mw,bias} = \frac{1}{\sqrt{3}} \cdot \begin{bmatrix} \|L_{mw,bias}\| \\ \|L_{mw,bias}\| \\ \|L_{mw,bias}\| \end{bmatrix}. \quad (3.3)$$

This means that when the momentum wheels are at their bias, they can only rotate the satellite 45° about any axis. A rotation beyond 45° would mean that the L_{total} vector would leave the first octant of the SBRF frame and the momentum wheels will reach their saturation limit, which means the magnetorquers will have to be used to desaturate the momentum wheels. For this reason a control supervisor will have to be implemented, to decide if an attitude manoeuvre is possible and if not when to desaturate the momentum wheels with the magnetorquers.

3.4 Detumbling Controller

The purpose of the detumbling controller is to detumble the satellite after it has been released from the launch vehicle. According to statement 1 in the system demands from Subsection 1.5.8 the satellite is considered detumbled, when it follows the magnetic field around the Earth. This means, that at an altitude of 700 [km], the angular velocity of the satellite, must be below 0.0021 [rad/s] according to statement 1 in the system demands for ADCS in Subsection 1.5.8 on page 17. This should be done by a robust and simple system, since this is the first attitude control task to be performed on the satellite after launch.

3.4.1 B-dot Controller

Because of its simplicity, a B-dot controller has been chosen as the detumbling controller. The controller only needs the derivative of the magnetic field as input, which makes it capable of functioning as long as the magnetometers and magnetorquers are functioning. The principle of the B-dot controller, is to minimize the rotational kinetic energy of the satellite. The rotational kinetic energy is reduced, if the derivative of it is negative. This can be expressed as

$$\dot{E}_{kin} = \boldsymbol{\omega}_s^T N_{mt} < 0, \quad (3.4)$$

where ω_s is the angular velocity of the satellite and N_{mt} is the torque from the magnetorquers. The torque can be described as

$$N_{mt} = m_{mt} \times B, \quad (3.5)$$

where m_{mt} is the magnetic moment of the magnetorquers, B is the Earth's magnetic field vector and N_{mt} is the torque caused by the magnetorquers. Inserting (3.5) into (3.4) yields

$$\omega_s^T (m_{mt} \times B) < 0 \quad \Leftrightarrow \quad -\omega_s^T (B \times m_{mt}) < 0. \quad (3.6)$$

This can be rewritten as

$$m_{mt}^T (\omega_s \times B) > 0. \quad (3.7)$$

This inequality can be solved by

$$m_{mt} = C_{B\text{-dot}} (\omega_s \times B), \quad (3.8)$$

where $C_{B\text{-dot}} > 0$ is a selectable scalar gain, which affects how fast the kinetic energy decreases. This solution only holds when ω and B are not parallel, in this case the result will be zero. The change in the B-field, \dot{B} , is caused by the rotation of the satellite, the orbit of the satellite around the Earth and the rotation of the Earth. However, the contributions from the orbit of the satellite and the rotation of the Earth, can be considered negligible compared to the contribution from the rotation of the satellite. This means that the derivative of the B-field can be written as [Wisniewski, page 142]

$$\dot{B} = B \times \omega_s \quad \Leftrightarrow \quad \dot{B} = -\omega_s \times B. \quad (3.9)$$

If (3.9) is inserted into (3.8), a simple control law can be stated

$$m_{mt} = -C_{B\text{-dot}} \dot{B}. \quad (3.10)$$

It is not possible to measure \dot{B} directly with the magnetometers and it may entail noise problems to differentiate the output. Therefore an estimate of \dot{B} will be used. This means that the B-dot control law can be stated as follows

$$m_{mt} = -C_{B\text{-dot}} \hat{\dot{B}}. \quad (3.11)$$

3.4.2 B-dot Estimation

To estimate \dot{B} a first order state variable filter is used. The filter can be seen in Figure 3.4.

The transfer function in the Laplace domain can be derived as

$$\frac{\hat{\dot{B}}}{B} = \frac{s\omega_c}{s + \omega_c}, \quad (3.12)$$

3.4. DETUMBLING CONTROLLER

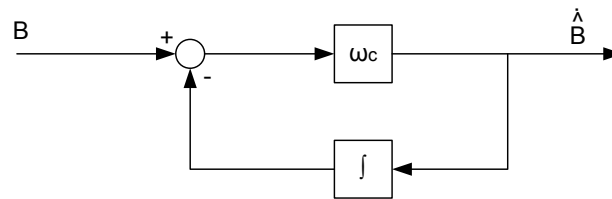


Figure 3.4: Block diagram of the first order state variable filter.

where ω_c is the cut-off frequency, which in [CubeSat ACS] is recommended to be 0.7 [rad/s] and simulations have proved this to be valid.

3.4.3 Implementation of B-dot Controller

This subsection will describe the implementation and simulation of the B-dot controller described. The SIMULINK implementation of the B-dot controller can be seen in Figure 3.5.

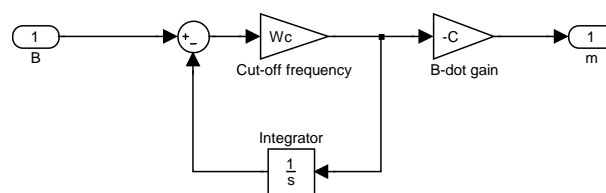


Figure 3.5: Block diagram from SIMULINK of the B-dot controller with filter for estimation of the derivative of B.

A simulation has been made with some preselected values of ω_c and $C_{B\text{-dot}}$ based on the recommendations made in [CubeSat ACS], where $\omega_c = 0.7$ and $C_{B\text{-dot}} = 11000$. Simulations were made with an initial angular velocity of 0.1 [rad/s] on each axis, the result can be seen in Figure 3.6.

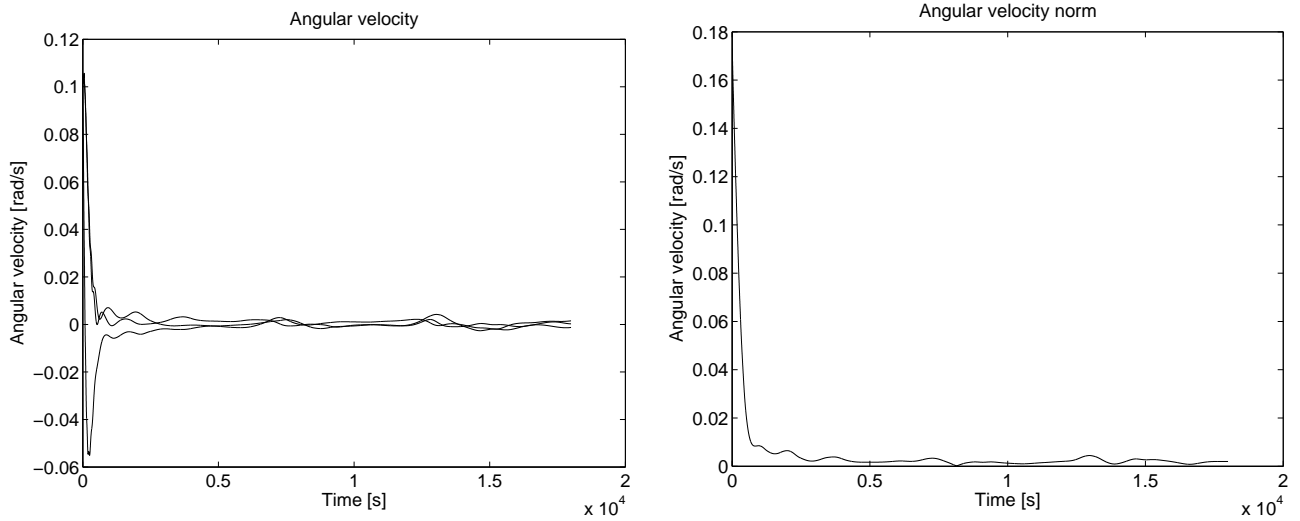


Figure 3.6: The angular velocity and norm with B-dot control enabled.

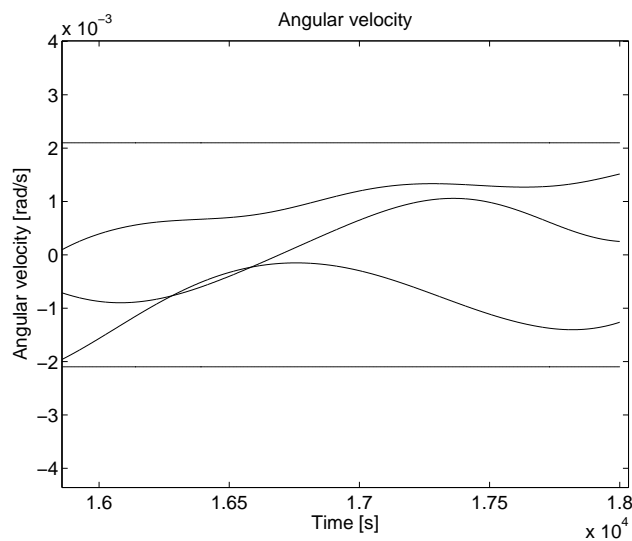


Figure 3.7: The angular velocity norm with B-dot control enabled.

Figure 3.7 shows a magnification of the angular velocity in Figure 3.6, where it can be seen that it is possible to reduce the angular velocity, to the required value of 0.0021 [rad/s] , within the specified time range of 3 orbits, which is approximately 18000 [s] at an altitude of 700 [km] .

The B-dot control has been derived and simulated without any constraints. But when it is implemented on the satellite it will not be possible to use the magnetometer and the magnetorquers simultaneously, because the magnetorquers will cause a disturbance in the measurements from the magnetometer. This means that it is necessary to switch between actuation and measuring the B-field, to avoid causing disturbances. To make the simulations as close to reality as possible, the B-dot estimation filter is Z-transformed to a discrete filter and the periodic actuation and measuring is implemented. The results can be seen in Figure 3.8.

3.4. DETUMBLING CONTROLLER

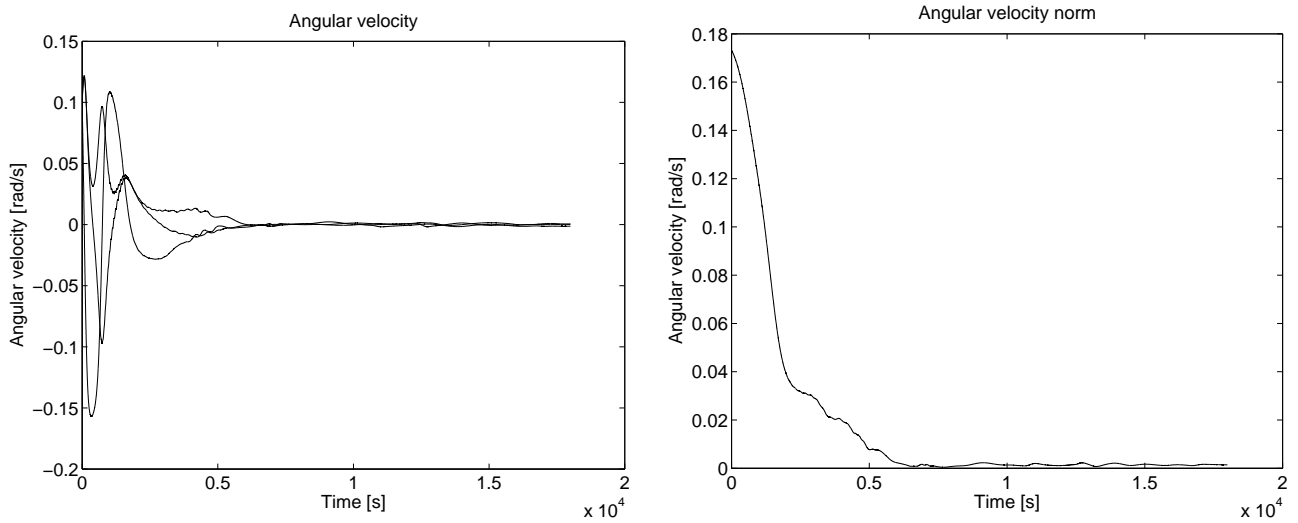


Figure 3.8: The angular velocity and norm with the discrete B-dot control enabled and with periodic actuation and measuring.

Figure 3.9 shows a close up of Figure 3.8.

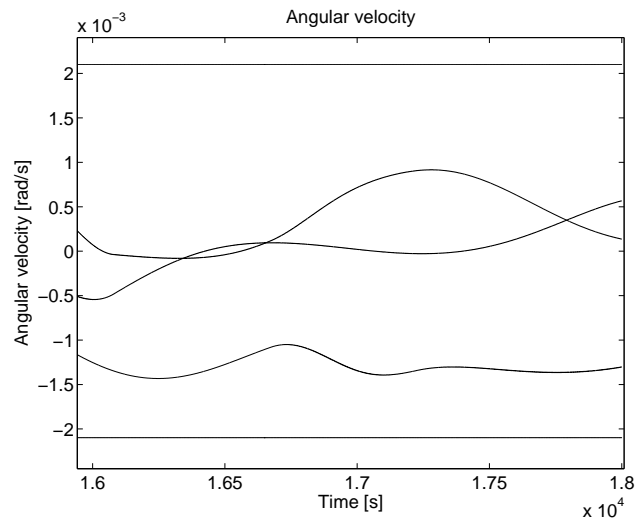


Figure 3.9: Close up of the angular velocity with the discrete B-dot control enabled and with periodic actuation and measuring.

As it can be seen from Figure 3.9, the discrete B-dot control algorithm with periodic actuation and measuring is able to meet the demands for detumbling. The design of the magnetorquers, introduces a saturation on the current running through them at 6.28 [mA], this is implemented in the discrete simulation of the B-dot controller. However the B-dot gain was designed for the continuous case with no saturation, this meant that the gain would have to be fitted to the discrete implementation. Simulations showed that 1500 was a suitable value, yielding the results seen in Figures 3.8 and 3.9. As expected the discrete case is slower due to the fact that actuation is only occurring half of the time and the B-dot gain is lowered, but the demands are met within the specified time range.

3.5 Optimal Controller for Attitude Control

The advantage of optimal control theory is that the controller is designed from the mathematical description of the satellite system using the state space description which includes the system dynamics and kinematics. Thereby information such as the gyro effect of the momentum wheels is taken into account in the regulator design.

In this section the design and implementation of an optimal controller for attitude control of the satellite is described. First a small and general introduction to Linear Quadratic Regulator (LQR) control is given, followed by the design and implementation using the AAUSAT-II SIMULINK model. Test specifications and results for the implemented attitude controller are given in Section 3.5.4.

3.5.1 LQ-Regulator

In optimal control the design is based on optimizing the controller by the performance index given by (3.13)

$$I = \sum_{k=0}^N \mathcal{H}(x(k), u(k)), \quad (3.13)$$

where k is the sample number, $x(k)$ is the state vector and $u(k)$ is the input vector. Under normal conditions it is preferred to bring the state vector from its initial state to origo. Thus the goal is to find an input sequence $u(k)$ which minimizes the performance index I . \mathcal{H} is the weighting function which defines the weight of the input signal $u(k)$ versus the state vector $x(k)$.

LQR in General

To give a small overview of control using an optimal controller a general description of LQR is reviewed for a simple system. The system is in state space form

$$\dot{\mathbf{x}}(t) = \underline{\mathbf{A}}\mathbf{x}(t) + \underline{\mathbf{B}}\mathbf{u}(t). \quad (3.14)$$

The system is put into discrete form for a computational approach

$$x(k+1) = \underline{\Phi}x(k) + \underline{\Gamma}u(k). \quad (3.15)$$

The system has n states and p inputs thereby $\underline{\Phi}$ will be an $n \times n$ quadratic matrix and $\underline{\Gamma}$ will be an $n \times p$ -matrix. The system is assumed to be controllable. The performance index is given by [Optimal, page 13]

$$I = \sum_{k=0}^{N-1} (x^T(k)\underline{\mathbf{Q}}_1x(k) + u^T(k)\underline{\mathbf{Q}}_2u(k)) + x^T(N)\underline{\mathbf{Q}}_N x(N), \quad (3.16)$$

where $\underline{\mathbf{Q}}_1$, $\underline{\mathbf{Q}}_2$ and $\underline{\mathbf{Q}}_N$ are quadratic weight matrices. They are inserted to punish big error values in steady state signals, state signals and the input signals. This means that a high weight of e.g. $\underline{\mathbf{Q}}_2$ will decrease the input signal to the system. In Figure 3.10 the block diagram for the system is shown.

From Figure 3.10 the simple control law is derived

$$u(k) = -\underline{\mathbf{L}}(k)x(k), \quad (3.17)$$

3.5. OPTIMAL CONTROLLER FOR ATTITUDE CONTROL

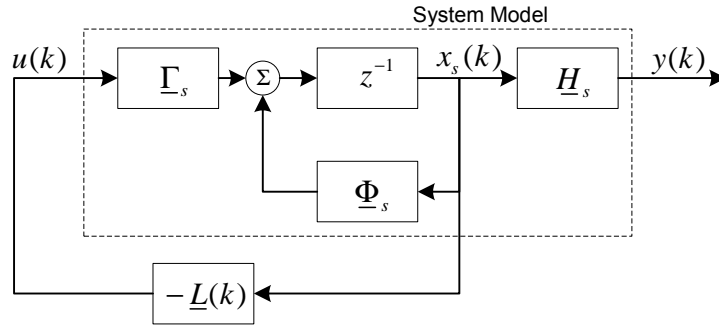


Figure 3.10: A simple LQR implementation.

where $\underline{L}(k)$ is the optimal proportional matrix that will bring the states to origo. $\underline{L}(k)$ is given by [Optimal, page 17]

$$\underline{L}(k) = [\underline{Q}_2 + \underline{\Gamma}^T \underline{S}(k+1) \underline{\Gamma}]^{-1} \underline{\Gamma}^T \underline{S}(k+1) \underline{\Phi}, \quad (3.18)$$

where $\underline{S}(k)$ is given as

$$\underline{S}(k) = \underline{Q}_1 + \underline{\Phi}^T \underline{S}(k+1) (\underline{\Phi} - \underline{\Gamma} \underline{L}(k)). \quad (3.19)$$

$\underline{S}(k)$ represents the optimal proportionality matrix derived from the associated Riccati equations using MATLAB.

3.5.2 Design of the Attitude Controller

The design of the optimal controller will include the following:

- The system equations are converted into discrete form.
- References and integrals for the state variables.
- A performance index for the system is derived.
- The weight matrices are derived from the performance index.
- The optimal gain matrices are calculated.
- A block diagram for the implemented regulator.

Discrete Form

The system is given in Subsection 2.7.3 on page 40 in state space form.

$$\begin{aligned} \dot{x}(t) &= \underline{A}x(t) + \underline{B}u(t) \\ y(t) &= \underline{C}x(t). \end{aligned} \quad (3.20)$$

The system equations are discretized using the `c2dm` function in MATLAB using zero order hold conditions

$$\begin{aligned} x(k+1) &= \underline{\Phi}_s x_s(k) + \underline{\Gamma}_s u(k) \\ y(k) &= \underline{H}_s x_s(k), \end{aligned} \quad (3.21)$$

where $\underline{\Phi}_s$ is the state matrix, $\underline{\Gamma}_s$ is the input matrix and \underline{H}_s is the output matrix of the system.

Controllability

With respect to the controllability considerations in Section 3.3 on page 55 the input matrix \underline{B} has to be modified in order to make the system controllable for a linear regulator. While the nonlinear B field is not considered in the system equations, the magnetorquers will make the system uncontrollable and therefore the input matrix is modified and will only include momentum wheels.

Steady State Disturbance Considerations

In order to take care of the steady state error caused by disturbances in the system as described in Section 2.3 on page 28 an integral state will be implemented in the optimal controller system to compensate for these uncontrollable disturbances. The important parameter for the attitude controller is the quaternion. The integrator is therefore designed with respect to the error signal between the measured quaternion value and the reference quaternion. In order to design the integrator, the reference and integral state shall be modelled. The reference model is described by

$$\begin{aligned} x_r(k+1) &= \underline{\Phi}_r x_r(k) \\ r(k) &= \underline{H}_r x_r(k). \end{aligned} \quad (3.22)$$

The integral model can be described as

$$x_i(k+1) = x_i(k) + e(k), \quad (3.23)$$

where $e(k) = r(k) - y(k)$ is the regulator error i.e.

$$x_i(k+1) = x_i(k) + r(k) - y(k). \quad (3.24)$$

Thereby the integral can be included in the system by

$$\begin{aligned} x_i(k+1) &= x_i(k) + e(k) \\ e(k) &= \underline{H}_r x_r(k) - \underline{H}_{sd} x_s(k), \end{aligned} \quad (3.25)$$

where \underline{H}_{sd} is the constructed output matrix for the integral states, which is different from the system matrix \underline{H}_s because the integral state will only integrate the quaternion states.

3.5. OPTIMAL CONTROLLER FOR ATTITUDE CONTROL

The Performance Index

The system equations for the whole system including the reference and integral states are listed below:

$$\text{Satellite state space equations} \quad x_s(k+1) = \underline{\Phi}_s x_s(k) + \underline{\Gamma}_s u(k) \quad (3.26)$$

$$y(k) = \underline{H}_s x_s(k) \quad (3.27)$$

$$\text{Reference model} \quad x_r(k+1) = \underline{\Phi}_r x_r(k) \quad (3.28)$$

$$r(k) = \underline{H}_r x_r(k) \quad (3.29)$$

$$\text{Integral model} \quad x_i(k+1) = x_i(k) + e(k) \quad (3.30)$$

$$e(k) = \underline{H}_r x_r(k) - \underline{H}_{sd} x_s(k) \quad (3.31)$$

From the system equations the following performance index is derived

$$\begin{aligned} I = & e^T(N) \underline{Q}_{Ne} e(N) + x_i^T(N) \underline{Q}_{Ni} x_i(N) \\ & + \sum_{k=0}^{N-1} e^T(k) \underline{Q}_{1e} e(k) + x_i^T(k) \underline{Q}_{1i} x_i(k) + u^T(k) \underline{Q}_2 u(k). \end{aligned} \quad (3.32)$$

From the performance index in (3.32) the weight matrices are shown. These matrices shall be determined in order to minimize the performance index. The general state space will now be expanded to include the reference and integral states

$$x(k) = [x_s^T(k) \quad x_r^T(k) \quad x_i^T(k)]^T. \quad (3.33)$$

Thereby the complete system equations are given in (3.34) to (3.37)

$$x(k+1) = \begin{bmatrix} \underline{\Phi}_{s9 \times 9} & \underline{0}_{9 \times 3} & \underline{0}_{9 \times 3} \\ \underline{0}_{3 \times 9} & \underline{\Phi}_{r3 \times 3} & \underline{0}_{3 \times 3} \\ -\underline{H}_{sd3 \times 9} & \underline{H}_{r3 \times 3} & \underline{1}_{3 \times 3} \end{bmatrix} x(k) + \begin{bmatrix} \underline{\Gamma}_{s9 \times 3} \\ \underline{0}_{3 \times 3} \\ \underline{0}_{3 \times 3} \end{bmatrix} u(k) = \underline{\Phi} x(k) + \underline{\Gamma} u(k) \quad (3.34)$$

$$y(k) = \begin{bmatrix} -\underline{H}_{sd3 \times 9} & \underline{0}_{3 \times 3} & \underline{0}_{3 \times 3} \end{bmatrix} x(k) = \underline{H}_y x(k) \quad (3.35)$$

$$e(k) = \begin{bmatrix} -\underline{H}_{sd3 \times 9} & \underline{H}_{r3 \times 3} & \underline{0}_{3 \times 3} \end{bmatrix} x(k) = \underline{H}_e x(k) \quad (3.36)$$

$$x_i(k) = \begin{bmatrix} \underline{0}_{3 \times 9} & \underline{0}_{3 \times 3} & \underline{1}_{3 \times 3} \end{bmatrix} x(k) = \underline{H}_i x(k) \quad (3.37)$$

Weight Matrices

The design parameters for the optimal controller are the weight matrices. By defining these matrices, the corresponding gain matrix $\underline{L}(k)$ is calculated. A commonly used design procedure is used to define the weight matrices.

First the important parameters to be controlled by the controller is defined and their maximum values are calculated. Now the weight matrices can be defined by diagonal matrices with elements as shown in (3.38)

3.5. OPTIMAL CONTROLLER FOR ATTITUDE CONTROL

$$\mathbf{Q}_1(i,i) = \frac{1}{x_{i,max}^2} \quad \mathbf{Q}_2(i,i) = \frac{1}{u_{i,max}^2}. \quad (3.38)$$

The purpose for the controller is to make precise pointing and keep the power consumption at a low level. The important parameters are defined to be the quaternion states and the input signals N_{mw} . As defined in Appendix A the norm of a quaternion is 1, i.e. $\|q\| = 1$ so this is used as the maximum value. It is decided that the maximum angular velocity for the momentum wheels is $10000 \text{ [rpm]} = 1047 \text{ [rad/s]}$ so the maximum torque for a momentum wheel is given as in (3.39)

$$L = \omega \cdot I = 1047 \cdot 137.7 \cdot 10^{-9} = 144.72 \cdot 10^{-6} \text{ [kg} \cdot \text{m}^2/\text{s]}. \quad (3.39)$$

The performance function in Equation (3.32) defines five weight matrices for design \underline{Q}_{Ne} , \underline{Q}_{Ni} , \underline{Q}_{1e} , \underline{Q}_{1i} and \underline{Q}_2 .

The \underline{Q}_{1e} matrix will punish the output error signal $e(k)$. \underline{Q}_{1e} is defined to be

$$\underline{Q}_{1e} = \begin{bmatrix} \frac{1}{q_{max}^2} & 0 & 0 \\ 0 & \frac{1}{q_{max}^2} & 0 \\ 0 & 0 & \frac{1}{q_{max}^2} \end{bmatrix}. \quad (3.40)$$

The \underline{Q}_{1i} matrix will punish integral states $x_i(K)$. By rewriting the performance index it can be seen that \underline{Q}_{1i} and \underline{Q}_{1e} are connected and therefore $\underline{Q}_{1i} = \underline{Q}_{1e}$. The \underline{Q}_2 weight matrix punishes the input signals $u(k)$. The \underline{Q}_2 matrix is defined to be

$$\underline{Q}_2 = \begin{bmatrix} \frac{1}{N_{mw,max}^2} & 0 & 0 \\ 0 & \frac{1}{N_{mw,max}^2} & 0 \\ 0 & 0 & \frac{1}{N_{mw,max}^2} \end{bmatrix}. \quad (3.41)$$

Because the main states are the quaternion states, the weight matrices \underline{Q}_{Ne} and \underline{Q}_{Ni} are set to \underline{Q}_{1e} and \underline{Q}_{1e} . Thereby the design parameters for the optimal controller is defined, when the controller is implemented it is tuned by adjusting the weight matrices.

The Gain Matrices

The design is now complete and the corresponding gain matrices can be calculated using the MATLAB function `dlqr` which takes the discrete equations and calculates the optimal controller using the Riccati equations

$$\underline{L} = \text{dlqr}(\underline{\Phi} \quad \underline{\Gamma} \quad \underline{Q}_1 \quad \underline{Q}_2). \quad (3.42)$$

The weight matrix \underline{Q}_1 by (3.42) is given by rewriting the performance index to the normal form and then \underline{Q}_1 is given as [Optimal, page 54]

$$\underline{Q}_1 = \underline{H}_e^T \underline{Q}_{1e} \underline{H}_e + \underline{H}_i^T \underline{Q}_{1i} \underline{H}_i. \quad (3.43)$$

The gain matrix can now be calculated

3.5. OPTIMAL CONTROLLER FOR ATTITUDE CONTROL

$$u(k) = -\underline{K}(0)x(k) = \begin{bmatrix} \underline{L}_s(0) & \underline{L}_r(0) & \underline{L}_i(0) \end{bmatrix} \begin{bmatrix} x_s(k) \\ x_r(k) \\ x_i(k) \end{bmatrix}, \quad (3.44)$$

where \underline{L}_s is the optimal proportional gain matrix, \underline{L}_r is the gain matrix for the reference and \underline{L}_i is the gain matrix for the integral.

Diagram

In Figure 3.11 a block diagram is illustrated for the implemented optimal controller calculated from the above theory and design.

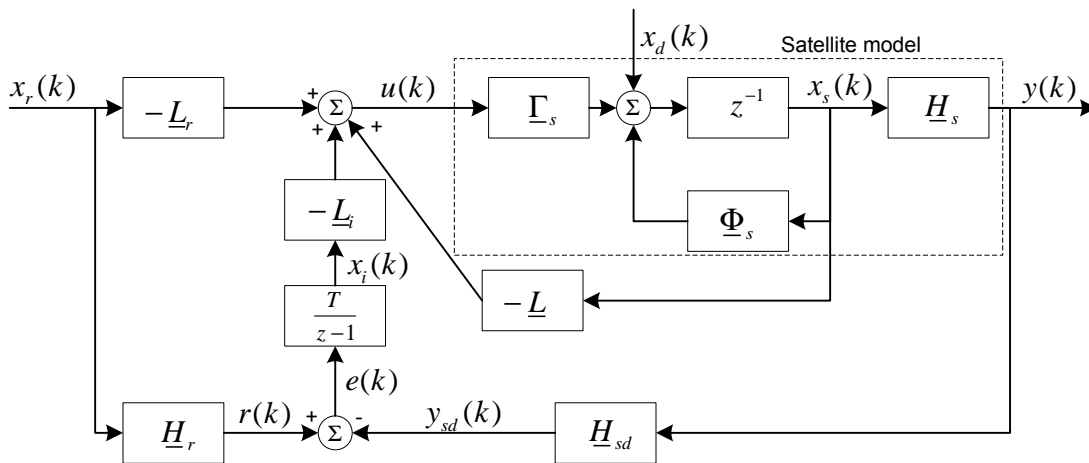


Figure 3.11: The implemented optimal controller.

3.5.3 Implementation

The optimal controller is implemented in the SIMULINK model as illustrated in Figure 3.11 though the interface in the SIMULINK model requires some modifications for operation. The optimal controller shall be stable, it shall work in the CRF, it shall interface to the momentum wheel controller and it shall be able to obtain any given attitude by rotating by a given reference quaternion.

Stability

While the controller will be used for attitude control, the measured quaternion reference will be changed and thereby be different from the working point. In order to avoid having to linearize the system for every new working point and thereby calculating a new controller, it is assumed that the controller will work if it prove to be stable. The stability is checked by looking at the closed loop poles (eigenvalues), which have to be inside the unit circle. The eigenvalues are found in MATLAB using $\text{eig}[\underline{\Phi} - \underline{\Gamma}\underline{L}]$ where \underline{L} is the calculated gain matrix. Because the reference $\underline{\Phi}_r$ is modelled by a unit matrix of size 3, the system will have eigenvalues on the unit circle, therefore the $\underline{\Phi}_r$ unit matrix is scaled with a factor 0.9999 to move these poles away from the unit circle.

Reference Frame

In order to minimize the computational operations generated by the controller the optimal controller is designed to operate in the CRF where the inertia matrix is a diagonal matrix. The controller will thereby control the satellite by rotations around the principal axes of the satellite and caused by the diagonal inertia matrix this will simplify the computational operations. The inertia matrix for the CRF is given in Subsection 2.1.2 on page 23.

Interface for Momentum Wheel Controller

The momentum wheels are controlled by adjusting the angular velocity of each wheel, but the optimal controller generates a reference torque for every wheel, therefore the torque is converted into an angular velocity. The angular momentum is given in (3.45)

$$L = \omega \cdot I. \quad (3.45)$$

In (3.46) the torque is given as a function of angular momentum

$$N = \frac{dL}{dt}. \quad (3.46)$$

Inserting (3.45) into (3.46) and solving with respect to ω gives

$$\omega = \int \frac{N}{I} dt, \quad (3.47)$$

where I is the moment of inertia of a momentum wheel. Therefore the torque input from the optimal controller is divided by the moment of inertia of the momentum wheel and integrated. A linear optimal controller will only work on small signals, therefore the angular momentum of the momentum wheel in bias is subtracted before entering the optimal controller. The angular velocity of the momentum wheels in the bias point is added to the input signal after the optimal controller. As described above the maximum angular velocity of a momentum wheel is 10000 [rpm]. The bias velocity of the momentum wheels has been chosen to 5500 [rpm] in order to avoid saturating the wheel at 0 [rpm] which will cause the non-linear dry friction and bring down the life time of the momentum wheels. The bias angular velocity will then be 576 [rad/s]. From (3.45) the angular momentum can be calculated as

$$L = \omega \cdot I = 79.31 \cdot 10^{-6} [\text{kg} \cdot \text{m}^2/\text{s}]. \quad (3.48)$$

Magnetorquers Feed Forward

For some attitude manoeuvring e.g. a 180[°] rotation the momentum wheels will saturate, therefore the desaturation controller is used to desaturate the momentum wheels when they are near their saturation point. The desaturation torque generated by the magnetorquers will cause disturbances in the manoeuvring and attitude, in order to compensate for this a feed forward coupling from the torque of the magnetorquers N_{mt} is inserted in the optimal controller.

3.5. OPTIMAL CONTROLLER FOR ATTITUDE CONTROL

Reference Quaternion Interface

This controller is for attitude control, therefore the important parameter for control is the rotation quaternion. The goal is to bring the satellite to a given attitude or rotation by rotating the satellite as described by the quaternion error (q_{err}) and thereby bring the quaternion error to origo (operation point). The rotational difference (q_{err}) between the current measured and the desired attitude has to be calculated which is given in Equation A.9 on page 83 to be

$$q_{err} = q_{att}q_{ref}^{-1}, \tag{3.49}$$

where q_{att} is the measured attitude quaternion and q_{ref} is the reference attitude quaternion given in the flight plan from ground or as a default reference.

From the linearized system in Subsection 2.7.3 on page 40 it can be derived that it is possible to achieve two attitudes because the controller only controls $q_{ref,1:3}$ so the fourth element in the quaternion is free. To avoid this, the error calculation is done with respect to (3.49) but when $q_{err,1:3}$ is calculated it will be multiplied with the sign of the $q_{err,4}$ in order to get the correct attitude. This is possible because

$$q_{err} = -q_{err}, \tag{3.50}$$

represent the same rotation.

The interface for the reference quaternion in SIMULINK can be seen in Figure 3.12.

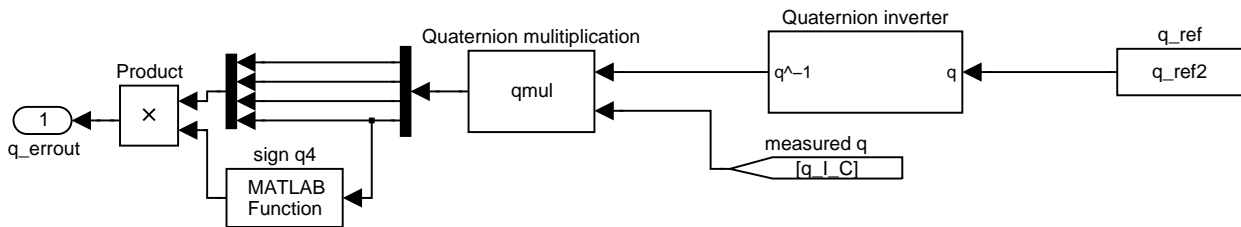


Figure 3.12: Interface for the reference quaternion. q_{ref} is the reference quaternion from the flight plan or a default desired attitude for the satellite. Measured q is the quaternion given by the measured attitude in CRF and q_{errout} is the input to the optimal controller.

SIMULINK Model

In Figure 3.13 the implemented SIMULINK model is shown.

The state interface is inserted by L_{mw} , Ω_c and the above described q_{errout} . N_{mt} feed forward is the feed forward from the desaturation controller. The above calculated gains and integral state for the optimal controller can be seen as well as the interface for the momentum wheel controller.

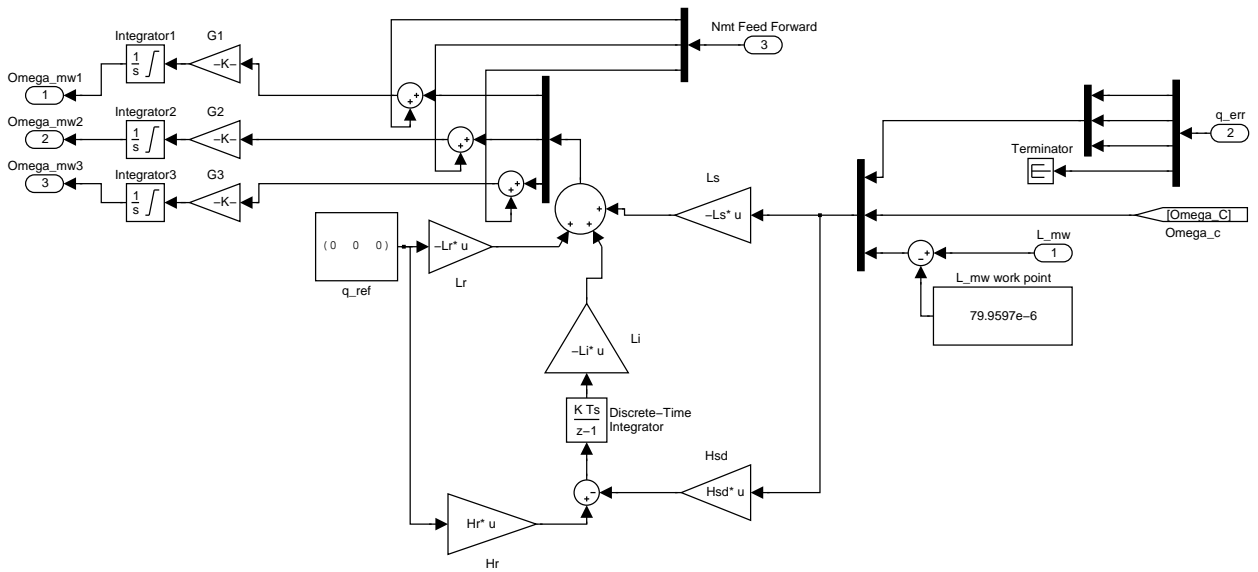


Figure 3.13: The implemented optimal controller.

3.5.4 Test

The tests are carried out by simulation in SIMULINK with the desaturation controller described in Section 3.6 on page 74 enabled.

Test Requirements

The requirements for the attitude controller in Section 1.5.2 on page 13 states that the satellite must be able to turn π [rad] over a period of 693 [s], the time of a ground station pass, in order to point the antenna towards the ground station. Therefore the satellite shall be able to maintain an angular velocity of minimum

$$\frac{\pi}{693} = 0.0045 \text{ [rad/s]} \quad (3.51)$$

during an overflight to ensure a stable communication link.

The second requirement is that the satellite must be able to point with an accuracy of $0.087 \text{ [rad]} \approx 5 \text{ [}^\circ\text{]}$.

Test Cases

Case 1

This test shall verify that the satellite is able to turn π [rad] during the time of a ground station pass. A set of quaternions corresponding to a rotation of π [rad] during 693 [s] are calculated and used as input to the SIMULINK model.

Case 2

The objective of this test is to verify that the ACS system is able to point in a certain direction with an accuracy better than $0.087 \text{ [rad]} \approx 5 \text{ [}^\circ\text{]}$. Five quaternions pointing in different directions, relative to the initial satellite

3.5. OPTIMAL CONTROLLER FOR ATTITUDE CONTROL

attitude, are calculated and it shall be verified by simulation that the pointing error is within the requirement. The properties of the generated quaternions are listed in Table 3.2.

Quaternion	Axes of rotation	Angle
Q1	x-axis	5 [°]
Q2	y-axis	25 [°]
Q3	z-axis	15 [°]
Q4	z-axis	-10 [°]
Q5	x-axis	35 [°]

Table 3.2: Quaternions for the pointing test.

Case 3

This test shall verify that the satellite is able to keep a constant attitude during a whole orbit. An attitude reference quaternion is set and a simulation of at least 5926.2 [s] is carried out. If the attitude is within ± 2.5 [°] at least 95% of the time the test is considered a success.

Test Results

Case 1

The results of the rotation test are shown in Figure 3.14. The quaternion reference is shown in 3.14 (a) and the quaternion error is shown in 3.14 (b). Figure 3.14 (c) depicts the angular velocity of the satellite and 3.14 (d) the rotation of the satellite about the x, y and z axes. Figure 3.14 (e) show the angular momentum of the momentum wheels.

The rotation of the satellite starts at $t=100$ [s] and stops at $t=793$ [s] and the largest quaternion error exists at these two points because the satellite must accelerate and decelerate respectively. In Figure 3.14 (c) and (d) it can be seen that the angular velocity of the satellite about the y-axis is stable during the rotation and that the final angle about the y-axis is 180 [°]. The angular momentum of the momentum wheels, depicted in Figure 3.14 (e), deviates from the bias point during the rotation and the momentum wheels are close to saturation. This means that the rotation manoeuvre pushes the satellite to its limits, however the rotation is successful and the test has verified that it is possible to rotate 180 [°] during a ground station pass.

Case 2

The results of the rotation test are shown in Figure 3.15. The quaternion reference is shown in 3.15 (a) and the satellite quaternion is shown in 3.15 (b). The quaternion error is shown in 3.15 (c) and Figure 3.15 (d) depicts the rotation of the satellite from its initial attitude. Figure 3.15 (e) shows the pointing error and a close up of the error is shown in Figure 3.15 (f).

Figure 3.15 (d) shows that the satellite turns to the expected angles and the pointing error in 3.15 (e) and (f) shows that once the satellite has settled the pointing error is below 0.01 [°]. This is well below the requirement of 0.087 [rad] ≈ 5 [°] and therefore the test is considered a success.

Case 3

The results of the constant attitude test are shown in Figure 3.16. The quaternion reference is shown in 3.16 (a) and the satellite quaternion is shown in 3.16 (b). The quaternion error is shown in 3.16 (c) and Figure 3.16 (d) depicts the rotation of the satellite from its initial attitude. Figure 3.16 (e) shows the pointing error and a close up of the error is shown in Figure 3.16 (f). Figure 3.16 (g) shows the angular velocity of the momentum wheels.

It can be seen from Figure 3.16 (f) that the pointing error deviates less than 0.01 [°] during an orbit. Figure

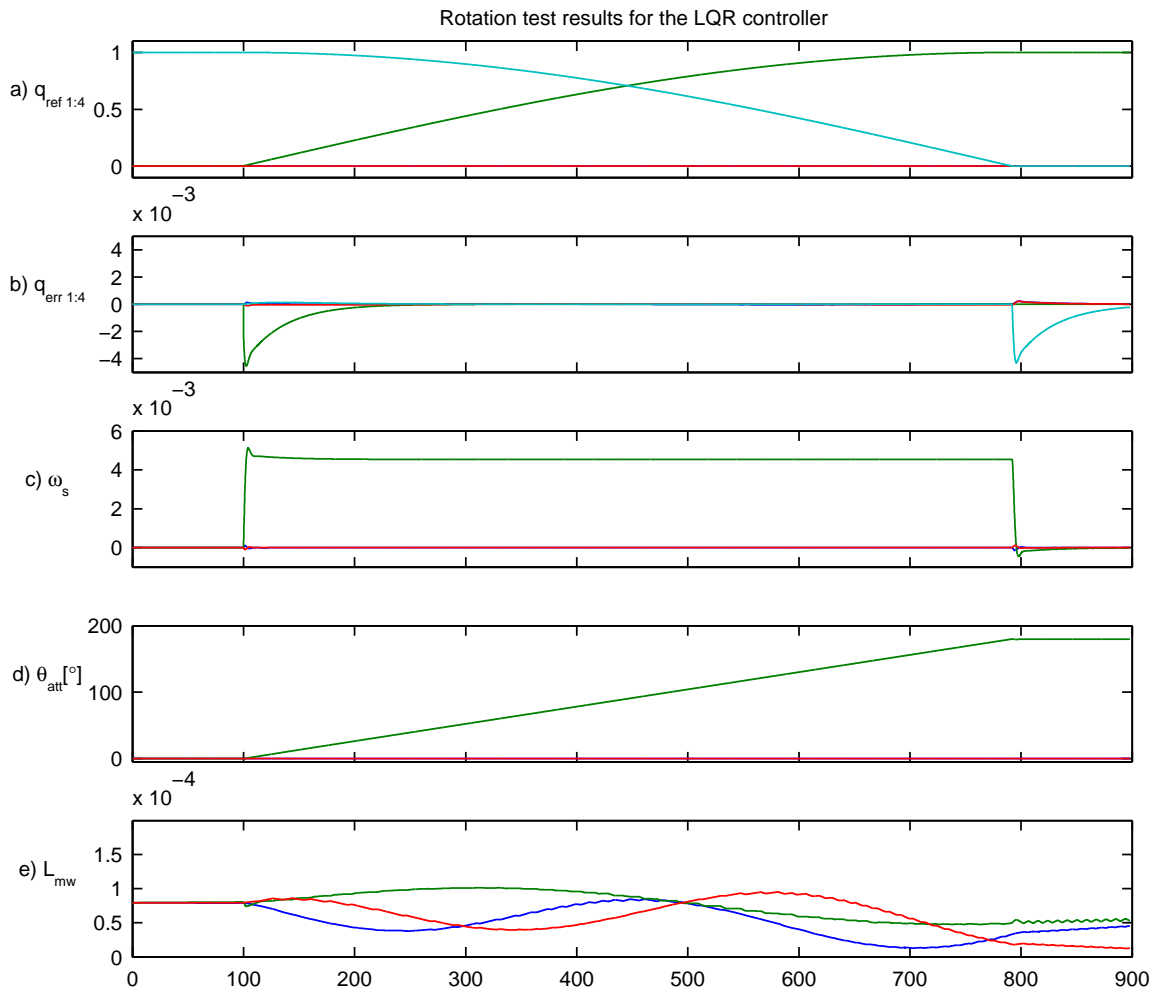


Figure 3.14: Test results for the rotation test. The x-axis is blue, the y-axis is green and the z-axis is red. The fourth quaternion element is cyan.

3.16 (g) shows that the angular velocity of the momentum wheels deviate around the bias speed of 576 [rad/s] but they never saturate and they are thereby able to keep a stable attitude of the satellite. The deviation of the pointing error is well below the requirement of $\pm 2.5 [^\circ]$ and therefore the test is considered a success.

3.5. OPTIMAL CONTROLLER FOR ATTITUDE CONTROL

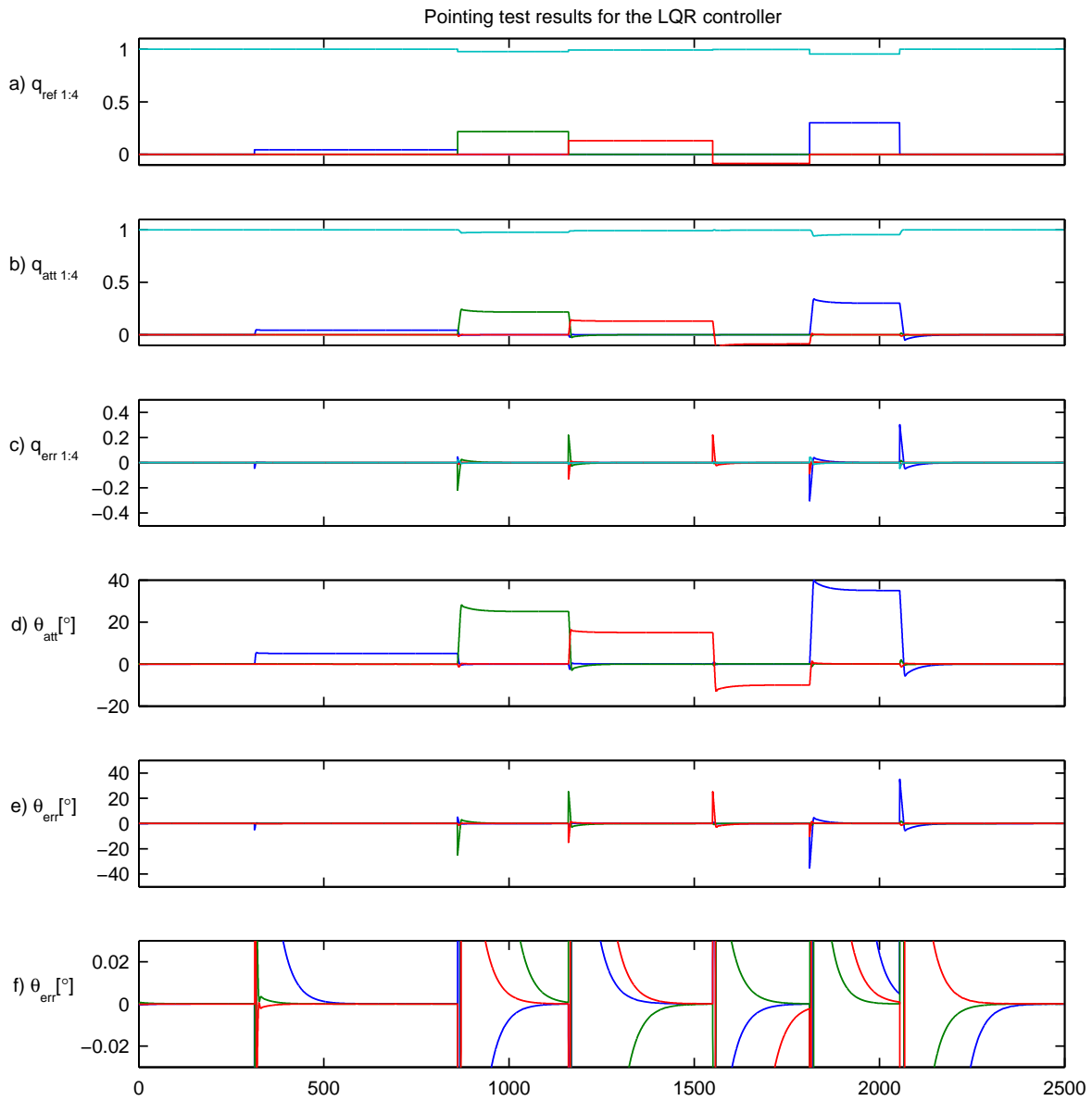


Figure 3.15: Test results for the pointing test. The x-axis is blue, the y-axis is green and the z-axis is red. The fourth quaternion element is cyan.

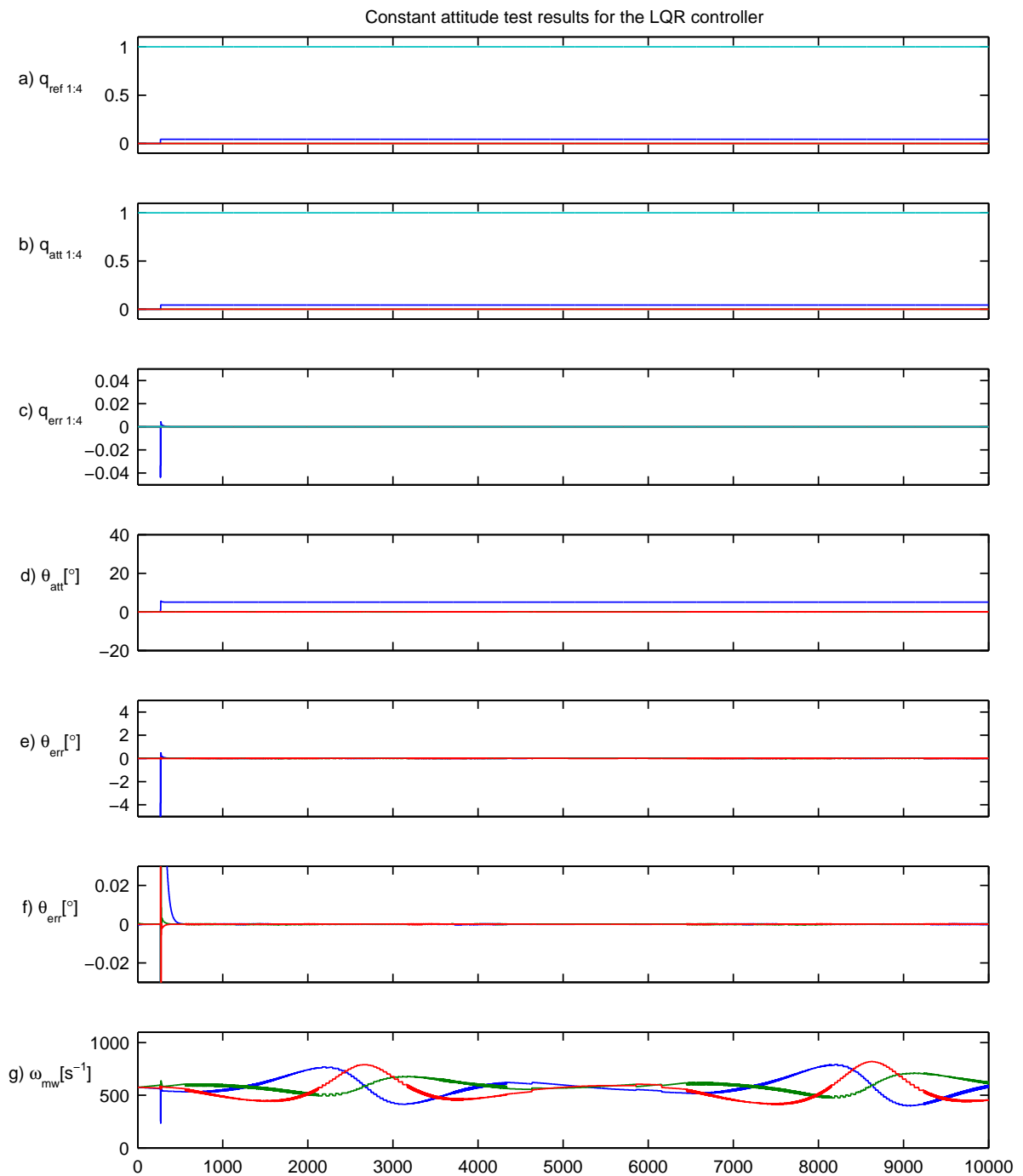


Figure 3.16: Test results for the constant attitude test. The x-axis is blue, the y-axis is green and the z-axis is red. The fourth quaternion element is cyan.

3.6 Desaturation Controller

When the attitude of the satellite is controlled by the momentum wheels they will absorb disturbances acting on the satellite and eventually reach their saturation limit. When this happens, they will no longer be able to maintain a stable attitude of the satellite. To avoid this, angular momentum must be moved from the satellite to the inertial system, which in this case is the Earth, by applying an external torque with the magnetorquers.

3.6.1 Desaturation Strategy

There are different ways to desaturate the momentum wheels. Some of the possibilities are:

- **Periodic B-dot**
The momentum wheels are set to their bias speed and the B-dot controller is activated until the satellite has been detumbled. This method will cause the satellite to spin and therefore it is not possible to control the attitude while desaturating the momentum wheels.
- **Continuous Desaturation**
Desaturation while maintaining attitude stability can be achieved with a magnetorquer controller that minimizes the momentum wheel bias error. The attitude controller shall be activated while a bias minimizing controller desaturates the momentum wheels.
- **Threshold Desaturation**
This method is the same as continuous desaturation mentioned above, but it is only activated when the bias error rises above a certain turn-on level. The desaturation controller shall be deactivated when the bias error falls below a certain off-level. The two different levels and a Schmitt trigger are introduced in order to avoid fast on and off switching.

The threshold desaturation controller is chosen for the AAUSAT-II, because it can be used in pointing mode and it is only active when necessary and thereby it is preserving power.

3.6.2 Controller Design

The objective of the controller is to desaturate the momentum wheels. This is done by unloading angular momentum, by the means of magnetic interaction with the Earth. By transferring angular momentum from the satellite to the Earth the bias error of the momentum wheels can be decreased. When the angular momentum of the momentum wheels have deviated sufficient from their bias point the controller is activated until the bias error again is within an acceptable range.

It is not always possible to desaturate the momentum wheels because of the two axes control constraint of the magnetorquers. The torque from the magnetorquers acting on the satellite is given by

$$N_{mt} = m_{mt} \times B_s, \quad (3.52)$$

where m_{mt} is the control input vector and B_s is the magnetic field of the Earth in the spacecraft frame.

The control law for the desaturation controller is given by

$$m_{mt} = C_{desat}(L_{err} \times B_s), \quad (3.53)$$

where L_{err} is the momentum wheel bias error given by

$$L_{err} = L_{wheel} - L_{wheel-bias}. \quad (3.54)$$

From (3.52) it can be seen that N_{mt} always lies in the normal plane to B_s . This means that only the part of L_{err} that is lying in the plane orthogonal to B_s , can be reduced by means of the magnetorquers. Therefore it is only possible to fully desaturate the momentum wheels, when L_{err} is orthogonal to B_s and it is not possible to remove any angular momentum from the momentum wheels when L_{err} is parallel to B_s .

If the desaturation controller is allowed to run while L_{err} is parallel to B_s it will only introduce an error and consume power, and none of these actions are beneficial for the satellite. However the amount of power consumed will be small because the magnitude of m_{mt} is dependent on the angle between B_s and L_{err} .

The supervisor that controls the desaturation controller shall use the part of L_{err} that lies in the normal plane to B_s given by

$$l_{err} = \|L_{err} \times B_s\|, \quad (3.55)$$

in order to determine when to enable the desaturation controller. This will ensure that the controller only is enabled while it can remove angular momentum error from the momentum wheels. The SIMULINK implementation of the desaturation controller and supervisor is shown in Figure 3.17.

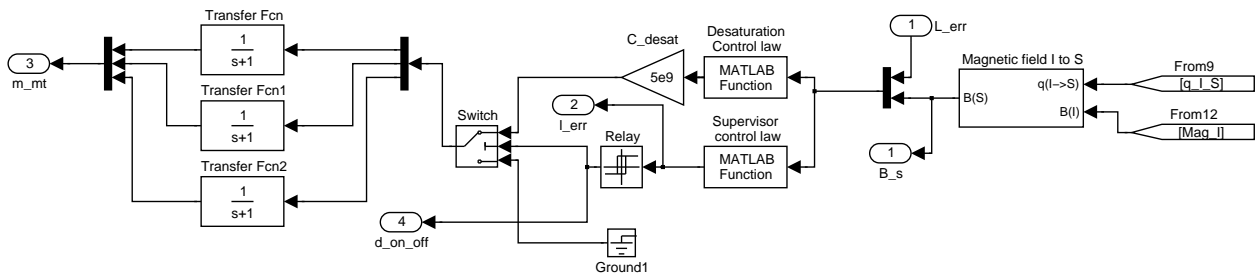


Figure 3.17: SIMULINK implementation of desaturation controller and supervisor.

3.6.3 Stability

The desaturation controller will render the system unstable if no stabilizing attitude controller is active and therefore the attitude controller must be able to maintain a stable attitude while the momentum wheels are desaturated.

3.6.4 Test

The desaturation controller has been tested with the LQR controller in SIMULINK with these parameters:

$$\begin{aligned} C_{desat} &= 5 \cdot 10^7 \\ l_{err\ on} &= 2 \cdot 10^{-11} \\ l_{err\ off} &= 7 \cdot 10^{-11} \\ L_{bias} &= [7.96 \ 7.96 \ 7.96] \cdot 10^{-6} \text{ [kgm}^2\text{/s]} \end{aligned}$$

3.6. DESATURATION CONTROLLER

The test results can be seen in Figure 3.18

During the test some manoeuvres have been simulated as can be seen from the attitude quaternion in Figure 3.18 (a) and 3.18 (b). Figure 3.18 (c) shows the angular velocity of the momentum wheels and Figure 3.18 (d) shows the angular velocity of the satellite. In Figure 3.18 (e) and 3.18 (f) the torque applied from the magnetorquers and the angular momentum error in the momentum wheels are shown. Figure 3.18 (g) shows the norm of the error that can be desaturated and Figure 3.18 (h) shows the on/off signal to the desaturation controller.

From Figure 3.18 it can be seen that the desaturation controller desaturates the momentum wheels after each manoeuvre. The supervisor shuts off the desaturation controller when no more angular momentum can be removed from the wheels and this can be seen at $t=90$ [s] and $t=800$ [s] where the magnitude of L_{err} is different at shut-off time. From $t=800$ [s] and forward no more manoeuvres are carried out and it is shown that the desaturation controller is activated briefly at $t=850$ [s] and $t=940$ [s] because it is possible to remove more angular momentum. This shows that the desaturation controller will keep the error at a minimum and thereby enable the LQR controller to keep the satellite stable over longer periods of time.

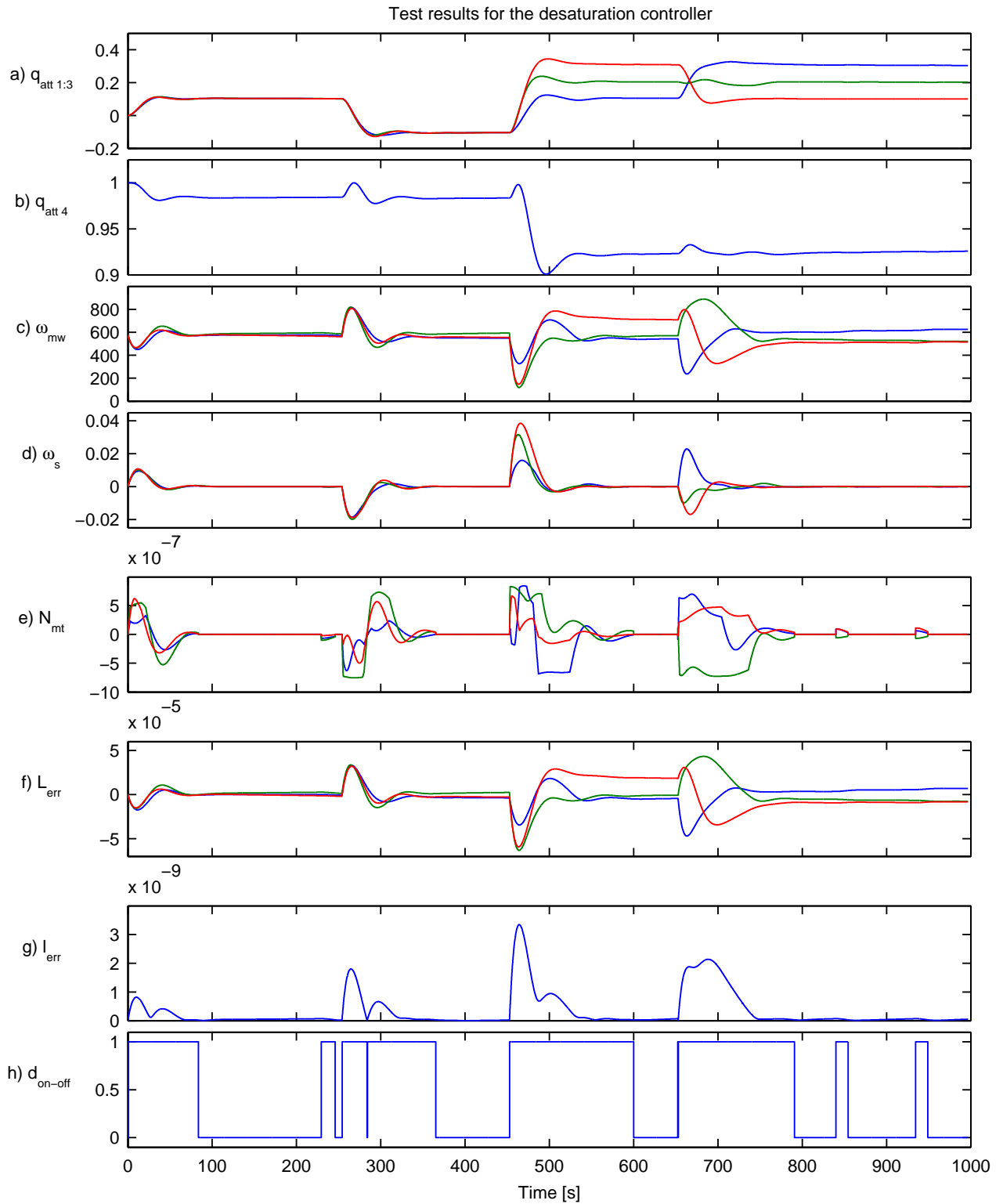


Figure 3.18: Test results from the desaturation controller with the LQR controller. The x-axis is blue, the y-axis is green and the z-axis is red.

Conclusion

This report concerns the development of the attitude control system for AAUSAT-II. Requirements have been outlined and the satellite and space environment have been modelled in SIMULINK. These assignments have been made in collaboration with the attitude determination system team, group 05GR833. Based on these models, different controllers have been developed which together constitute a complete ACS system which enables the satellite to detumble and do pointing manoeuvres. The controllers have been tested in the SIMULINK simulation environment.

System demands for the ADCS system have been outlined in Section 1.5 on page 12. These demands concern:

- Detumbling below 0.0021 [rad/s] within three orbits.
- Maintaining an average minimum angular velocity of 0.0045 [rad/s] during an overflight of the ground station.
- Maintaining a given attitude within 0.087 [rad].
- Implementation such that new controller algorithms may be uploaded.

These demands are to be fulfilled by the overall ADCS system, but have been applied to the ACS system alone, since the ADS system and the ACS system have not yet been integrated.

In collaboration with the ADS team, group 05GR833, a model of the environment for the satellite have been developed, including the spacecraft dynamics and kinematics. Different reference frames have been defined in order to reduce the complexity of the model and computational power needed to run the ADCS system on-board the satellite. A simulation library, containing the satellite and space environment has been developed in SIMULINK. It contains both satellite sensors and actuators, but since the ACS system does not use the sensors directly, the modelling of those have been left out of this report. The simulation environment contains disturbances in space and parts of the model have been made generic, offering the possibility of simulating the behaviour of other satellites.

Only verification of the orbit model and the magnetic field model has been conducted. Verifications of the other simulation models have not been carried out, because reliable test methods are hard to find. No test data of the satellite in orbit is available and hence there is no data to test the model up against.

A supervisor for managing the controllers of the attitude control system has been designed in order to switch between detumbling mode and pointing mode. The supervisor also detects if the angular velocity of the satellite increases in pointing mode, and switches to detumbling mode if it does, to ensure the safety of the satellite.

A detumbling controller, based on the B-dot algorithm has been designed to make the satellite follow the magnetic field of the Earth. The detumbling controller is designed as a simple and robust controller to increase the possibility of being able to detumble the satellite after deployment from the launch vehicle. Tests of the B-dot controller indicate that it is capable of reducing the angular velocity of the satellite below 0.0021 [rad/s] within the specified three orbits. It is able to detumble the satellite within approximately one orbit and hence performs better than expected.

An optimal controller was designed for the momentum wheels to control the attitude of the satellite. To keep

the momentum wheels from reaching their limits of angular velocity, a supervisor to control the desaturation of the momentum wheels, has been designed. This composition provides the pointing controller for the satellite. Tests show that the pointing controller is capable of maintaining a given attitude of the satellite within 0.087 [rad]. Furthermore the pointing controller is capable of maintaining an average angular velocity of minimum 0.0045 [rad/s] which is necessary in order to be able to point the antennas towards the ground station during an ideal overflight.

The tests of the controllers imply that the attitude of the satellite may be controlled using the designed controllers. Though the controllers have not yet been implemented on the satellite, as no hardware is complete yet. Furthermore the ACS also requires testing with the ADS and the ADCS hardware teams before it can be verified if the complete ADCS system meets the demands. Even if ACS and ADS alone are able to fulfil the system demands for ADCS, there is no guarantee that the systems combined are stable as they depend on each other. Therefore the complete ADCS requires combined testing before implementation on the satellite.

4.1 Future Work

Before the ACS may be considered finished, some improvements need to be implemented. The detumbling controller has been tested while switching the magnetorquers on and off to be able to use the magnetometers for measuring the magnetic field. This feature needs to be implemented on the desaturation controller as well.

When the controllers have been tuned and implemented to fulfil all requirements from the hardware, the controllers may be implemented on the satellite. This requires the models in SIMULINK to be ported to the on-board computer on the satellite. After implementation it needs to be tested if new controllers can be uploaded to the ADCS system, in order to fulfil the last statement of the system demands.

Bibliography

- [04GR830a] Group 04GR830a Aalborg University. *Attitude Control System for AAUSAT-II*. 2004. /doc/ACS04.pdf on the enclosed CD-ROM.
- [04GR830b] Group 04GR830b Aalborg University. *Attitude Determination System for AAUSAT-II*. 2004. /doc/ADS04.pdf on the enclosed CD-ROM.
- [ADS05] Group 05GR833 Aalborg University. *Attitude Determination System for AAUSAT-II*. 2005. /doc/ADS05.pdf on the enclosed CD-ROM.
- [Anderson et al.] Dennis J. Sweeney David R. Anderson and Thomas A. Williams. *Modern Business Statistics with Microsoft Excel*. South Western, 2003. ISBN 0-324-12174-1.
- [Bhanderi] Dan Bhanderi. *Spacecraft Attitude Determination with Albedo Corrected Sun Sensor Measurements.*, 2005. Not Published.
- [Braeunig] Robert Braeunig. *Orbital Mechanics*, 2005. <http://www.braeunig.us/space/orbmech.htm>.
- [Chou] *IEEE Transactions on Robotics and Automation*. Quaternion kinematic and dynamic differential equations. Jack C. K. Chou. nr. 1. February 1992. side 53 –64.
- [COM] Group 05GR834 Aalborg University. *The AAUSAT-II Communication System*. 2005. /doc/com.pdf on the enclosed CD-ROM.
- [CubeSat ACS] Michael Kvist Frederiksen Torben Graversen and Søren Vejlgård Vedstesen. *Attitude Control System for AAU CubeSat*. 2002. /doc/cubesat-ACS.pdf on the enclosed CD-ROM.
- [CubeSat ADS] Kristian Krogh and Elmo Schreder. *Attitude Determination for AAU CubeSat*. 2002. /doc/cubesat-ADS.pdf on the enclosed CD-ROM.
- [Franklin et al.] Michael Workman Gene F. Franklin, J. David Powell. *Digital Control of Dynamic Systems*. Addison Wesley Longman, Inc., 1998. ISBN 0-201-82054-4.
- [MECH-WWW] Mechanical group of AAUSAT-II. "Mechanical System - AAUSAT-II", May 17th 2005. http://www.aausatii.auc.dk/wiki/index.php/Mechanical_System/doc/satellite-frame.jpg on the enclosed cd.
- [IAGA V-MOD] IAGA V-MOD Working Group. *IAGA V-MOD Geomagnetic Field Modeling: International Geomagnetic Reference Field IGRF-10*, Downloaded May 2005. <http://www.ngdc.noaa.gov/IAGA/vmod/igrf.html>.
- [ADCS HW ICD] ADCS Hardware. *ADCS Hardware ICD*, May 2005. /doc/adcs-icd.txt on the enclosed CD-ROM.
- [Hmnao] Hmnao. *The Astronomical Almanac for the Year 2003*. The Stationery Office, 2003. ISBN 0-11-887320-2.
- [Hoots & Roehrich] Felix R. Hoots and Ronald L. Roehrich. *SPACETRACK REPORT NO. 3 - Models for Propagation of NORAD Element Sets*, 1980. <http://celestrak.com/NORAD/documentation/spacetrk.pdf> /doc/spacetrk.pdf on the enclosed CD-ROM.

- [Hughes] Peter C. Hughes. *Spacecraft Attitude Dynamics*. Wiley and Sons, Inc, 1986. ISBN 0-471-81842-9.
- [Kelso] T. S. Kelso. *Frequently Asked Questions: Two-Line Element Set Format*, 1998. <http://celestrak.com/columns/v04n03/>.
- [Kuipers] Jack B. Kuipers. *Quaternions and Rotation Sequences: A Primer with Applications to Orbits, Aerospace, and Virtual Reality*. Princeton University Press, 2002. ISBN 0-691-10298-8.
- [MECH-Mail] MECH. *Email from MECH concerning the inertia matrix of the satellite.*, 2005. /doc/inertia_mech.pdf on the enclosed CD-ROM.
- [Maxon RE10] Maxon Motor. *Maxon DC motor RE 10 data sheet*, April 2005. http://www.maxonmotor.com/docsx/Download/catalog_2005/Pdf/05_053_e.pdf/datasheets/Maxon_RE-10.pdf on the enclosed CD-ROM.
- [NASA/GSFC] Ozone Processing Team NASA/GSFC Code 916. *Total Ozone Mapping Spectrometer*. NASA and Goddard Space Flight Center, Downloaded April 2005. <http://toms.gsfc.nasa.gov>.
- [Powell et al.] J. David Powell Gene Franklin and Abbas Emami-Naeini. *Feedback Control of Dynamic Systems*. Prentice-Hall, Inc., 2002. ISBN 0-13-098041-2.
- [LM628] National Semiconductor. *LM628/LM629 Precision Motion Controller*, Downloaded March 2005. <http://www.national.com/ds.cgi/LM/LM628.pdf/datasheets/LM628.pdf> on the enclosed CD-ROM.
- [Serway & Beichner] Raymond A. Serway and Robert J. Beichner. *Physics For Scientists and Engineers with Modern Physics*. Harcourt College Publishers, 2000. ISBN 0-03-022657-0.
- [Sidi] Marcel J. Sidi. *Spacecraft Dynamics and Control*. Cambridge University Press, 1997. ISBN 0-521-55072-6.
- [Space Track] Space-Track.Org. *Space Track - The Source for Space Surveillance Data*, Downloaded April 2005. <http://www.space-track.org>.
- [BGS] British Geological Survey. *An Overview of the Earth's Magnetic Field*, Downloaded May 2005. <http://www.geomag.bgs.ac.uk/earthmag.html>.
- [Princeton] Princeton Satellite Systems. *Princeton Satellite Systems, moonV2.m*, 1993. /aausatii-sim/lib/space_environment_emulation/ephemeris/MoonV2.m on the enclosed CD-ROM.
- [Optimal] Ole Sørensen. *Introduction to Optimal Control*, August 1995. /doc/optimalcontrol.pdf on the enclosed CD-ROM.
- [CPSU] California Polytechnic State University. *CubeSat Program*, 2005. http://cubesat.calpoly.edu/_new/index.html.
- [Weisstein Cofactor] Eric W. Weisstein. *Cofactor*, Downloaded March 2005. <http://mathworld.wolfram.com/Cofactor.html>.
- [Weisstein Ellipse] Eric W. Weisstein. *Ellipse*, Downloaded March 2005. <http://mathworld.wolfram.com/Ellipse.html>.
- [Wertz & Larson] James R. Wertz and Wiley J. Larson. *Space Mission Analysis*. Microcosm Press and Kluwer Academic Publishers, 1999. ISBN 1-881883-10-8.
- [Wertz] James R. Wertz. *Spacecraft Attitude Determination and Control*. Kluwer Academic Publishers, 1978. ISBN 90-277-0959-9.
- [Wie] Bong Wie. *Space Vehicle Dynamics and Control*. American Institute of Aeronautics and Astronautics, Inc, 1998. ISBN 1-56347-261-9.
- [Wisniewski] Rafał Wiśniewski. *Satellite Attitude Control Using Only Electromagnetic Actuation*. Department of Control Engineering, Aalborg University, 1996. /doc/Wisniewski.pdf on the enclosed CD-ROM.

Quaternions

A

Since the kinematics of the satellite are best expressed in quaternion form for calculation purposes this appendix includes quaternion definitions and describes the fundamental algebraic properties of quaternions. As sources for this appendix [Wertz, page 758-759] and [Chou] are used.

A.1 Quaternion Definitions

A quaternion is a hyper complex number and can be defined as

$$q = \hat{i}q_1 + \hat{j}q_2 + \hat{k}q_3 + q_4, \quad (\text{A.1})$$

where the hyperimaginary numbers \hat{i} , \hat{j} and \hat{k} satisfy the following conditions

$$\begin{aligned} \hat{i}^2 &= \hat{j}^2 = \hat{k}^2 = -1 \\ \hat{i}\hat{j} &= -\hat{j}\hat{i} = \hat{k} \\ \hat{j}\hat{k} &= -\hat{k}\hat{j} = \hat{i} \\ \hat{k}\hat{i} &= -\hat{i}\hat{k} = \hat{j}. \end{aligned} \quad (\text{A.2})$$

In (A.1) the parameter q_4 is also known as the real part or the scalar part. The first three terms in (A.1) are normally denoted the imaginary part or vector part. By defining the vector part as

$$q_{1:3} = \hat{i}q_1 + \hat{j}q_2 + \hat{k}q_3, \quad (\text{A.3})$$

it is possible to make the following representation of (A.1)

$$q = (q_{1:3}, q_4). \quad (\text{A.4})$$

When quaternions are used for attitude descriptions and generally for rotation of objects the four parameters (q_1, q_2, q_3, q_4) are defined as

$$q_1 = e_1 \sin(\theta/2) \quad (\text{A.5})$$

$$q_2 = e_2 \sin(\theta/2) \quad (\text{A.6})$$

$$q_3 = e_3 \sin(\theta/2) \quad (\text{A.7})$$

$$q_4 = \cos(\theta/2). \quad (\text{A.8})$$

where $e_1^2 + e_2^2 + e_3^2 = 1$ which implies that $\|q\| = 1$ and further that the use of this subset of quaternions performs rotations while preserving lengths.

The difference between two quaternions, i.e. the attitude error can be calculated as

$$q_{\text{err}} = q_{\text{att}} q_{\text{ref}}^{-1}, \quad (\text{A.9})$$

where q_{att} is the calculated attitude quaternion and q_{ref} is the reference attitude quaternion given by the dynamics and kinematics of the satellite.

A.2 Quaternion Algebra

The fundamental mathematical operations that will be described in this section are addition and subtraction of quaternions, the norm and inverse of quaternions and multiplication of quaternions.

A.2.1 Addition and Subtraction

The addition and subtraction of quaternions obey the associative and commutative laws and are defined as

$$q_A \pm q_B = (q_{A1:3} \pm q_{B1:3}) + (q_{A4} \pm q_{B4}). \quad (\text{A.10})$$

Quaternions are added and subtracted as normal complex numbers or vectors.

A.2.2 Norm and Inverse

The norm of a quaternion is calculated like the norm of a complex number and is defined as

$$\|q\| = \sqrt{q_1^2 + q_2^2 + q_3^2 + q_4^2}. \quad (\text{A.11})$$

The inverse of a quaternion is defined as

$$q^{-1} = \frac{q^*}{\|q\|}, \quad (\text{A.12})$$

where q^* is the complex conjugate of q , which is defined as

$$q = -\hat{i}q_1 - \hat{j}q_2 - \hat{k}q_3 + q_4 = (-q_{1:3} + q_4). \quad (\text{A.13})$$

From (A.12) it should be noticed that when the norm of a quaternion is 1 the inverse of that quaternion is equal to the complex conjugate of that same quaternion.

A.2.3 Multiplication

Quaternion multiplication is performed in the same way as multiplication of complex numbers. However, the order of operation must be taken into account as quaternion multiplication does not obey the commutative law, i.e., $q_A q_B \neq q_B q_A$.

The following expression defines the multiplication of two quaternions q_A and q_B .

A.2. QUATERNION ALGEBRA

$$q_C = q_A q_B = (q_{A_4} + \hat{i}q_{A_1} + \hat{j}q_{A_2} + \hat{k}q_{A_3})(q_{B_4} + \hat{i}q_{B_1} + \hat{j}q_{B_2} + \hat{k}q_{B_3}). \quad (\text{A.14})$$

Using (A.2) it is possible to express (A.14) as

$$\begin{aligned} q_C = q_A q_B &= \hat{i}(q_{A_1}q_{B_4} + q_{A_2}q_{B_3} - q_{A_3}q_{B_2} + q_{A_4}q_{B_1}) \\ &\quad + \hat{j}(-q_{A_1}q_{B_3} + q_{A_2}q_{B_4} + q_{A_3}q_{B_1} + q_{A_4}q_{B_2}) \\ &\quad + \hat{k}(q_{A_1}q_{B_2} - q_{A_2}q_{B_1} + q_{A_3}q_{B_4} + q_{A_4}q_{B_3}) \\ &\quad + (-q_{A_1}q_{B_1} - q_{A_2}q_{B_2} - q_{A_3}q_{B_3} + q_{A_4}q_{B_4}). \end{aligned} \quad (\text{A.15})$$

In matrix form (A.15) becomes

$$\begin{bmatrix} q_{C_1} \\ q_{C_2} \\ q_{C_3} \\ q_{C_4} \end{bmatrix} = \begin{bmatrix} q_{B_4} & q_{B_3} & -q_{B_2} & q_{B_1} \\ -q_{B_3} & q_{B_4} & q_{B_1} & q_{B_2} \\ q_{B_2} & -q_{B_1} & q_{B_4} & q_{B_3} \\ -q_{B_1} & -q_{B_2} & -q_{B_3} & q_{B_4} \end{bmatrix} \begin{bmatrix} q_{A_1} \\ q_{A_2} \\ q_{A_3} \\ q_{A_4} \end{bmatrix}. \quad (\text{A.16})$$

Given two successive rotations q_A and q_B , (A.16) gives the components of the quaternion that describes the combined rotation.

Rotations

This appendix explains different rotation methods such as the direction cosine matrix denoted attitude matrix, Euler angles and Eulers eigenaxis rotation theorem. Furthermore, this appendix deals with the derivation of the kinematic differential equation for the attitude matrix. This appendix is based on [Kuipers] and [Wie, pages 307-329].

B.1 Direction Cosine

In the following two reference frames will be used, A and B, which are both right handed and have bases formed by the orthogonal sets of unit vectors $(\hat{a}_1, \hat{a}_2, \hat{a}_3)$ and $(\hat{b}_1, \hat{b}_2, \hat{b}_3)$ respectively. A rotation matrix transforming A into B can be found by expressing the basis of B in terms of A

$$\hat{b}_1 = C_{11}\hat{a}_1 + C_{12}\hat{a}_2 + C_{13}\hat{a}_3 \quad (\text{B.1})$$

$$\hat{b}_2 = C_{21}\hat{a}_1 + C_{22}\hat{a}_2 + C_{23}\hat{a}_3 \quad (\text{B.2})$$

$$\hat{b}_3 = C_{31}\hat{a}_1 + C_{32}\hat{a}_2 + C_{33}\hat{a}_3. \quad (\text{B.3})$$

(B.1), (B.2) and (B.3) can be written in matrix notation as

$$\begin{bmatrix} \hat{b}_1 \\ \hat{b}_2 \\ \hat{b}_3 \end{bmatrix} = \begin{bmatrix} C_{11} & C_{12} & C_{13} \\ C_{21} & C_{22} & C_{23} \\ C_{31} & C_{32} & C_{33} \end{bmatrix} \begin{bmatrix} \hat{a}_1 \\ \hat{a}_2 \\ \hat{a}_3 \end{bmatrix} = {}^B_A\underline{C} \begin{bmatrix} \hat{a}_1 \\ \hat{a}_2 \\ \hat{a}_3 \end{bmatrix}, \quad (\text{B.4})$$

where ${}^B_A\underline{C}$ is called the attitude matrix as each element is calculated by projection,

$${}^B_A\underline{C} = \begin{bmatrix} \hat{b}_1 \cdot \hat{a}_1 & \hat{b}_1 \cdot \hat{a}_2 & \hat{b}_1 \cdot \hat{a}_3 \\ \hat{b}_2 \cdot \hat{a}_1 & \hat{b}_2 \cdot \hat{a}_2 & \hat{b}_2 \cdot \hat{a}_3 \\ \hat{b}_3 \cdot \hat{a}_1 & \hat{b}_3 \cdot \hat{a}_2 & \hat{b}_3 \cdot \hat{a}_3 \end{bmatrix}, \quad (\text{B.5})$$

where ${}^B_A C_{ij} = \hat{b}_i \cdot \hat{a}_j = \cos(\alpha_{ij})$ as the basis¹ of A and B consists of unit vectors and α_{ij} is the angle between the two elements. Analogously the rotation from B to A can be found as

$$\begin{bmatrix} \hat{a}_1 \\ \hat{a}_2 \\ \hat{a}_3 \end{bmatrix} = {}^A_B\underline{C} \begin{bmatrix} \hat{b}_1 \\ \hat{b}_2 \\ \hat{b}_3 \end{bmatrix}, \quad (\text{B.6})$$

¹Hence the commonly used notion direction cosine matrix.

B.2. EULER ANGLES

where

$$\underline{\underline{C}}_{\text{B}}^{\text{A}} = \begin{bmatrix} \hat{a}_1 \cdot \hat{b}_1 & \hat{a}_1 \cdot \hat{b}_2 & \hat{a}_1 \cdot \hat{b}_3 \\ \hat{a}_2 \cdot \hat{b}_1 & \hat{a}_2 \cdot \hat{b}_2 & \hat{a}_2 \cdot \hat{b}_3 \\ \hat{a}_3 \cdot \hat{b}_1 & \hat{a}_3 \cdot \hat{b}_2 & \hat{a}_3 \cdot \hat{b}_3 \end{bmatrix}. \quad (\text{B.7})$$

B.2 Euler Angles

There exist three special forms of the attitude matrix which each rotates the reference frame about one of its axes - these are called elementary rotations.

Rotation around the third axis as depicted in Figure B.1

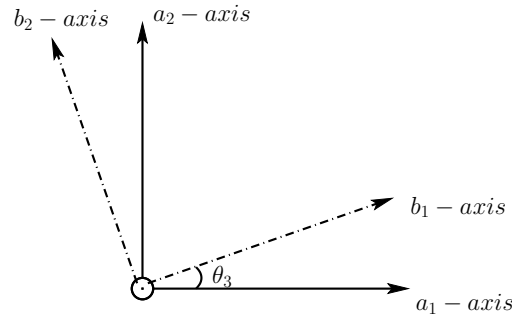


Figure B.1: Example of Euler rotation around the z-axis

yields the transformation matrix

$$\underline{\underline{C}}_3 = \begin{bmatrix} \hat{b}_1 \cdot \hat{a}_1 & \hat{b}_1 \cdot \hat{a}_2 & \hat{b}_1 \cdot \hat{a}_3 \\ \hat{b}_2 \cdot \hat{a}_1 & \hat{b}_2 \cdot \hat{a}_2 & \hat{b}_2 \cdot \hat{a}_3 \\ \hat{b}_3 \cdot \hat{a}_1 & \hat{b}_3 \cdot \hat{a}_2 & \hat{b}_3 \cdot \hat{a}_3 \end{bmatrix}. \quad (\text{B.8})$$

The two reference frames have the same third-axis and the three axes are orthogonal, hence $\hat{b}_1 \cdot \hat{a}_3 = \hat{b}_2 \cdot \hat{a}_3 = \hat{b}_3 \cdot \hat{a}_1 = \hat{b}_3 \cdot \hat{a}_2 = 0$ and $\hat{b}_3 \cdot \hat{a}_3 = 1$ This yields

$$\underline{\underline{C}}_3 = \begin{bmatrix} \hat{b}_1 \cdot \hat{a}_1 & \hat{b}_1 \cdot \hat{a}_2 & 0 \\ \hat{b}_2 \cdot \hat{a}_1 & \hat{b}_2 \cdot \hat{a}_2 & 0 \\ 0 & 0 & 1 \end{bmatrix}. \quad (\text{B.9})$$

The remaining dot products can be calculated by inspecting the projection of \hat{a}_1 and \hat{a}_2 on the \hat{b}_1 and \hat{b}_2 unit vectors which yields

$$\underline{\underline{C}}_3 = \begin{bmatrix} \cos(\theta_3) & \sin(\theta_3) & 0 \\ -\sin(\theta_3) & \cos(\theta_3) & 0 \\ 0 & 0 & 1 \end{bmatrix}. \quad (\text{B.10})$$

Similar calculations for the second- and first-axis yields

$$\underline{C}_2 = \begin{bmatrix} \cos(\theta_2) & 0 & -\sin(\theta_2) \\ 0 & 1 & 0 \\ \sin(\theta_2) & 0 & \cos(\theta_2) \end{bmatrix} \quad \text{and} \quad \underline{C}_1 = \begin{bmatrix} 1 & 0 & 0 \\ 0 & \cos(\theta_1) & \sin(\theta_1) \\ 0 & -\sin(\theta_1) & \cos(\theta_1) \end{bmatrix}. \quad (\text{B.11})$$

Note that the sign of the sine terms are opposite when rotating about the second axis, due to the properties of the righthanded reference frame.

By combining three of the Euler rotations, without having two successive rotations around the same axis, it is possible to obtain an arbitrary rotation. Thus, there exists 12 possible sets of Euler rotations.

B.3 Euler's Eigenaxis Rotation Theorem

Euler's eigenaxis rotation theorem uses a vector fixed in one reference frame during rotation rather than one of the axes. Consider a reference frame B rotated an angle of θ around a unit vector \hat{e} to coincide with reference frame A,

$$\hat{e} = e_1 \hat{a}_1 + e_2 \hat{a}_2 + e_3 \hat{a}_3 \quad (\text{B.12})$$

$$= e_1 \hat{b}_1 + e_2 \hat{b}_2 + e_3 \hat{b}_3. \quad (\text{B.13})$$

As \hat{e} is fixed in reference frame A, (B.12) and (B.13) can be expressed as an attitude matrix,

$$\begin{bmatrix} e_1 \\ e_2 \\ e_3 \end{bmatrix} = \begin{bmatrix} C_{11} & C_{12} & C_{13} \\ C_{21} & C_{22} & C_{23} \\ C_{31} & C_{32} & C_{33} \end{bmatrix} \begin{bmatrix} e_1 \\ e_2 \\ e_3 \end{bmatrix} = \underline{C} \begin{bmatrix} e_1 \\ e_2 \\ e_3 \end{bmatrix}. \quad (\text{B.14})$$

The rotation matrix \underline{C} can be expressed as three successive rotations. First A is rotated to the point where the unit vector \hat{a}_1 is aligned with \hat{e} thus constructing a new reference frame A'. This is done using the rotation matrix

$$\underline{R} = \begin{bmatrix} e_1 & e_2 & e_3 \\ R_{21} & R_{22} & R_{23} \\ R_{31} & R_{32} & R_{33} \end{bmatrix}. \quad (\text{B.15})$$

Second the reference frames A and A' are rotated around \hat{e} by an angle of θ . After this rotation the A frame will be aligned with the B frame and A' will construct a new reference frame A'' via the rotation matrix

$${}_{A'}^{A''} \underline{C} = \begin{bmatrix} 1 & 0 & 0 \\ 0 & \cos \theta & \sin \theta \\ 0 & -\sin \theta & \cos \theta \end{bmatrix}. \quad (\text{B.16})$$

It is important to notice that the relative rotation of B to A'' is equal to the rotation from A to A' i.e. ${}_{B}^{A''} \underline{C} = {}_{A}^{A'} \underline{C} = \underline{R}$.

B.4. ATTITUDE MATRIX AND KINEMATICS

The third of the three successive rotations needs to align the reference frame A'' with B. This is done by rotating A'' through an inverse matrix $\underline{R}^{-1} = \underline{R}^T$ since ${}^B_{A''}\underline{C} = \underline{R}^{-1}$. It is now possible to describe the rotation from A to B by the attitude matrix ${}^B_{A'}\underline{C}$ expressed as

$${}^B_{A'}\underline{C} = {}^B_{A''}\underline{C} {}^{A''}_{A'}\underline{C} {}^{A'}_{A}\underline{C}. \quad (\text{B.17})$$

By inserting (B.15) and (B.16) in (B.17) the elements of the matrix ${}^B_{A'}\underline{C}$ can be expressed as

$$\begin{aligned} C_{11} &= e_1^2 + (R_{21}^2 + R_{31}^2) \cos(\theta) \\ C_{12} &= e_1 e_2 + (R_{21} R_{22} + R_{31} R_{32}) \cos(\theta) + (R_{21} R_{32} - R_{22} R_{31}) \sin(\theta) \\ C_{13} &= e_1 e_3 + (R_{21} R_{23} + R_{31} R_{33}) \cos(\theta) + (R_{21} R_{33} - R_{23} R_{31}) \sin(\theta) \\ &\vdots \\ C_{33} &= e_3^2 + (R_{23}^2 + R_{33}^2) \cos(\theta). \end{aligned} \quad (\text{B.18})$$

Utilizing the orthonormality condition $\underline{R}^T \underline{R} = \underline{I}$, yields

$$\begin{aligned} e_1^2 + R_{21}^2 + R_{31}^2 &= 1 \\ e_2^2 + R_{22}^2 + R_{32}^2 &= 1 \\ e_3^2 + R_{23}^2 + R_{33}^2 &= 1 \\ e_1 e_2 + R_{21} R_{22} + R_{31} R_{32} &= 0 \\ e_2 e_3 + R_{22} R_{23} + R_{32} R_{33} &= 0 \\ e_1 e_3 + R_{21} R_{23} + R_{31} R_{33} &= 0, \end{aligned}$$

and calculating the cofactor of each of the elements (e_1, e_2, e_3) [Weisstein Cofactor],

$$\begin{aligned} e_1 &= R_{22} R_{33} - R_{32} R_{23} \\ e_2 &= R_{23} R_{31} - R_{21} R_{33} \\ e_3 &= R_{21} R_{32} - R_{31} R_{22}, \end{aligned}$$

it is possible to obtain the rotation matrix

$${}^B_{A'}\underline{C} = \begin{bmatrix} c\theta + e_1^2(1 - c\theta) & e_1 e_2(1 - c\theta) + e_3 s\theta & e_1 e_3(1 - c\theta) - e_2 s\theta \\ e_2 e_1(1 - c\theta) - e_3 s\theta & c\theta + e_2^2(1 - c\theta) & e_2 e_3(1 - c\theta) + e_1 s\theta \\ e_3 e_1(1 - c\theta) + e_2 s\theta & e_3 e_2(1 - c\theta) - e_1 s\theta & c\theta + e_3^2(1 - c\theta) \end{bmatrix}, \quad (\text{B.19})$$

where $c\theta \equiv \cos(\theta)$, $s\theta \equiv \sin(\theta)$ and e_i are the direction cosines of the Euler axis. The parameters (e_1, e_2, e_3) are not independent but constrained by $e_1^2 + e_2^2 + e_3^2 = 1$.

B.4 Attitude Matrix and Kinematics

In order to derive the kinematic differential equation, two reference frames, A and B, are used. A time varying angular velocity vector in the reference frame B is denoted as ω . This vector can also be expressed in terms of the unit vectors of reference frame B which yields

$$\omega = \hat{\omega}_1 \hat{b}_1 + \hat{\omega}_2 \hat{b}_2 + \hat{\omega}_3 \hat{b}_3. \quad (\text{B.20})$$

In (B.4) the attitude matrix $\underline{C} = {}^B_A C$ was defined such that

$$\begin{bmatrix} \hat{b}_1 \\ \hat{b}_2 \\ \hat{b}_3 \end{bmatrix} = \underline{C} \begin{bmatrix} \hat{a}_1 \\ \hat{a}_2 \\ \hat{a}_3 \end{bmatrix}. \quad (\text{B.21})$$

Because the attitude matrix \underline{C} is an orthonormal matrix (B.21) can be rewritten to the following

$$\begin{bmatrix} \hat{a}_1 \\ \hat{a}_2 \\ \hat{a}_3 \end{bmatrix} = \underline{C}^T \begin{bmatrix} \hat{b}_1 \\ \hat{b}_2 \\ \hat{b}_3 \end{bmatrix}. \quad (\text{B.22})$$

Since the two reference frames, A and B, are rotating relative to each other then the attitude matrix and its elements C_{ij} are time dependent. Taking the time derivative of (B.22) in A yields the following equation

$$\begin{bmatrix} 0 \\ 0 \\ 0 \end{bmatrix} = \dot{\underline{C}}^T \begin{bmatrix} \hat{b}_1 \\ \hat{b}_2 \\ \hat{b}_3 \end{bmatrix} + \underline{C}^T \begin{bmatrix} \dot{\hat{b}}_1 \\ \dot{\hat{b}}_2 \\ \dot{\hat{b}}_3 \end{bmatrix}. \quad (\text{B.23})$$

Because the unit vectors \hat{b}_i are fixed in reference frame B are rotating relative to A, the rate of change in \hat{b}_i is only caused by ω . This means that the time derivative of the unit vector \hat{b}_i , must be normal to both \hat{b}_i and ω . Thus (B.23) can be expressed as

$$\begin{bmatrix} 0 \\ 0 \\ 0 \end{bmatrix} = \dot{\underline{C}}^T \begin{bmatrix} \hat{b}_1 \\ \hat{b}_2 \\ \hat{b}_3 \end{bmatrix} + \underline{C}^T \begin{bmatrix} \omega \times \hat{b}_1 \\ \omega \times \hat{b}_2 \\ \omega \times \hat{b}_3 \end{bmatrix}. \quad (\text{B.24})$$

By introduction of the skew symmetric matrix

$$\begin{aligned} \underline{S}(\omega) &= \omega^T \times \omega = -\omega \times \omega^T = - \begin{bmatrix} \hat{\omega}_1 \\ \hat{\omega}_2 \\ \hat{\omega}_3 \end{bmatrix} \times \begin{bmatrix} \hat{\omega}_1 & \hat{\omega}_2 & \hat{\omega}_3 \end{bmatrix} \\ &\equiv - \begin{bmatrix} \hat{\omega}_1 \times \hat{\omega}_1 & \hat{\omega}_1 \times \hat{\omega}_2 & \hat{\omega}_1 \times \hat{\omega}_3 \\ \hat{\omega}_2 \times \hat{\omega}_1 & \hat{\omega}_2 \times \hat{\omega}_2 & \hat{\omega}_2 \times \hat{\omega}_3 \\ \hat{\omega}_3 \times \hat{\omega}_1 & \hat{\omega}_3 \times \hat{\omega}_2 & \hat{\omega}_3 \times \hat{\omega}_3 \end{bmatrix} \end{aligned} \quad (\text{B.25})$$

$$= \begin{bmatrix} 0 & -\hat{\omega}_3 & \hat{\omega}_2 \\ \hat{\omega}_3 & 0 & -\hat{\omega}_1 \\ -\hat{\omega}_2 & \hat{\omega}_1 & 0 \end{bmatrix}, \quad (\text{B.26})$$

it is possible to substitute the cross product in (B.24) with a multiplication [Hughes, page 524], and rewrite (B.23) to

B.4. ATTITUDE MATRIX AND KINEMATICS

$$\begin{bmatrix} 0 \\ 0 \\ 0 \end{bmatrix} = \left[\underline{\dot{\mathbf{C}}}^T - \underline{\mathbf{C}}^T \underline{\mathbf{S}}(\omega) \right] \begin{bmatrix} \hat{b}_1 \\ \hat{b}_2 \\ \hat{b}_3 \end{bmatrix}, \quad (\text{B.27})$$

which is again rewritten to

$$0 = \underline{\dot{\mathbf{C}}}^T - \underline{\mathbf{C}}^T \underline{\mathbf{S}}(\omega). \quad (\text{B.28})$$

By transposing both sides of (B.27) and utilizing the relationship $\underline{\mathbf{S}}^T(\omega) = -\underline{\mathbf{S}}(\omega)$ the following expression is obtained

$$0 = \underline{\dot{\mathbf{C}}} + \underline{\mathbf{S}}(\omega) \underline{\mathbf{C}}. \quad (\text{B.29})$$

This expression is the kinematic differential equation for the direct cosine matrix.



Two Line Elements

When the satellite has been deployed an initial position of the satellite must be obtained for use in the on-board model. The North American Aerospace Defense Command (NORAD) tracks objects that orbit the Earth. Data concerning the orbit of these objects e.g. Keplerian elements, are distributed using Two Line Elements (TLE), which can be obtained free of charge [Space Track] and are updated on a daily basis. A TLE can thus be used to initialize the orbit model.

A TLE has the following format:

```
AAAAAAAAAAAAAAAAAAAAAAAAAAAAAAAA
1 BBBBBC DDEEEFFF GGHHH.HHHHHHHH +.IIIIIIII +JJJJJ-J +KKKKK-K L MMMMN
2 BBBB OOO.OOOO PPP.PPPP QQQQQQ RRR.RRRR SSS.SSSS TT.TTTTTTTUUUUUN
```

Each of the elements in the TLE denoted by the letters are described in Table C.1, and an example of a TLE from the AAU CubeSat can be seen below:

```
AAU CUBESAT
1 27846U 03031G 04070.99002110 -.00000777 00000-0 -34070-3 0 1720
2 27846 98.7298 79.6436 0008339 275.9042 84.1157 14.20604785 36102
```

In the following the elements of the TLE are described further based on [Kelso]. Referring to Table C.1, the elements A through F are used to identify the object to which the TLE is related. Elements G and H define the reference time for the element set and are jointly referred to as the epoch. Elements I and J are primarily used in older orbit models such as the SGP model, and are not used in the SGP4 model. The perturbations modelled by the SGP4 model include aerodynamic drag where element K is a coefficient. Element L is related to the model (i.e. SGP/SGP4) used for generating the TLE. The element is used internally only, and all distributed TLEs have the element set to zero. The element M is used for keeping track of the received number of TLEs and the value is increased each time a new TLE is generated.

The elements O through R have been described in Section 2.1.1. Element S, the mean anomaly is defined by $M = 2\pi (\frac{\Delta t}{P})$, where P is the orbital period and Δt is the time since perigee passage of the satellite. Element U has the following definition: A revolution begins when the satellite is at the ascending node of the orbit and a revolution is the period between successive ascending nodes. The period from launch to the first ascending node is considered to be revolution 0 and revolution 1 begins when the first ascending node is reached.

Element N is used for checksum on each line and represents a modulo-10 checksum of the data on the current line. To calculate the checksum the values of all the numbers must be added on each line. All letters, spaces, periods, and plus signs are ignored, and all minus signs are assigned the value 1.

Element	Description
A	Satellite name
1	Line 1 of element data
B	Satellite number
C	Classification (U=Unclassified)
D	Last two digits of launch year
E	Launch number of the year
F	Item number of the launch
G	Last two digits of epoch year
H	Epoch day and fractional portion of the day
I	First time derivative of the mean motion [m/s ²]
J	Second time derivative of the mean motion [m/s ³]
K	BSTAR drag term
L	Ephemeris type
M	Element number
N	Checksum
2	Line 2 of element data
O	Inclination [°]
P	RAAN [°]
Q	Eccentricity (Decimal point assumed)
R	Argument of perigee [°]
S	Mean anomaly [°]
T	Mean motion [Revolutions per day]
U	Revolution number at epoch
N	Checksum

Table C.1: The format of a Two Line Element.

Linearization

From Equation 2.74 on page 41 the system equations are given. In order to use the system equations e.g. for optimal control or a Kalman Filter, these nonlinear equations have to be linearized. The satellite kinematics and dynamics equations are given by

$$\begin{bmatrix} \dot{\omega} \\ \dot{q} \end{bmatrix} = \begin{bmatrix} \mathbf{I}^{-1}(N_{\text{ext}} + N_{\text{ctrl}} - \underline{S}(\omega)(\mathbf{I}\omega + L_{\text{mw}})) \\ \frac{1}{2}\underline{\Omega}q \end{bmatrix}. \quad (\text{D.1})$$

A linear description of the satellite attitude will be found by linearizing (D.1) about an operating point. Thereby the satellite dynamics and kinematics can be expressed in state space.

D.1 Linearization of the Satellite Kinematic Equation

The satellite kinematic equation is expressed as

$$\dot{q} = \frac{1}{2}\underline{\Omega}q. \quad (\text{D.2})$$

Linearizations of quaternions are used in order to linearize (D.2). The quaternion can then be expressed as

$$q = q(t + \Delta t) = q(t)q(\Delta t) = \bar{q}\tilde{q}, \quad (\text{D.3})$$

where \bar{q} is the quaternion in the operating point $q(t)$ and \tilde{q} is the small signal quaternion, $q(\Delta t)$, representing a small change in attitude. Using the fact that $q^{-1} = q^*$, then \tilde{q} can be derived from (D.3) as

$$\tilde{q} = \bar{q}^*q, \quad (\text{D.4})$$

where \bar{q}^* is the complex conjugate of \bar{q} .

It is possible to rewrite the kinematic equation of the satellite in (D.2) into a multiplication of two quaternions, using the multiplicative properties of a quaternion as expressed in (D.5). The result can be seen in (D.6).

D.1. LINEARIZATION OF THE SATELLITE KINEMATIC EQUATION

$$\begin{aligned}
 qq_\omega &= (q_4 + q_1\hat{i} + q_2\hat{j} + q_3\hat{k}) \cdot (0 + \omega_1\hat{i} + \omega_2\hat{j} + \omega_3\hat{k}) \\
 &= \underbrace{\begin{bmatrix} 0 & \omega_3 & -\omega_2 & \omega_1 \\ -\omega_3 & 0 & \omega_1 & \omega_2 \\ \omega_2 & -\omega_1 & 0 & \omega_3 \\ -\omega_1 & -\omega_2 & \omega_3 & 0 \end{bmatrix}}_{\underline{\Omega}} \underbrace{\begin{bmatrix} q_1 \\ q_2 \\ q_3 \\ q_4 \end{bmatrix}}_q, \tag{D.5}
 \end{aligned}$$

$$\dot{q} = \frac{1}{2}qq_\omega, \tag{D.6}$$

where q_ω is defined as

$$q_\omega = \begin{bmatrix} \omega_{3 \times 1} \\ 0 \end{bmatrix} = \begin{bmatrix} \bar{\omega}_{3 \times 1} + \tilde{\omega}_{3 \times 1} \\ 0 \end{bmatrix} = q_\omega + q_{\bar{\omega}}. \tag{D.7}$$

In the following calculations the properties of the complex conjugate of the quaternion $(qq_\omega)^* = q_\omega^*q^*$ and $q_{\bar{\omega}}^* = -q_{\bar{\omega}}$ will be used as the scalar part of $q_{\bar{\omega}}$ is zero. Taking the derivative of (D.4) with respect to time and utilizing (D.6), yields

$$\begin{aligned}
 \dot{q} &= \dot{q}^*q + \bar{q}^*\dot{q} \\
 &= \frac{1}{2}[(\bar{q}q_\omega)^*q + \bar{q}^*(qq_\omega)] \\
 &= \frac{1}{2}[(\bar{q}q_\omega)^*q + \tilde{q}q_\omega] \\
 &= \frac{1}{2}[q_\omega^*\bar{q}^*q + \tilde{q}q_\omega] \\
 &= \frac{1}{2}[-q_{\bar{\omega}}\tilde{q} + \tilde{q}q_\omega]. \tag{D.8}
 \end{aligned}$$

Inserting (D.7) into (D.8) yields

$$\begin{aligned}
 \dot{q} &= \frac{1}{2}[-q_{\bar{\omega}}\tilde{q} + \tilde{q}q_\omega] \\
 &= \frac{1}{2}[-q_{\bar{\omega}}\tilde{q} + \tilde{q}q_{\bar{\omega}} + \tilde{q}q_\omega] \\
 &= \frac{1}{2}[-q_{\bar{\omega}}\tilde{q} + \tilde{q}q_{\bar{\omega}}] + \frac{1}{2}\tilde{q}q_\omega. \tag{D.9}
 \end{aligned}$$

Calculating the quaternion products $q_{\bar{\omega}}\tilde{q}$ in (D.9) yields

$$\begin{aligned}
 q_{\bar{\omega}}\tilde{q} &= \begin{bmatrix} -\underline{S}(\tilde{q}_{1:3}) + \tilde{q}_4 \underline{1}_{3 \times 3} & \tilde{q}_{1:3} \\ -\tilde{q}_{1:3}^T & \tilde{q}_4 \end{bmatrix} \begin{bmatrix} \bar{\omega} \\ 0 \end{bmatrix} \\
 &= \begin{bmatrix} \underline{S}(\bar{\omega})\tilde{q}_{1:3} + \tilde{q}_4 \underline{1}_{3 \times 3} \bar{\omega} \\ -\tilde{q}_{1:3}^T \bar{\omega} \end{bmatrix}. \tag{D.10}
 \end{aligned}$$

D.1. LINEARIZATION OF THE SATELLITE KINEMATIC EQUATION

Note that $\underline{S}(\omega)$ is the skew symmetric matrix described in Equation 2.53 on page 38 and that $\underline{S}(\omega)q = -\underline{S}(q)\omega$. The multiplication of $\tilde{q}q_{\tilde{\omega}}$ can be found as follows

$$\begin{aligned}\tilde{q}q_{\tilde{\omega}} &= \begin{bmatrix} -\underline{S}(\tilde{\omega}) & \tilde{\omega} \\ -\tilde{\omega}^T & 0 \end{bmatrix} \begin{bmatrix} \tilde{q}_{1:3} \\ \tilde{q}_4 \end{bmatrix} \\ &= \begin{bmatrix} -\underline{S}(\tilde{\omega})\tilde{q}_{1:3} + \tilde{\omega}\tilde{q}_4 \\ -\tilde{\omega}^T\tilde{q}_{1:3} \end{bmatrix}.\end{aligned}\tag{D.11}$$

Finally the multiplication of $\tilde{q}q_{\tilde{\omega}}$ must be derived. In this case note that each quaternion represents a rotation and it has a vector part, $q_{1:3}$, with dimensions 3×1 and a scalar part (q_4). Therefore small rotations yields.

$$\lim_{\text{rotation} \rightarrow 0} q = \lim_{\theta \rightarrow 0} \begin{bmatrix} q_{1:3} \\ q_4 \end{bmatrix} = \lim_{\theta \rightarrow 0} \begin{bmatrix} e_1 \sin\left(\frac{\theta}{2}\right) \\ e_2 \sin\left(\frac{\theta}{2}\right) \\ e_3 \sin\left(\frac{\theta}{2}\right) \\ \cos\left(\frac{\theta}{2}\right) \end{bmatrix} = \begin{cases} q_{1:3} \rightarrow 0 \\ q_4 \rightarrow 1 \end{cases}\tag{D.12}$$

Therefore $\tilde{q}q_{\tilde{\omega}}$ can be approximated with $q_{\tilde{\omega}}$ as shown in (D.13).

$$\begin{aligned}\tilde{q}q_{\tilde{\omega}} &= \begin{bmatrix} -\underline{S}(\tilde{\omega}) & \tilde{\omega} \\ -\tilde{\omega}^T & 0 \end{bmatrix} \begin{bmatrix} \tilde{q}_{1:3} \\ \tilde{q}_4 \end{bmatrix} = \begin{bmatrix} -\underline{S}(\tilde{\omega})\tilde{q}_{1:3} + \tilde{\omega}\tilde{q}_4 \\ -\tilde{\omega}^T\tilde{q}_{1:3} \end{bmatrix} \\ &\approx \begin{bmatrix} 0 + \begin{bmatrix} \tilde{\omega}_1 \\ \tilde{\omega}_2 \\ \tilde{\omega}_3 \\ 0 \\ 0 \end{bmatrix} \tilde{q}_4 \\ \end{bmatrix} = \begin{bmatrix} \tilde{\omega}_1 \\ \tilde{\omega}_2 \\ \tilde{\omega}_3 \\ 0 \end{bmatrix} \\ &= q_{\tilde{\omega}}.\end{aligned}\tag{D.13}$$

Now it is possible to substitute the results of (D.10), (D.11) and (D.13) into (D.9), yielding the following linear expression for the kinematics of the satellite.

$$\begin{aligned}\dot{q} &= \frac{1}{2} \left(- \begin{bmatrix} \underline{S}(\tilde{\omega})\tilde{q}_{1:3} + \tilde{q}_4 \mathbb{1}_{3 \times 3} \tilde{\omega} \\ -\tilde{q}_{1:3}^T \tilde{\omega} \end{bmatrix} + \begin{bmatrix} -\underline{S}(\tilde{\omega})\tilde{q}_{1:3} + \tilde{q}_4 \mathbb{1}_{3 \times 3} \tilde{\omega} \\ -\tilde{\omega}^T \tilde{q}_{1:3} \end{bmatrix} \right) + \frac{1}{2} \tilde{q}q_{\tilde{\omega}} \\ &= \begin{bmatrix} -\underline{S}(\tilde{\omega})\tilde{q}_{1:3} \\ 0 \end{bmatrix} + \frac{1}{2} \tilde{q}q_{\tilde{\omega}} \\ &\approx \begin{bmatrix} -\underline{S}(\tilde{\omega})\tilde{q}_{1:3} \\ 0 \end{bmatrix} + \frac{1}{2} q_{\tilde{\omega}}.\end{aligned}\tag{D.14}$$

as the $a^T b = b^T a$ applies.

D.2 Linearization of Satellite Dynamic Equation

The satellite dynamic equation is stated in Equation 2.74 on page 41 as

$$\dot{\omega} = \mathbb{I}^{-1} [N_{\text{ext}} + N_{\text{ctrl}} - \underline{\mathbf{S}}(\omega)(\mathbb{I}\omega + L_{\text{mw}})]. \quad (\text{D.15})$$

To linearize the dynamic equation, it is necessary to choose an operating point $\bar{\omega}$ for the system. The operating point varies in different time steps but is constant in each specific time step. The change in angular velocity is modelled with the small signal $\tilde{\omega}$ in the operating point. This yields

$$\omega = \omega(t + \Delta t) = \bar{\omega} + \tilde{\omega}. \quad (\text{D.16})$$

The derivative of (D.16) with respect to time yields

$$\dot{\omega} = \dot{\tilde{\omega}}. \quad (\text{D.17})$$

Taking (D.15) into consideration it is possible to assume N_{ext} as constant about the operating point within the time frame Δt . Therefore, $\dot{\omega}$ becomes a function of ω , N_{ctrl} and L_{mw} . (D.15) is linearized using first order Taylor expansion.

$$\begin{aligned} \dot{\omega}(\omega, L_{\text{mw}}, N_{\text{ctrl}}) \approx & -\mathbb{I}^{-1} \left. \frac{d}{d\omega} \underline{\mathbf{S}}(\omega)(\mathbb{I}\omega + L_{\text{mw}}) \right|_{\omega=\bar{\omega}, L_{\text{mw}}=\bar{L}_{\text{mw}}} \cdot \tilde{\omega} \\ & - \mathbb{I}^{-1} \left. \frac{d}{dL_{\text{mw}}} \underline{\mathbf{S}}(\omega)(\mathbb{I}\omega + L_{\text{mw}}) \right|_{\omega=\bar{\omega}, L_{\text{mw}}=\bar{L}_{\text{mw}}} \cdot \tilde{L}_{\text{mw}} \\ & + \mathbb{I}^{-1} \left. \frac{d}{dN_{\text{ctrl}}} N_{\text{ctrl}} \right|_{N_{\text{ctrl}}=\bar{N}_{\text{ctrl}}} \cdot \tilde{N}_{\text{ctrl}}. \end{aligned} \quad (\text{D.18})$$

By rewriting the $\tilde{\omega}$ term and expanding the \tilde{N}_{ctrl} and \tilde{L}_{mw} terms, (D.18) can be expressed in the form

$$\begin{aligned} \dot{\omega} = & -\mathbb{I}^{-1} \left[\left. \frac{d}{d\omega} \underline{\mathbf{S}}(\omega)\mathbb{I}\bar{\omega} \right|_{\omega=\bar{\omega}} + \left. \frac{d}{d\omega} \underline{\mathbf{S}}(\bar{\omega})\mathbb{I}\bar{\omega} \right|_{\omega=\bar{\omega}} + \left. \frac{d}{d\omega} \underline{\mathbf{S}}(\bar{\omega})\bar{L}_{\text{mw}} \right|_{\omega=\bar{\omega}} \right] \tilde{\omega} \\ & - \mathbb{I}^{-1} \left. \frac{d}{dL_{\text{mw}}} \underline{\mathbf{S}}(\bar{\omega})L_{\text{mw}} \right|_{\omega=\bar{\omega}, L_{\text{mw}}=\bar{L}_{\text{mw}}} \cdot \tilde{L}_{\text{mw}} + \mathbb{I}^{-1} \tilde{N}_{\text{ctrl}}. \end{aligned} \quad (\text{D.19})$$

Using the fact that $\underline{\mathbf{S}}(\omega)\mathbb{I}\bar{\omega} = -\underline{\mathbf{S}}(\mathbb{I}\bar{\omega})\bar{\omega}$ then (D.19) can be expressed as

$$\begin{aligned} \dot{\omega} = & \mathbb{I}^{-1} \left[\left. \frac{d}{d\omega} \underline{\mathbf{S}}(\mathbb{I}\bar{\omega})\bar{\omega} \right|_{\omega=\bar{\omega}} - \left. \frac{d}{d\omega} \underline{\mathbf{S}}(\bar{\omega})\mathbb{I}\bar{\omega} \right|_{\omega=\bar{\omega}} + \left. \frac{d}{d\omega} \underline{\mathbf{S}}(\bar{L}_{\text{mw}})\bar{\omega} \right|_{\omega=\bar{\omega}} \right] \tilde{\omega} \\ & - \mathbb{I}^{-1} \underline{\mathbf{S}}(\bar{\omega})\tilde{L}_{\text{mw}} + \mathbb{I}^{-1} \tilde{N}_{\text{ctrl}}. \end{aligned} \quad (\text{D.20})$$

From (D.20) the linearized dynamic differential equation shown in (D.21) is obtained as

$$\dot{\omega} = \mathbb{I}^{-1} [\underline{\mathbf{S}}(\mathbb{I}\bar{\omega}) - \underline{\mathbf{S}}(\bar{\omega})\mathbb{I} + \underline{\mathbf{S}}(\bar{L}_{\text{mw}})] \tilde{\omega} - \mathbb{I}^{-1} \underline{\mathbf{S}}(\bar{\omega})\tilde{L}_{\text{mw}} + \mathbb{I}^{-1} \tilde{N}_{\text{ctrl}}. \quad (\text{D.21})$$

D.3 Linear Equation for the Satellite Attitude

Using the results given in the two previous sections, it is possible to obtain the linear system equation for the satellite, which is expressed as

$$\begin{aligned}
 \begin{bmatrix} \dot{\tilde{q}}_{1:3} \\ \tilde{\omega} \\ \dot{\tilde{L}}_{\text{mw}} \end{bmatrix} &= \begin{bmatrix} -\underline{S}(\tilde{\omega}) & \frac{1}{2}\underline{1}_{3 \times 3} & \underline{0}_{3 \times 3} \\ \underline{0}_{3 \times 3} & \underline{I}^{-1} [\underline{S}(\underline{I}\tilde{\omega}) - \underline{S}(\tilde{\omega})\underline{I} + \underline{S}(\tilde{L}_{\text{mw}})] & -\underline{I}^{-1}\underline{S}(\tilde{\omega}) \\ \underline{0}_{3 \times 3} & \underline{0}_{3 \times 3} & \underline{0}_{3 \times 3} \end{bmatrix} \begin{bmatrix} \tilde{q}_{1:3} \\ \tilde{\omega} \\ \tilde{L}_{\text{mw}} \end{bmatrix} \\
 &+ \begin{bmatrix} \underline{0}_{3 \times 3} & \underline{0}_{3 \times 3} \\ \underline{I}^{-1} & -\underline{I}^{-1} \\ \underline{0}_{3 \times 3} & \underline{1}_{3 \times 3} \end{bmatrix} \begin{bmatrix} \tilde{N}_{\text{mt}} \\ \tilde{N}_{\text{mw}} \end{bmatrix}. \tag{D.22}
 \end{aligned}$$

Note that in this equation the scalar element of the quaternion, q_4 , does not yield a contribution as it is approximated to be 1 for small angles. See (D.12). $\underline{S}(\tilde{\omega})$ and $\underline{S}(\tilde{L}_{\text{mw}})$ are constant in their operating points and they are calculated in each operating point using the measurements from the gyros and the tachometers on the momentum wheels. \tilde{N}_{mt} and \tilde{N}_{mw} are small changes in the torques exerted by the actuators within the Δt time frame.

Implementation of Simulation

The models deducted in the report have all been implemented in MATLAB and SIMULINK to be able to test the ADCS system. In the following chapter the implementation of the different models will be presented. The implementation is based on the work done by group 04gr830a [04GR830a] and 04gr830b [04GR830b], Aalborg University. The implementation is available on the enclosed CD.

E.1 Simulation Environment

This section presents the implementation of the models related to the simulation environment.

E.1.1 Disturbance Models

The following SIMULINK disturbance models have been implemented:

- Aerodynamic drag.
- Gravity gradient.
- Magnetic residual.
- Solar radiation.

For verification and test of the disturbance models, see [04GR830a] and [04GR830b].

Aerodynamic Drag Model

The SIMULINK model of the aerodynamic drag has two inputs.

- The attitude of the satellite.
- The velocity of the satellite (ECI).

The output of the model are the torque in the SBRF frame and the force in the ECI frame.

Gravity Gradient Model

The SIMULINK model for the gravity gradient disturbance, seen in Figure E.2, has two input.

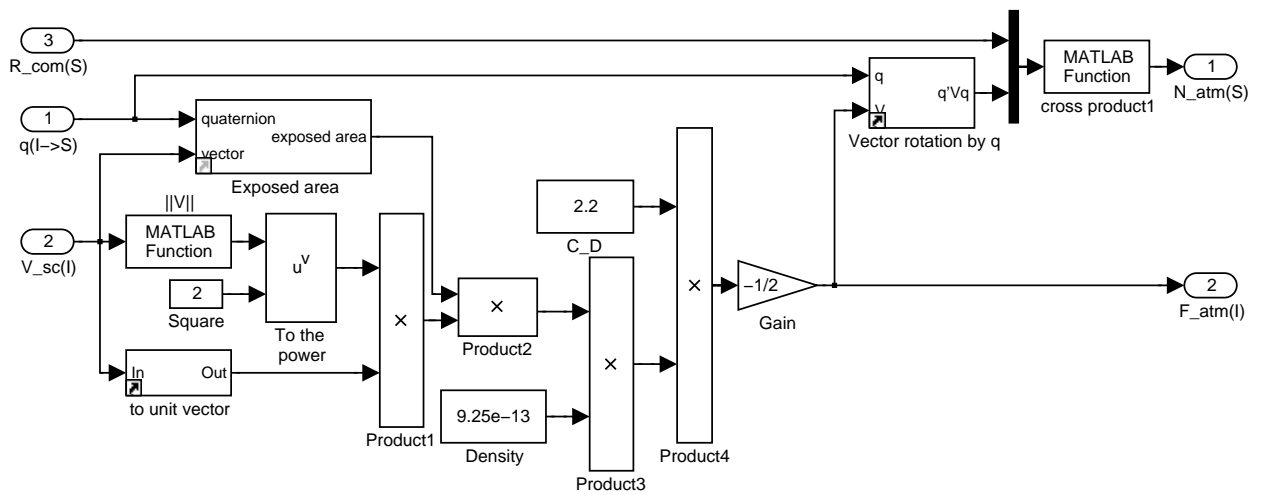


Figure E.1: SIMULINK model of the aerodynamic drag.

- A vector pointing from the center of the Earth to the satellite in SBRF.
- The attitude of the satellite.

The model has a single output, which is the gravity gradient torque in SBRF.

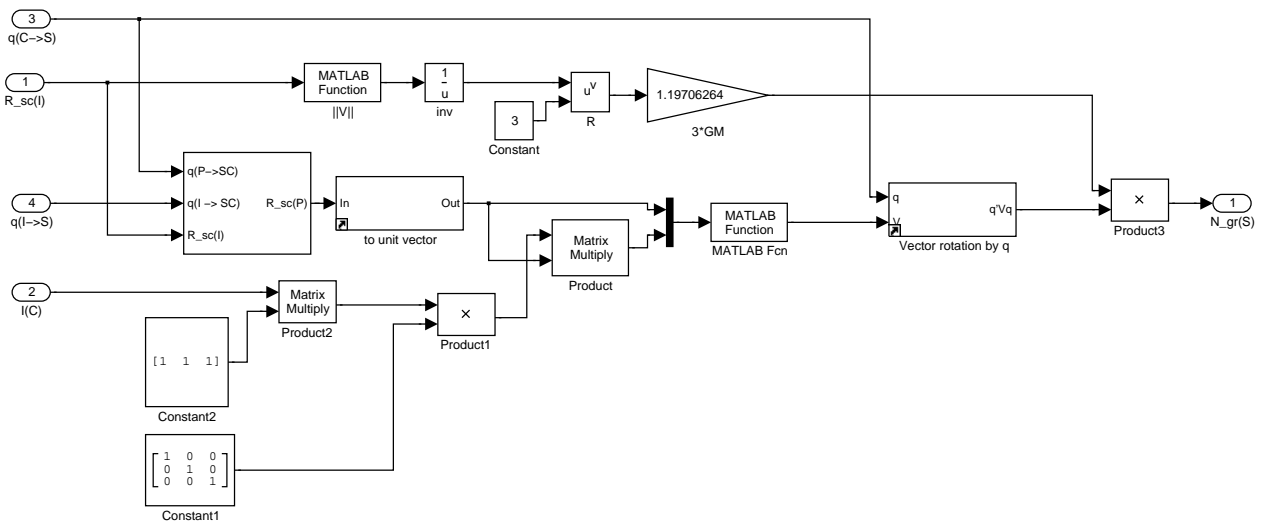


Figure E.2: SIMULINK model of the gravity gradient.

Magnetic Residual Model

The SIMULINK model of the magnetic residual, seen in Figure E.3, has four input

- The magnetic dipole moment (SBRF).
- The satellite attitude.

E.1.2 Satellite Dynamics and Kinematics

The implementation of the model of the dynamics and kinematics of the satellite is depicted in Figure E.5. The central part is implemented in a S-function programmed in C. The block has three variable input.

- The angular momentum of the momentum wheels (SBRF).
- The torque of the actuators (SBRF).
- The torque exerted on the satellite due to disturbances (SBRF).

The block also has four constant input.

- Initial values for angular velocity.
- Initial attitude quaternion of the satellite.
- The inertia matrix (CRF)
- A quaternion describing the rotation from SBRF to CRF.

The block has two output.

- The angular velocity of the satellite (SBRF).
- The attitude quaternion of the satellite.

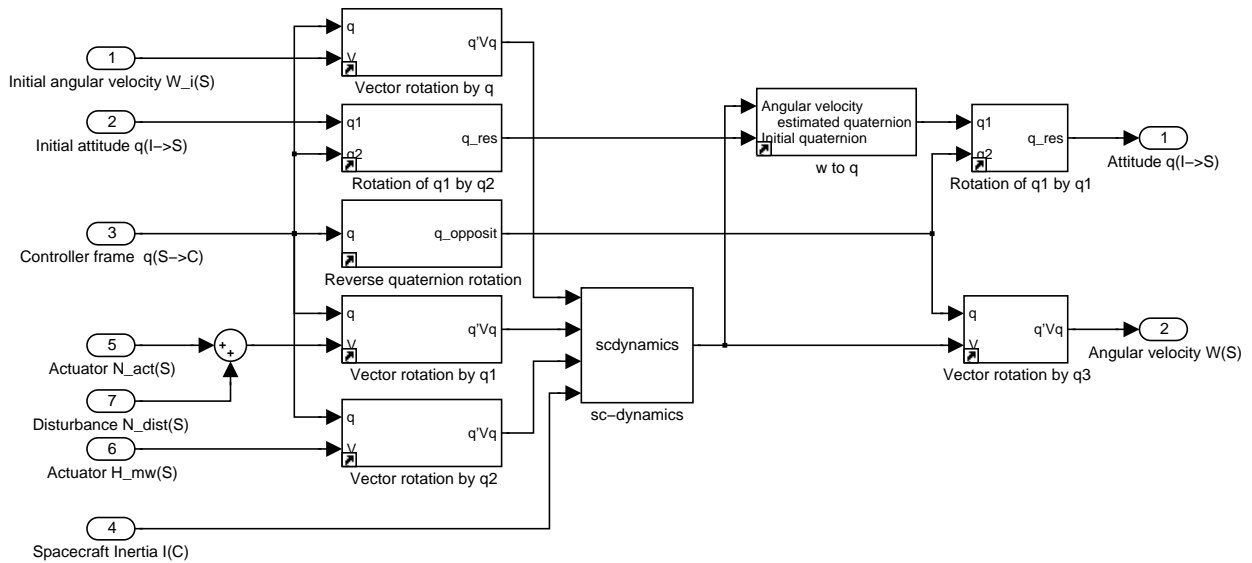


Figure E.5: SIMULINK implementation of dynamics and kinematics of the satellite.

E.1.3 Ephemeris Model

The calculation of the positions of the Sun and Moon, and the rotation of the Earth (ECI to ECEF) are performed in the Ephemeris model. The Spacecraft Control Toolbox from Princeton Satellite Systems is used for calculation of the Sun and Moon positions and the implementation consist of two MATLAB script files. The rotation of the Earth is also implemented in a MATLAB script file. The SIMULINK implementation is depicted in Figure E.6. The input for the block is

E.1. SIMULATION ENVIRONMENT

- The simulation time in Julian Date format.

and the output are

- Moon position (ECI).
- Sun position (ECI).
- A quaternion describing the rotation of the Earth.

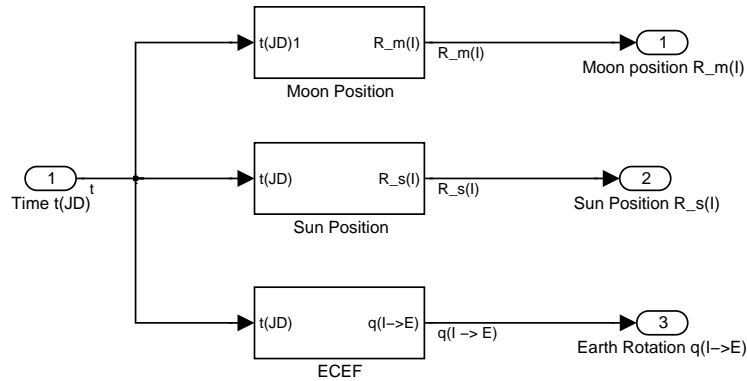


Figure E.6: SIMULINK implementation of the ephemeris model.

E.1.4 Orbit Propagator, Magnetic Field Model, Eclipse Model, and Albedo Model

The input to this block are.

- Sun position (ECI).
- Quaternion describing the rotation of the Earth.
- Initial time (JD).

The output are.

- Position vector for the satellite (ECI).
- Velocity vector for the satellite (ECI).
- Magnetic field vector (ECI).
- Reflectivity matrix.
- The simulation time (JD).
- Boolean indication of Eclipse.

The SIMULINK implementation depicted in Figure E.7 facilitates the first three output vectors either based on the SGP4/IGRF models or based on position measurements from the Ørsted satellite. The selection is done in a SIMULINK mask on the sub-system. Both the SGP4 model and the IGRF model is implemented in S-functions programmed in C. The precision of the SGP4 model and the IGRF model are treated in Appendix F and G.

The reflectivity matrix is generated using the Albedo Toolbox as described in [Bhanderi].

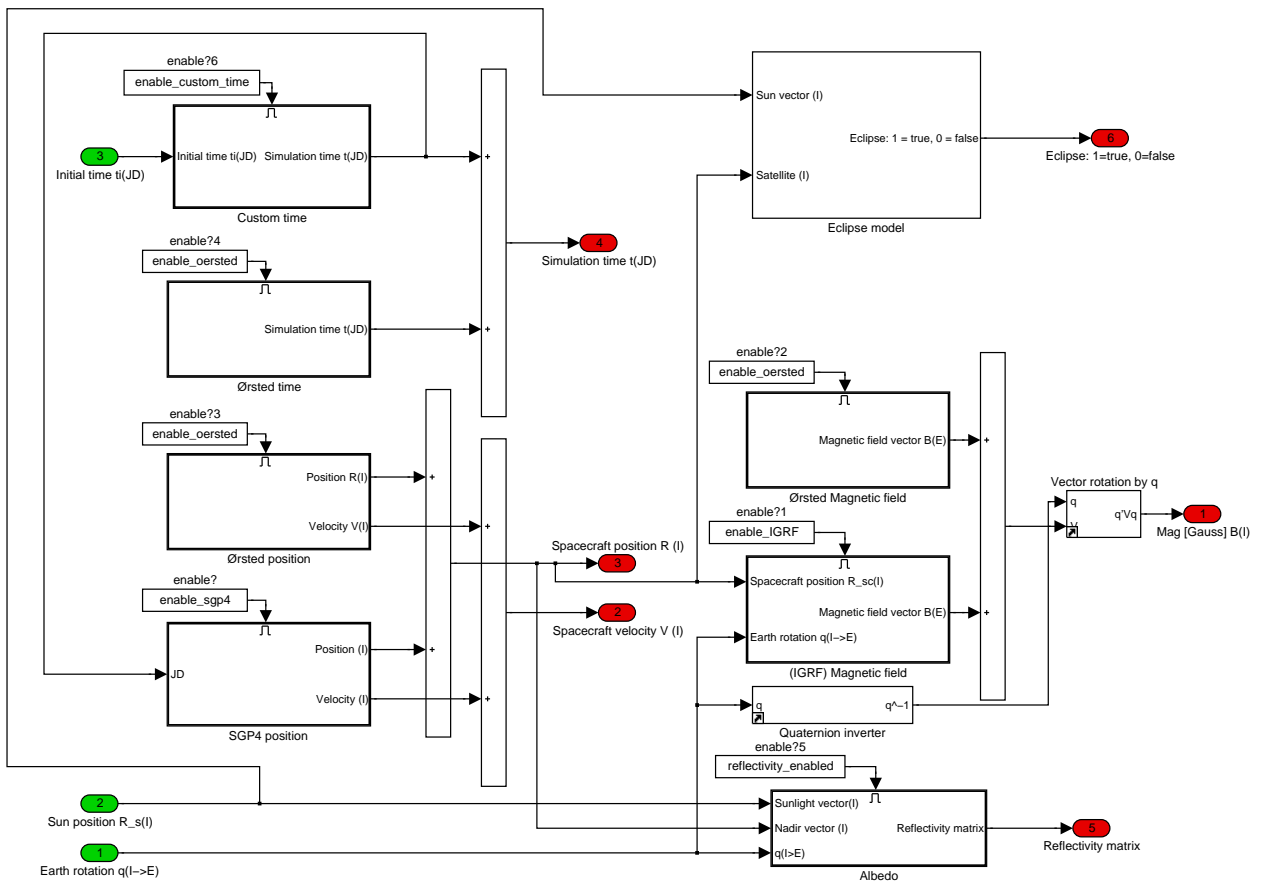


Figure E.7: SIMULINK implementation of the orbit propagator, magnetic field model, eclipse model, and albedo model.

E.1.5 Sensor Emulation

The purpose of the sensor emulation block is to map the output of the environment models to an output appropriate for the given sensors. The top level of the block is shown in Figure E.8. As the sensors are temperature dependent, a block containing an emulation of the temperature sensors on the satellite has been added. However, it is considered outside the scope of the report to model the temperature. At the time of this writing the block contains a constant value for the temperature, and it is possible to create a deviation of the measured temperature by introducing an offset to the measured temperature.

E.1.6 Emulation of Gyros

The implementation of the emulation of the gyros is done according to Figure E.9. The parameters such as `e_scale` depicted in the figure are defined in a mask on the sub-system which eases the overview of the parameters. The block has the following two input.

- The angular velocity of the satellite in the SBRF.
- The temperature.

The output of the block is a vector containing the emulated output voltages of the six gyros in [mV].

E.1. SIMULATION ENVIRONMENT

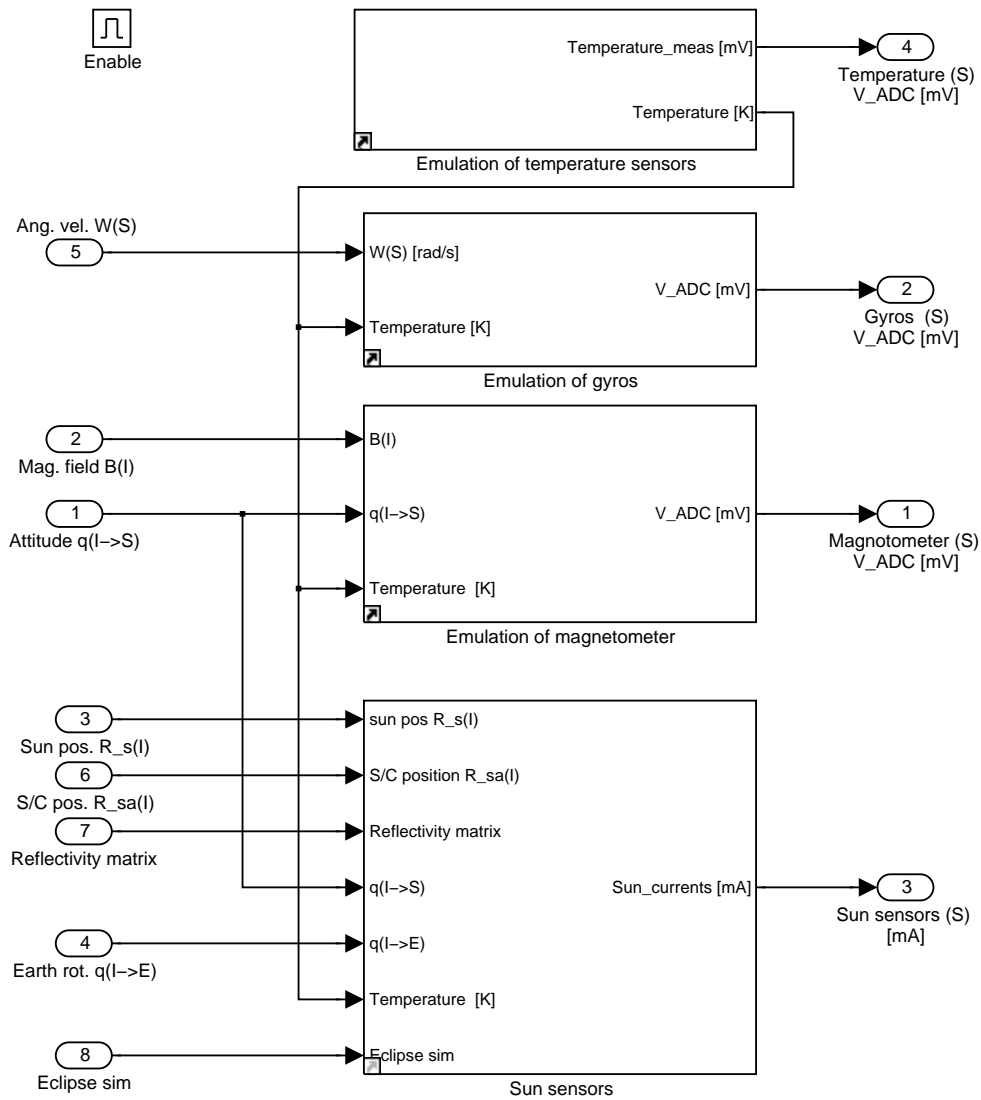


Figure E.8: Top level view of the SIMULINK implementation of the sensor emulation.

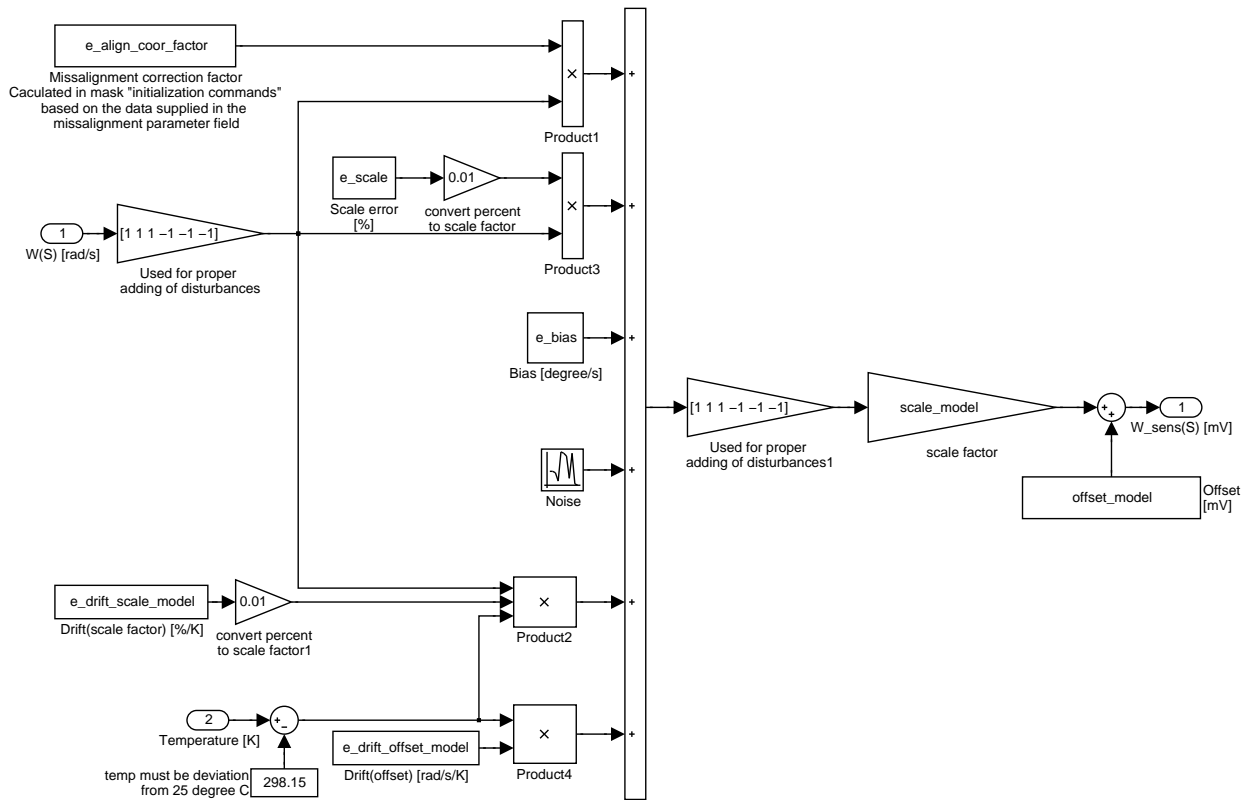


Figure E.9: SIMULINK implementation of the gyro emulation.

E.1.7 Emulation of the Magnetometer

The SIMULINK implementation of the magnetometer is depicted in Figure E.10. The block has the following input.

- A magnetic field vector (ECI).
- A quaternion describing the rotation from ECI to SBRF.
- The temperature.

The attitude quaternion is used to rotate the magnetic field vector from ECI to SBRF. The output of the block is a vector containing the output voltages of the magnetometer in [mV].

E.1.8 Emulation of Sun Sensors

The block emulating the Sun sensors has six input.

- A position vector to the Sun (ECI).
- A position vector to the satellite (ECI).
- Reflectivity matrix.
- A quaternion describing the rotation of Earth (ECI to ECEF).

E.1. SIMULATION ENVIRONMENT

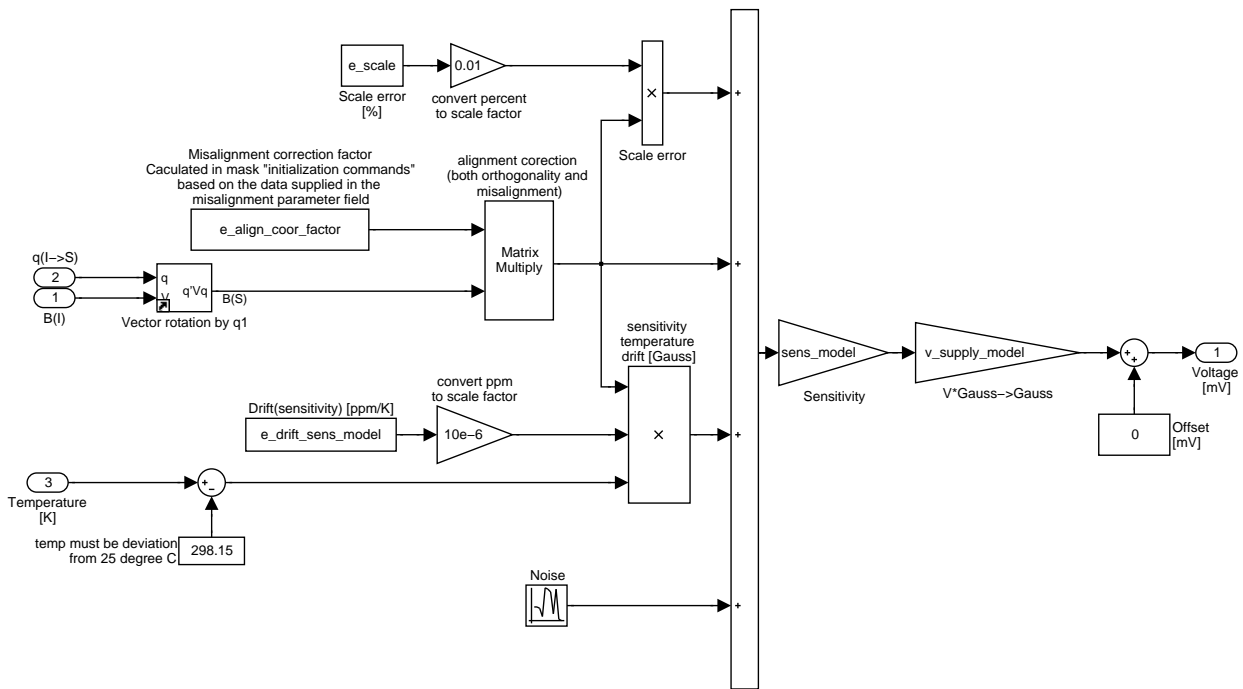


Figure E.10: SIMULINK implementation of the magnetometer emulation.

- A quaternion describing the attitude of the satellite.
- The temperature.

The reflectivity matrix is generated using the albedo toolbox as previously described. The output of the block is as shown in Figure E.11 a vector containing the emulated output currents of the six sun sensors.

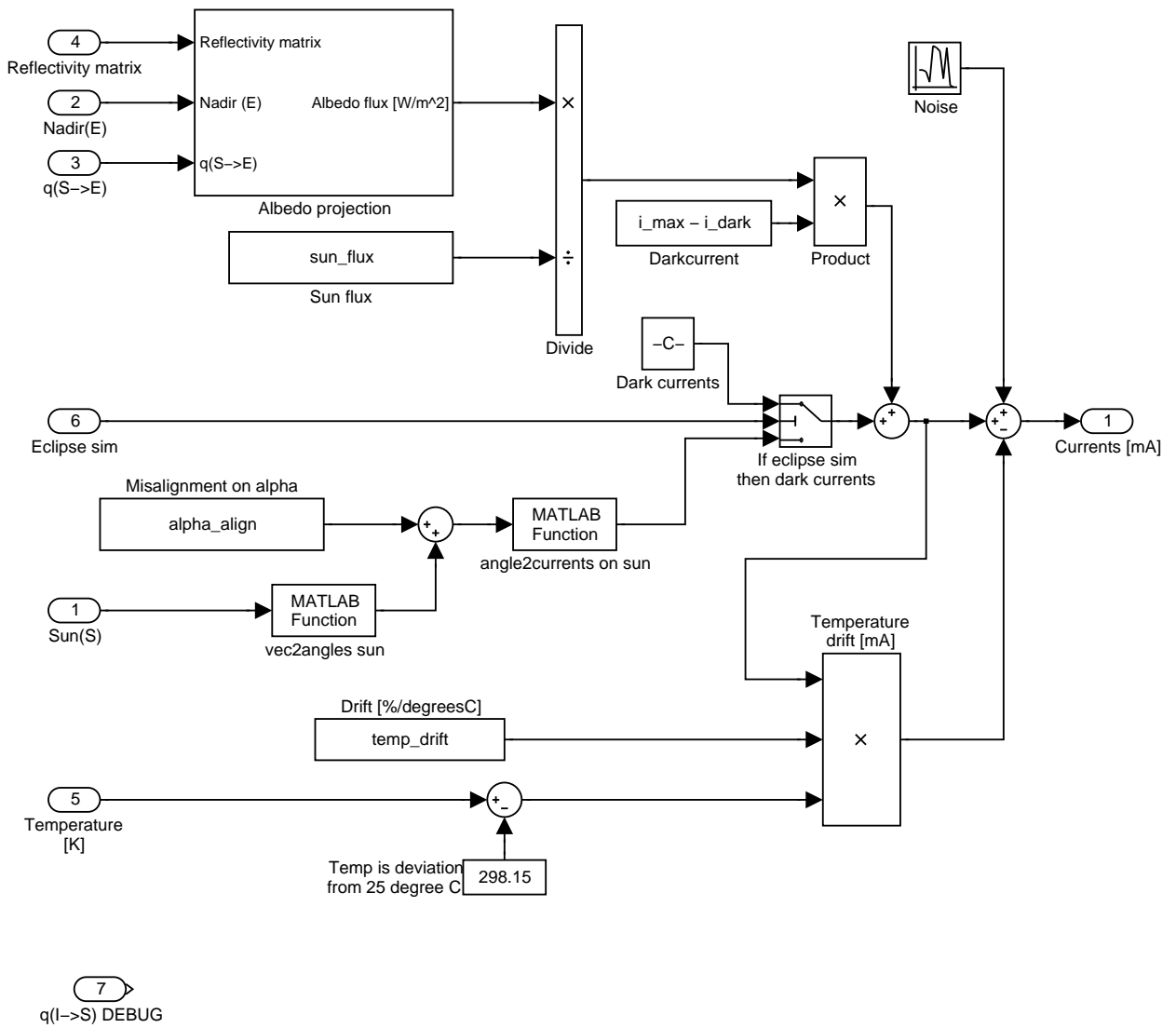


Figure E.11: SIMULINK implementation of the sun sensor emulation.

Orbit Propagator Accuracy

F

In the following the SGP4 orbit model and the Kepler orbit model are compared with position measurements from an existing satellite in orbit. The measurements originates from the Ørsted satellite and a TLE from this satellite is used for the two models (For further information concerning the Ørsted measurement data see [CubeSat ADS, page 110]).

The position of the Ørsted satellite is determined using a GPS-receiver, and in the following comparison the accuracy of this GPS-receiver is expected to be much better than the accuracy of the investigated models. Thus errors related in position generated by the GPS-receiver are not considered.

The SIMULINK implementation used for comparing the Kepler and SGP4 models with the Ørsted measurement data is shown in Figure F.1.

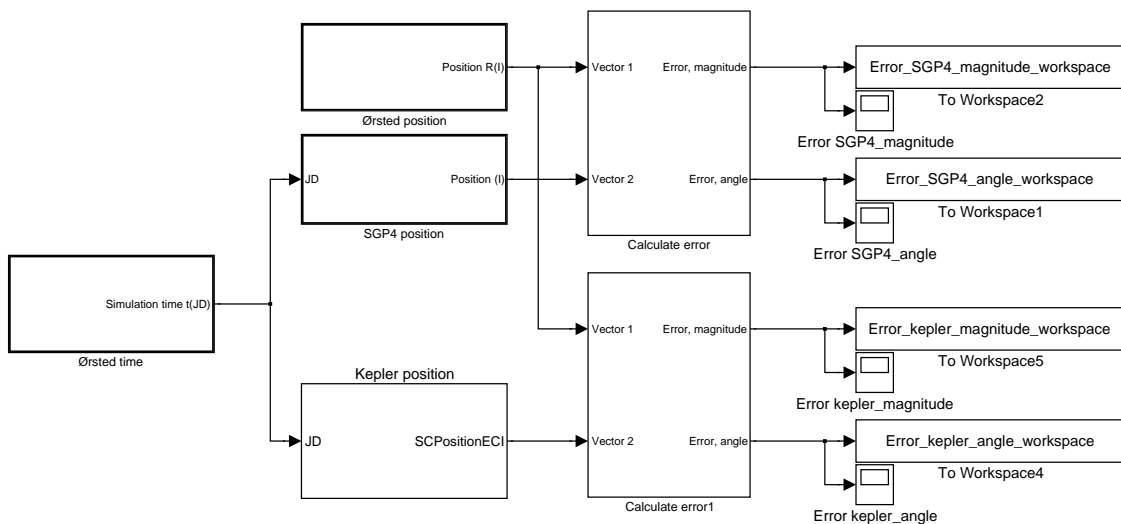
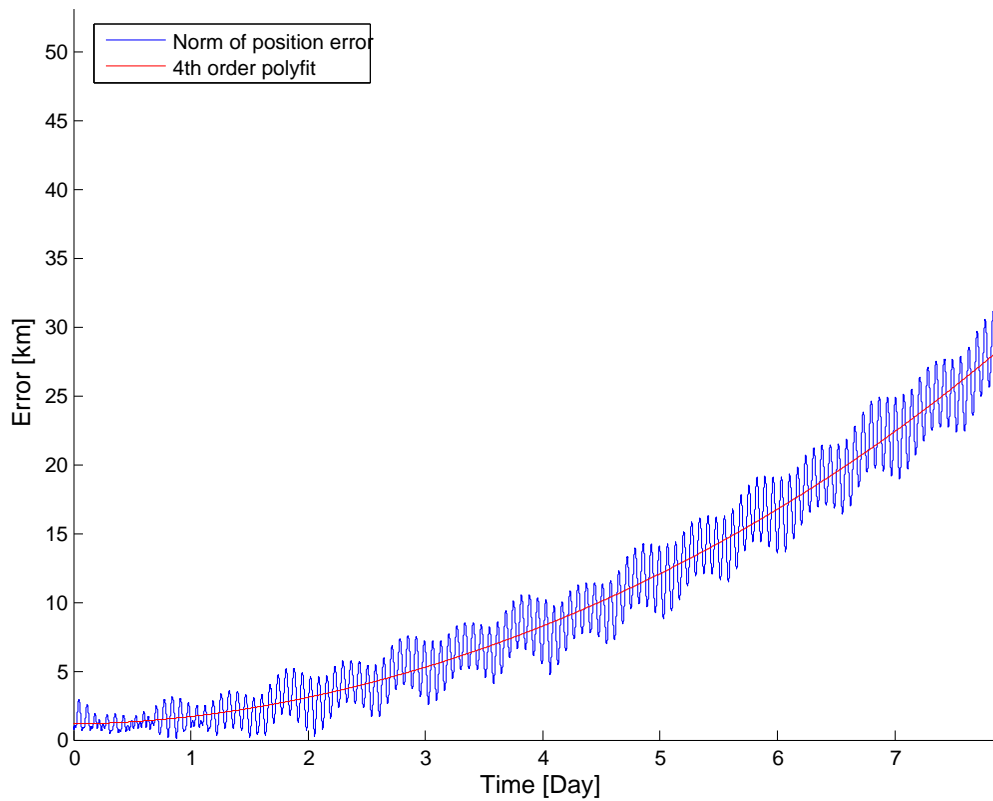
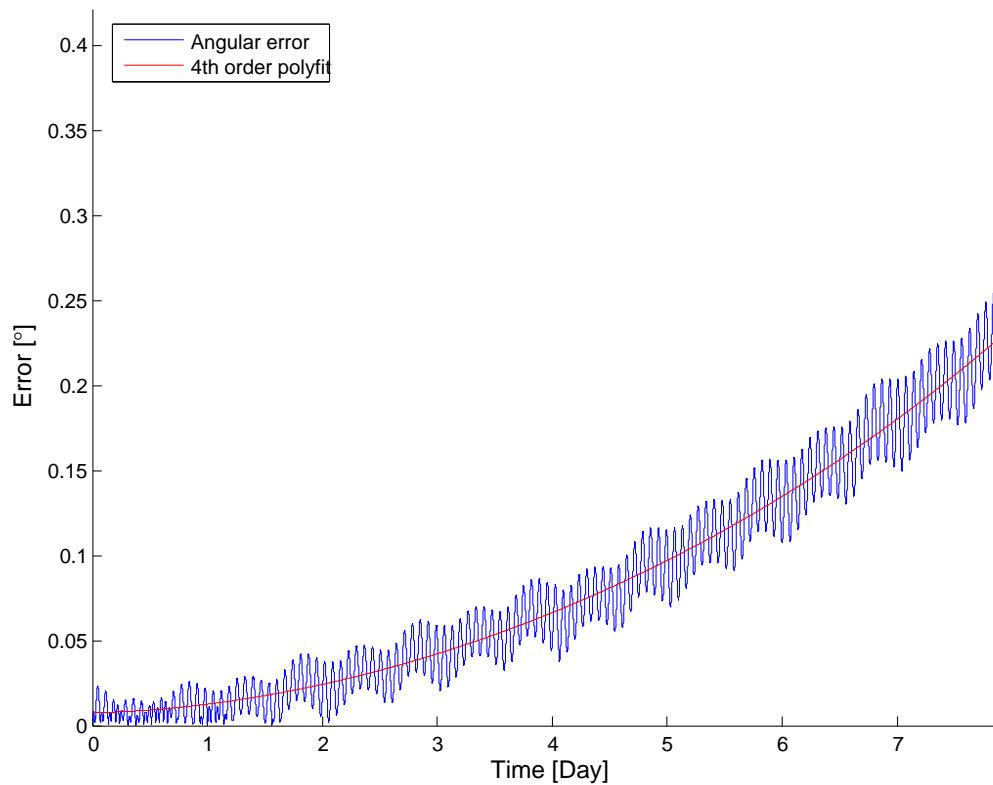


Figure F.1: SIMULINK model used for comparing the SGP4 model and Kepler model with in-orbit position measurements from the Ørsted satellite.

The error of the SGP4 orbit model compared to the measured position of the Ørsted satellite is depicted in Figure F.2 and the error of the Kepler orbit model compared to the measured position of the Ørsted satellite is depicted in F.3. In all of the plots the values have been fitted to a 4th order polynomial to emphasize the tendency of the errors using the function `polyfit` available in MATLAB. Figure F.2 and F.3 indicate that the accuracy of both models decrease with time when compared to the measured position of the Ørsted satellite. However, the error in the SGP4 model is generally smaller than the error in the Kepler orbit model.

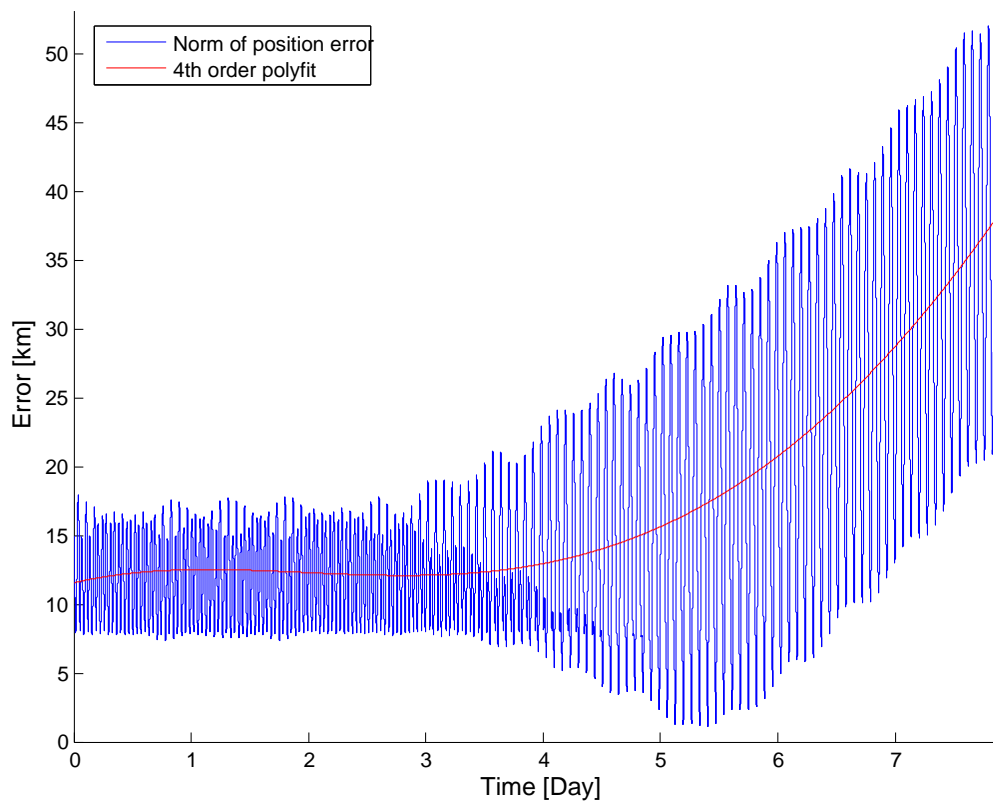


(a) Norm of the position error.

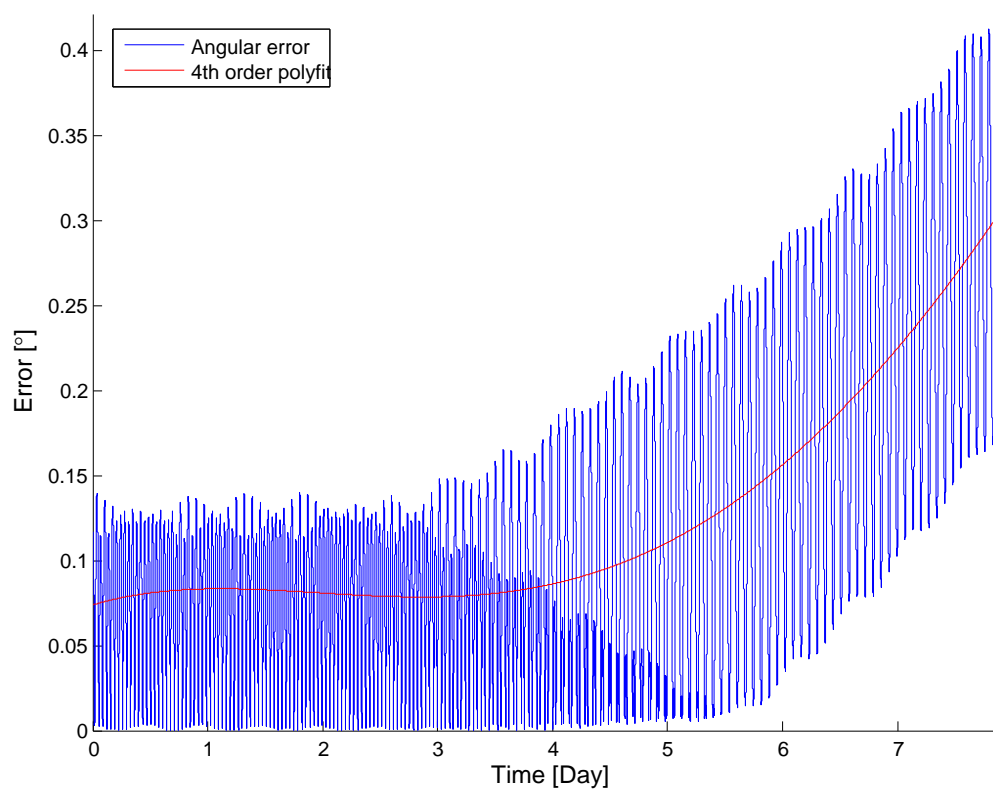


(b) Angular error.

Figure F.2: The SGP4 orbit model compared to the measured position of the Ørsted satellite. The data was recorded between the 10th of February 2002 and the 17th of February 2002.



(a) Norm of position error.



(b) Angular error.

Figure F.3: The Kepler orbit model compared to the measured position of the Ørsted satellite. The data was recorded between the 10th of February 2002 and the 17th of February 2002.

Magnetic Field Model Accuracy



To verify the accuracy of the model a number of simulations have been performed using the SIMULINK model depicted in Figure G.1. In the SIMULINK model an 7th order IGRF model is used.

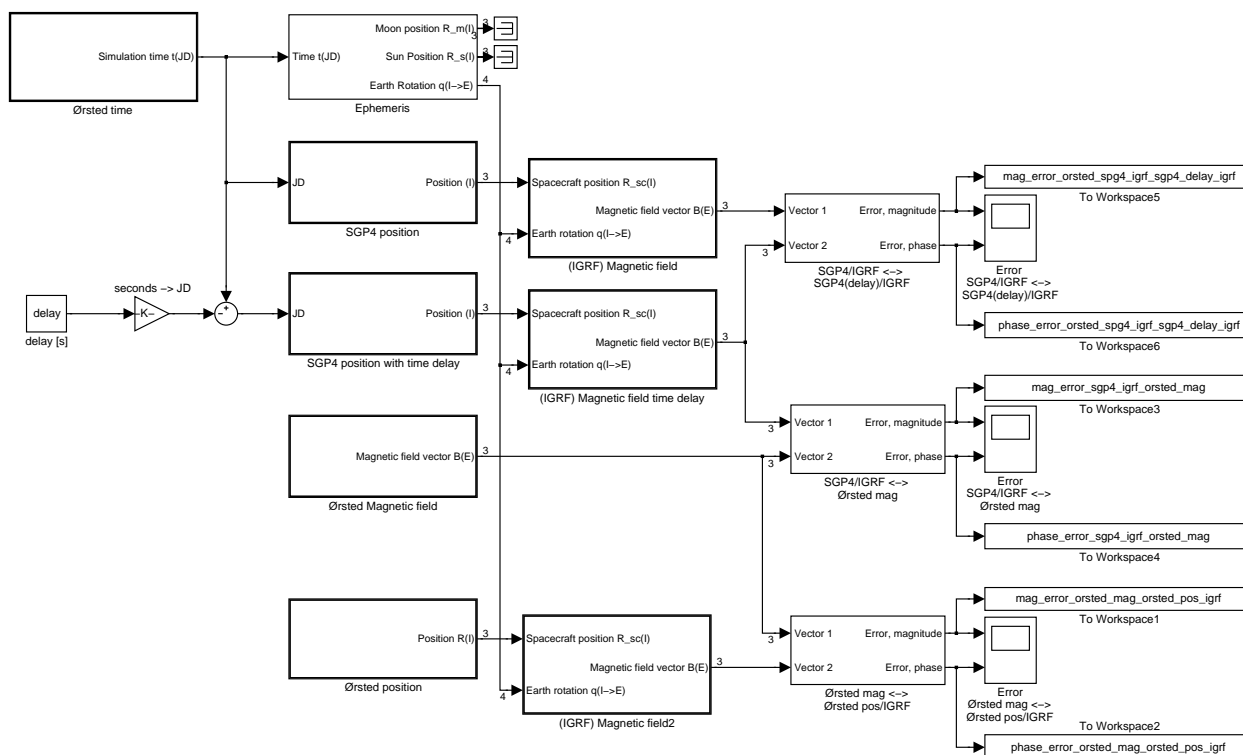
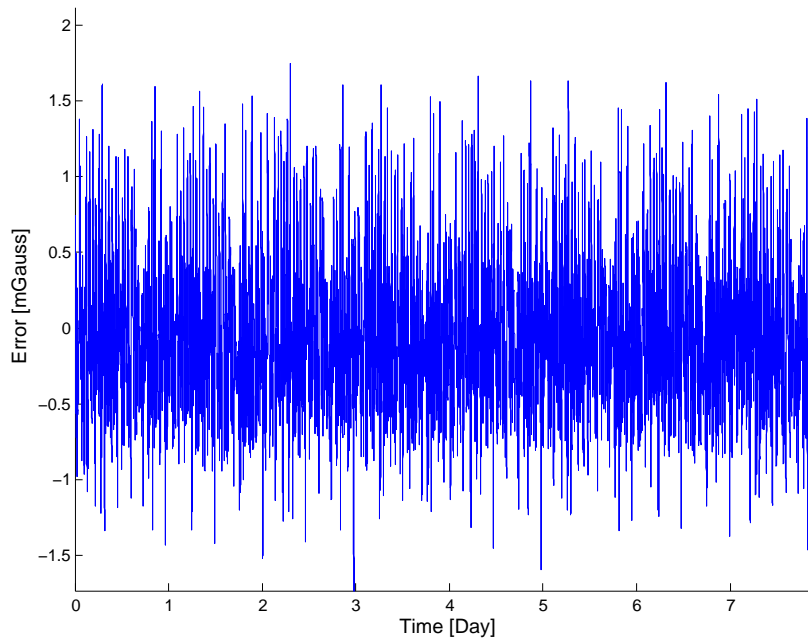


Figure G.1: The SIMULINK model used for accuracy verification of the IGRF model.

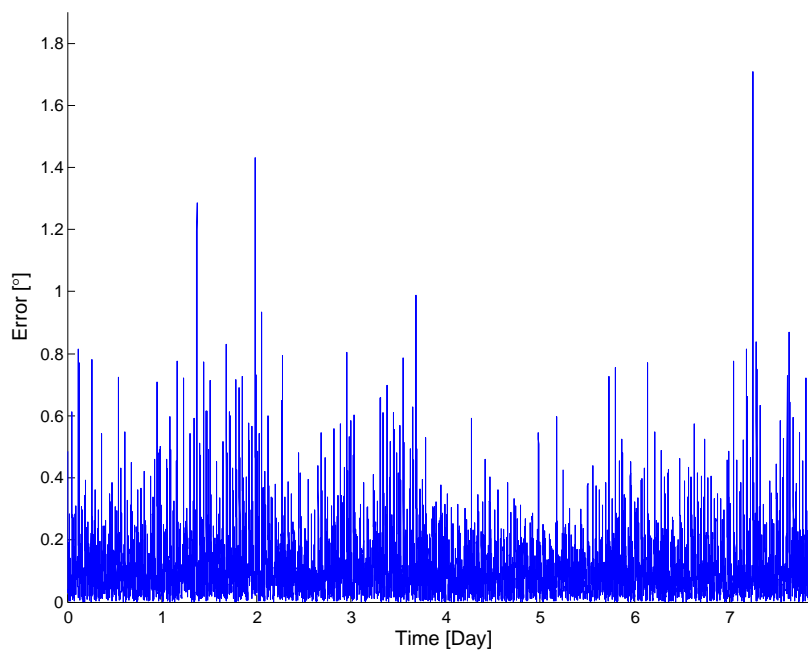
To examine the accuracy of the IGRF model the output is compared with measurements of the magnetic field performed by the Ørsted satellite. Besides measurements of magnetic field vectors and positions, the data from the Ørsted satellite also contains time stamps for each measurement. Therefore it is possible to use position data for the Ørsted satellite orbit in the simulation instead of the SGP4 orbit model. The Ørsted measurement data is further described in [CubeSat ADS, page 110]. The results of the simulation are shown in Figure G.2.

The accuracy of the IGRF model is dependent on the accuracy of the SGP4 orbit model. The influence can be determined by using position data from the SGP4 orbit model to generate a model output of the IGRF model. The output is compared with magnetic field data from the Ørsted satellite. A simulation has been performed using the SIMULINK model depicted in Figure G.1 and the results are depicted in Figure G.3.

As expected the mean angular error of the IGRF model output using SGP4 position data is larger than when using Ørsted position data. Figure G.3 also indicates that the angular error increases during the the simula-



(a) Error in magnetic field intensity.



(b) Angular error.

	Intensity error [mGauss]	Angular error [°]
Mean	-0.0482	0.112
Max	1.7450	1.707

(c) Mean and maximum values of errors.

Figure G.2: Magnetic field vector error between the IGRF model and Ørsted position and magnetic field data.

tion. The error is time dependent which traces back to the SGP4 orbit model in which the position error also increases with time. This is described in Appendix F on page 108. To keep the IGRF error as low as possible the SGP4 orbit model should be reinitialised with a new TLE at a regular basis.

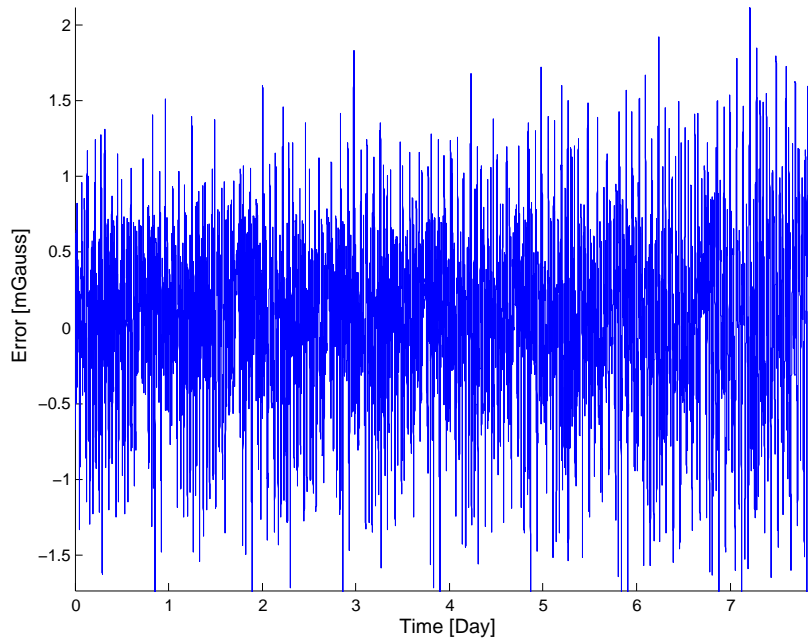
In order for the SGP4 orbit model to produce a valid position vector to the satellite it requires the correct time in Julian Date. If the time used in the SGP4 algorithm is not synchronized with the time used when generating the TLE the result will be an error in the position vector to the satellite. To examine the impact of the errors on the IGRF model on the IGRF model, the output of a combination of the IGRF model and the SGP4 model, with and without time offset, are compared.

Figure G.1 shows the SIMULINK model used for the simulation with the SGP4 model with different time offsets and the results are shown in Table G.1.

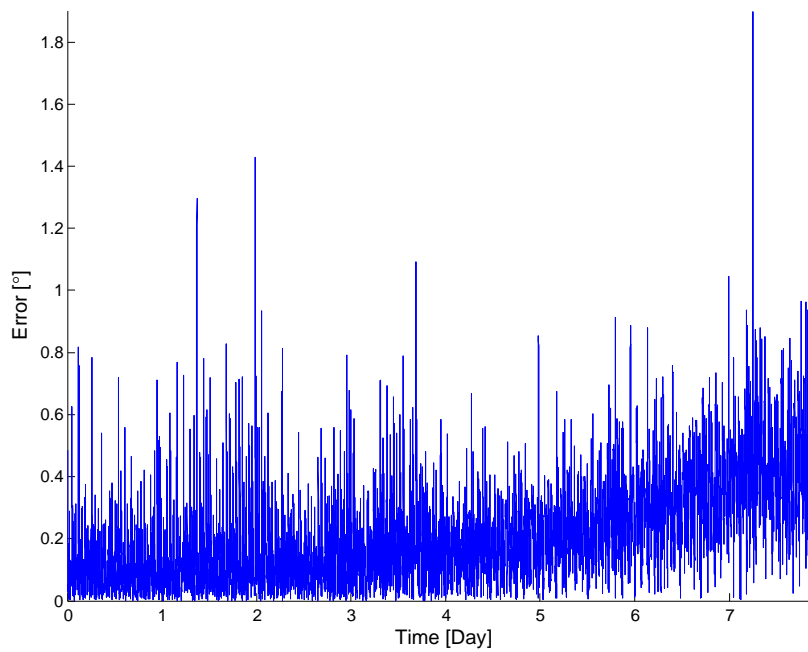
(a) Intensity error.										
Offset [s]	0.5	1.0	1.5	2.0	2.5	3.0	3.5	4.0	4.5	5.0
Mean [mGauss]	0.049	0.049	0.049	0.049	0.048	0.048	0.048	0.048	0.048	0.047
Max [mGauss]	2.001	1.885	1.799	1.788	1.777	1.765	1.861	1.992	2.123	2.255

(b) Angular error.										
Offset [s]	0.5	1.0	1.5	2.0	2.5	3.0	3.5	4.0	4.5	5.0
Mean [°]	0.221	0.200	0.198	0.214	0.245	0.287	0.335	0.387	0.441	0.498
Max [°]	1.867	1.835	1.803	1.772	1.740	1.710	1.679	1.649	1.619	1.641

Table G.1: Magnetic field vector error between Ørsted data and the IGRF model using the SGP4 orbit model with a time offset.



(a) Error in magnetic field strength.



(b) Angular error.

	Magnitude error [mGauss]	Angular error [°]
Mean	0.0493	0.2082
Max	2.1175	1.8986

(c) Mean and maximal values of error.

Figure G.3: Magnetic field vector error between the IGRF model using the SGP4 orbit model and Ørsted magnetic field measurements.